(2)

S-CUBED

A Division of Maxwell Laboratories, Inc.

AFOSR-TR- 89 0020

SSS-DFR-89-10153

ADVANCED CONSTITUTIVE MODELING OF PLAIN AND REINFORCED CONCRETES

G. A. Hegemier, H. E. Read
K. C. Valanis and H. Murakami

Final Report

Prepared for

Air Force Office of Scientific Research
Bolling AFB, DC 20322

under

AFOSR Contract No. F49620-84-C-0029

December, 1988

P. O. Box 1620, La Jolla, California 92038-1620
(619) 453-0060

UNCLASSIFIED
SECURITY CLASSIFICATION OF THIS PAGE

ADA204746

REPORT DOCUMENTATION PAGE

1a REPORT SECURITY CLASSIFICATION: Unclassified	1b RESTRICTIVE MARKINGS: N/A since Unclassified
2a SECURITY CLASSIFICATION AUTHORITY: N/A since Unclassified	3 DISTRIBUTION / AVAILABILITY OF REPORT: Approved for public release; distribution unlimited
2b DECLASSIFICATION / DOWNGRADING SCHEDULE	
4 PERFORMING ORGANIZATION REPORT NUMBER(S): SSS-DFR-89-10153	5 MONITORING ORGANIZATION REPORT NUMBER(S): AFOSR-TR- 89-0020
6a NAME OF PERFORMING ORGANIZATION: S-CUBED, A Division of Maxwell Laboratories, Inc. / 6b OFFICE SYMBOL (If applicable)	7a NAME OF MONITORING ORGANIZATION: Air Force Office of Scientific Research
6c ADDRESS (City, State, and ZIP Code): P.O.Box 1620, La Jolla, CA 92038-1620	7b ADDRESS (City, State, and ZIP Code): Bolling AFB, DC 20332 BK1 410
8a NAME OF FUNDING / SPONSORING ORGANIZATION: AFOSR / 8b OFFICE SYMBOL (If applicable): NA	9 PROCUREMENT INSTRUMENT IDENTIFICATION NUMBER: F49620-84-C-0029
8c ADDRESS (City, State, and ZIP Code): Bolling AFB, DC 20332 BK1 410	10 SOURCE OF FUNDING NUMBERS: PROGRAM ELEMENT NO 61102F; PROJECT NO 2302; TASK NO C2; WORK UNIT ACCESSION NO

11 TITLE (Include Security Classification)
ADVANCED CONSTITUTIVE MODELING OF PLAIN AND REINFORCED CONCRETES

12 PERSONAL AUTHOR(S)
Hegemier, G. A., Read, H.E., Valanis, K. C., and Murakami,H.,

13a TYPE OF REPORT	13b TIME COVERED	14 DATE OF REPORT (Year, Month, Day)	15 PAGE COUNT
Final	FROM 840301 TO 880731	881231	

16. SUPPLEMENTARY NOTATION

17 COSATI CODES			18. SUBJECT TERMS (Continue on reverse if necessary and identify by block number)
FIELD	GROUP	SUB-GROUP	Plain concrete, Constitutive modeling, Reinforced concrete, Steel-concrete interaction, Endochronic theory, Continuous damage theory, (SRS)

19. ABSTRACT (Continue on reverse if necessary and identify by block number)

This report summarizes research conducted by S-CUBED to develop advanced constitutive models of plain and reinforced concrete for ultimate use in the cost-effective design and hardness assessment of concrete protective structures. The specific goals of the research are two-fold: namely, (1) development of a mixture theory which can accurately account for steel-concrete interaction and (2) formulation of an advanced constitutive theory for plain concrete which can accurately portray its nonlinear, inelastic behavior, including developing damage and macrocracking, for arbitrary loading histories. The importance of steel-concrete interaction and nonlinear inelastic behavior of the plain concrete, including cracking, is emphasized. The progress made toward achieving these goals is described..

20. DISTRIBUTION / AVAILABILITY OF ABSTRACT	21 ABSTRACT SECURITY CLASSIFICATION
☐ UNCLASSIFIED/UNLIMITED ☒ SAME AS RPT. ☐ DTIC USERS	UNCLASSIFIED
22a. NAME OF RESPONSIBLE INDIVIDUAL: Dr. Spencer T. Wu	22b. TELEPHONE (Include Area Code): (202) 767-6962 / 22c. OFFICE SYMBOL: AFOSR/NA

DD FORM 1473, 84 MAR — 83 APR edition may be used until exhausted. All other editions are obsolete.

SECURITY CLASSIFICATION OF THIS PAGE
UNCLASSIFIED

S-CUBED
A Division of Maxwell Laboratories, Inc.

SSS-DFR-89-10153

ADVANCED CONSTITUTIVE MODELING OF PLAIN AND REINFORCED CONCRETES

G. A. Hegemier, H. E. Read
K. C. Valanis and H. Murakami

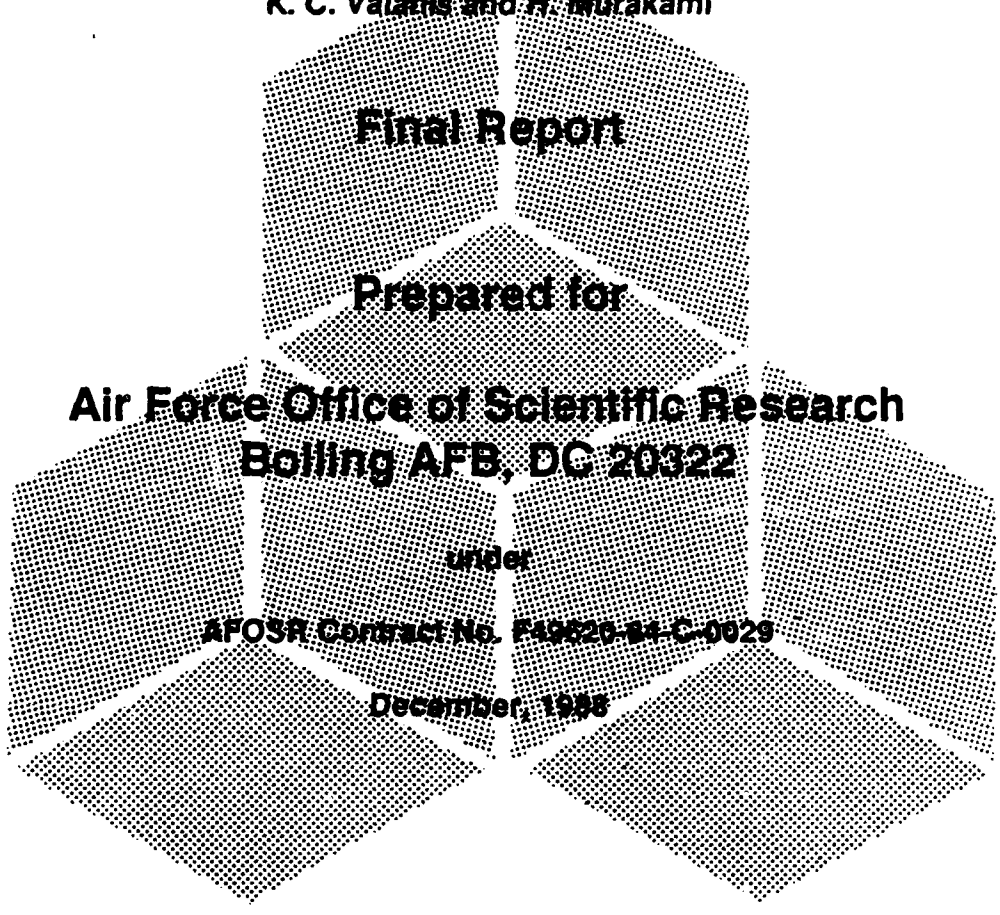

Final Report

Prepared for

Air Force Office of Scientific Research
Bolling AFB, DC 20322

under

AFOSR Contract No. F49620-84-C-0029

December, 1988

P. O. Box 1620, La Jolla, California 92038-1620
(619) 453-0060

FOREWORD

This final report summarizes the research performed by S-CUBED under AFOSR Contract F49620-84-C-0029 during the period from March 1, 1984, to July 31, 1988. Partial support for portions of the research was provided by the Defense Nuclear Agency under Contract DNA001-84-C-0127. The Co-Principal Investigators for the project were Dr. G. A. Hegemier and Dr. H. E. Read. The AFOSR Contract Technical Monitors were, initially, Lt. Col. L. D. Hokanson and, later on, Dr. Spencer T. Wu.

Drs. Hegemier and Murakami, Consultants to S-CUBED, are also, respectively, Professor and Associate Professor of Applied Mechanics at the University of California, San Diego. Dr. Valanis, an S-CUBED Consultant, presently operates his own research and consulting company, called ENDOCHRONICS, Inc.

The authors express their appreciation to Dr. D. H. Brownell and Mr. R. G. Herrmann, who provided excellent computational support throughout the course of the research.

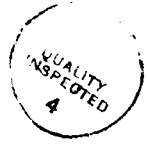

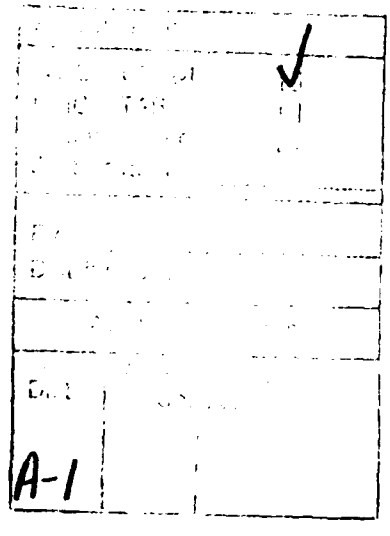

TABLE OF CONTENTS

Section		Page
	Foreword	ii
1	INTRODUCTION	1
	1.1 Background	1
	1.2 Objective	1
2	REINFORCED CONCRETE	3
	2.1 The Problem	3
	2.2 Accomplishments	3
	2.3 Future Studies	5
3	PLAIN CONCRETE	6
	3.1 The Problem	6
	3.2 Accomplishments	6
	3.3 Future Studies	10
4	PUBLICATIONS	12
	APPENDICES	
	APPENDIX A: ON MIXTURE MODELS WITH MICROSTRUCTURE FOR REINFORCED CONCRETE	A-1
	APPENDIX B: ENDOCHRONIC PLASTIC-FRACTURING THEORY WITH APPLICATION TO PLAIN CONCRETE	B-1

ADVANCED CONSTITUTIVE MODELING OF PLAIN AND REINFORCED CONCRETES

Section 1
INTRODUCTION

1.1 BACKGROUND.

During the past several years, the Air Force has been deeply involved in an extensive effort to develop, and assess the feasibility and relative effectiveness of, various candidate modes for basing the MX strategic weapons system. In most of these basing modes, the key elements are large reinforced concrete structures, called protective structures, which are designed to protect a missile from the shock loads prescribed by the design attack scenarios. The enormous costs involved in constructing the large number of such structures required by the system dictates that their design be not only safe, but cost-effective as well.

In the event that the enemy threat changes, it is also important for the strategic system designer to know the ultimate hardness of the concrete protective structures, so that the survivability of the system with regard to the new threat can be readily assessed. The most expeditious and economical way to do this is through the use of validated analytical models of the structure's behavior. There is, accordingly, a need to have reliable analytical models that can predict the loading environments for which complex reinforced concrete structures will collapse, or incur sufficient damage to render them functionally inoperable.

1.2 OBJECTIVE

The objective of the overall research program described here is to construct an advanced, nonlinear, multi-axial, non-phenomenological constitutive model of reinforced concrete that will provide simulation accuracy in the nonlinear response regime that is superior to existing models. The term 'advanced nonlinear multi-axial' implies a model that provides greater accuracy than existing models in the inelastic, nonlinear response regime and for arbitrary paths in multi-axial stress or strain space. The term 'non-phenomenological' implies a model that is capable of synthesizing the global properties of reinforced concrete from knowledge of the plain concrete and steel properties, the concrete-steel interface properties, and the geometry of the steel reinforcement.

A non-phenomenological reinforced concrete theory requires, as input, constitutive models for each of the basic constituents, namely, steel rebar and plain concrete. The accuracy of the resulting reinforced concrete theory depends heavily on the accuracy with which one can model these two constituents. The constitutive properties of steel are well known and can be adequately represented by reasonable simple elasto-plastic models. Plain concrete, on the other hand, is one of the most complex structural materials in current use and, despite numerous efforts in recent years to mathematically model its properties, there is today still no model which can adequately describe its nonlinear constitutive properties over a wide range of behavior, including damage accumulation and post-cracking response. As a result, the major challenges that one faces in attempting to develop an accurate constitutive theory for reinforced concrete are twofold; namely, (1) development of a mixture theory which accurately accounts for the interaction between the rebar and plain concrete; and (2) formulation of a constitutive theory for plain concrete which adequately describes its nonlinear, inelastic properties, including damage and cracking, for arbitrary, multi-axial load paths. Accordingly, two major areas of research have been pursued in parallel, concurrent efforts under the present program; namely, (1) development of a mixture theory which accounts for concrete-rebar interaction in a realistic manner; and (2) development of a plain concrete model.

Detailed documentation of the research conducted during the first three years of this study can be found in the Annual Reports by Hegemier, Read, Valanis and Murakami (1985, 1986, 1987).* Details of the research performed during the past (fourth) year are described in the topical reports by Hegemier, Murakami and Sweet (1988) and by Read (1988).** The major accomplishments made during the course of the entire program are summarized in this report, and the reader is referred to either the Annual Reports or to the various published papers and Topical reports for further details of the research accomplishments.

---

* A list of the publications which resulted from this contract is given in Section 4.

** These topical reports are included as part of the present report in Appendices A and B.

Section 2
REINFORCED CONCRETE

2.1 THE PROBLEM.

The nonlinear, inelastic behavior of reinforced concrete is dominated by complex interactions between the steel rebar and the concrete. These interactions have a major effect on structural characteristics such as stiffness, strength, damping and ductility. As a result, it is necessary that a model of reinforced concrete reflect these phenomena in an accurate and realistic manner. Further, in an effort to minimize the number and types of tests necessary to define model parameters, it is desirable that the model be non-phenomenological, i.e., that the global properties of reinforced concrete be synthesized from the properties of (1) the steel and concrete, (2) the steel-concrete interface physics and (3) the steel layout.

2.2 ACCOMPLISHMENTS.

A theoretical formulation of the type outlined above constitutes a new, advanced model of reinforced concrete which has predictive capabilities far superior to existing models. In an effort to bring such a model to fruition, the following tasks were accomplished as part of this program:

1. Formulation of a methodology for constructing an advanced theoretical model of reinforced concrete which correctly reflects steel-concrete interaction;

2. Construction of a first generation model of reinforced concrete using the results from the above task;

3. Construction of numerical algorithms and a special-purpose computer program which allows one to exercise the developed model for a limited class of test problems;

4. Simulation of special problems (case studies) using the special purpose code developed under the above task.

5. Conduct of a detailed literature search and evaluation of available experimental data on the behavior of reinforced concrete.

6. Performance of model validations consisting of experimental-theoretical comparisons of important response features.

7. Performance of a parametric study in an effort to determine the influence of basic material and geometric properties on damage accumulation and failure conditions.

Under Tasks 1 and 2, a new, advanced model of reinforced concrete with a dense unidirectional steel layout was constructed (Hegemier and Murakami, 1985; Murakami and Hegemier, 1986; Hegemier, Read, Valanis and Murakami, 1986). The construction technique was based upon the use of multivariable asymptotic expansions, a variational principle, and certain smoothing operations. The resulting model was cast into the form of a binary mixture which resembles an overlay of two continua: steel and concrete. These continua interact via body forced which are functionals of the relative global displacements of the continua. The theory is fully nonlinear and it incorporates the following basic physical phenomena; rebar yielding, steel-concrete bond degradation and slip, dowel action, and progressive concrete cracking (which is treated explicitly). The model furnishes both global and local (to a certain degree of accuracy) measures of deformation, stress and damage. Response characteristics such as stiffness degradation, ductility, hysteresis, strain hardening, and certain failure models evolve naturally as the deformation proceeds.

The validations performed under Task 6 reveal that the theoretical framework developed leads to a model of reinforced concrete which is capable of accurate predictions of complex response characteristics. (Hageman, Murakami and Hegemier, 1986; Hegemier, Murakami and Hageman, 1984; Hegemier and Murakami, 1986; Murakami and Hegemier, 1986.) Specifically, the validation tests performed to-date clearly indicate that the model correctly simulates progressive concrete primary cracking (Hegemier, Murakami and Hageman, 1984), steel-concrete bond degradation and slip (Hageman, Murakami and Hegemier, 1986; Hegemier, Murakami and Hageman, 1984), steel-concrete dowel action (Murakami and Hegemier, 1986), and certain failure modes (Hegemier, Read, Valanis and Murakami, 1986).

Under Task 7, an extensive parametric study (Hegemier, Murakami, and Sweet, 1988), which is included herein as Appendix A for the convenience of the reader, was performed using the developed advanced reinforced concrete model. The purpose of this study was to ascertain the influence of fundamental material, interface, and

geometric properties on the nonlinear response characteristics of reinforced concrete. Of primary interest in this study was damage accumulation, overall ductility, and failure modes/conditions. The damage mechanisms that were examined included progressive concrete cracking, steel-concrete bond slip, and rebar yielding. Parameters that were varied included the concrete tensile strength, the steel-concrete bond strength, and rebar yield stress and hardening characteristics, the steel volume fraction, and the total steel surface area. Combinations of these parameters were discovered that allowed a concise graphical description of their affects on material response. The latter should be of considerable value to the practicing engineer.

Finally, during the last research period the unidirectional theory noted above was extended to include multidirectional steel layouts. The latter was selected in the form of an orthogonal net. Details concerning the derivation and form of the resulting theory are contained in Appendix A.

2.3 FUTURE STUDIES

It is recommended that future studies be focused upon two main areas. These are: (1) advanced validation tests in the form of response simulations of elementary structural elements under shear, bending, direct compression, and combinations thereof; and (2) the development and application of smoothing operations for the crack field. Item (1) is self-evident. Item (2), however, deserves comment.

Currently the model development process homogenizes the steel and concrete via appropriate smoothing operations. These operations lead, as was noted previously, to a model which resembles an overlay of two continua: steel and concrete. The evolving concrete crack field, however, is <u>not</u> homogenized, i.e., cracks must presently be followed explicitly. This feature of the model renders it difficult to use from a computational standpoint. As a consequence, some form of crack field smoothing should be explored in an effort to simplify the model computationally.

Section 3
PLAIN CONCRETE

3.1 THE PROBLEM.

The ultimate success of the mixture theory for reinforced concrete, discussed above, hinges very strongly on the ability of the constitutive model of plain concrete, used with the theory, to accurately describe the behavior of plain concrete over the wide range of response that can be expected in practice. Any deficiencies in the plain concrete model will surely be reflected -- and possibly enhanced -- when the model is used in conjunction with the mixture theory to describe reinforced concrete. Clearly, the accuracy of the mixture theory can never be greater than the accuracy of the plain concrete model used with it. Because of this, every effort should be made to develop an accurate model of plain concrete.

During the past ten years, considerable research has been devoted to understanding and modeling the constitutive behavior of plain concrete. From this has come a variety of different constitutive models for plain concrete which provide reasonably accurate descriptions of plain concrete behavior for stress paths which generally do not differ greatly from the standard paths followed in the usual laboratory testing. Largely, due to the lack of available appropriate data, little proof-testing of the models has been done to examine their predictive capabilities for complex stress or strain paths that are expected to occur in practice. Many of the models are limited to the stress range below failure, since they contain no provision for treating cracking. A few of the models do, however, attempt to treat cracking and post-cracking behavior as well. Generally speaking, however, the problems of developing a constitutive model of plain concrete capable of realistically describing the full spectrum of behavior from pre-cracking to cracking and finally post-cracking response still remains basically unsolved. The goal of the present research is to address this need.

3.2 ACCOMPLISHMENTS.

A new constitutive model of plain concrete was developed which appears to have remarkable capabilities for predicting the nonlinear inelastic behavior of concrete for stress states below failure (Valanis and Read, 1985; 1986). The model is formulated on the basis of the endochronic theory of plasticity and, as such, does not require a yield surface nor the specification of loading or unloading criteria, as in classical plasticity. It predicts that plastic flow will occur from the onset of loading, a feature

which makes the model attractive and appropriate for describing the behavior of concrete, which does not exhibit a well-defined yield point. Basically, the model is isotropic (when referred to its initial state), rate-independent and satisfies the second law of thermodynamics (Clausius-Duhem inequality). It realistically portrays the major features of nonlinear inelastic behavior exhibited by plain concrete, including shear-volumetric coupling, effect of hydrostatic pressure on shear response, hardening, hysteresis and stress-path dependence.

The foregoing model was applied to an extensive set of laboratory data generated by the University of Colorado, using a true triaxial device. The test programs consisted of six different series of stress-controlled tests, each of which was designed to explore a particular facet of material behavior. Altogether, the response of concrete to over 45 complex stress paths was investigated. In all cases, the stress paths were such that no significant macrocracking occurred during the tests.

The model was fit to a very small subset of the data, after which it was proof-tested by driving it around over 20 complex stress paths to predict the corresponding deformation histories. None of the data from the complex stress path tests were used in fitting the model parameters and no optimization techniques were employed.

As shown by Valanis and Read (1985,1986), the proof-tests were remarkably successful and revealed the powerful predictive capability of this new model. In all cases, the model captured the essential features of the concrete behavior and exhibited excellent agreement with the data. For nonlinear, inelastic behavior inside the failure surface, i.e., where significant macrocracking has not occurred, the endochronic concrete model appears to provide the most accurate description of concrete behavior of any of the existing concrete models.

To approach the problem of extending the basic endochronic model to account for cracking, anisotropy and dilatancy, the constitutive behavior of a brittle elastic solid was first considered. From this effort, there resulted a new continuous damage theory for brittle solids (Valanis, 1985), which possessed a number of desirable features not found in other models. In this model, damage (microcracking) accumulates in a gradual manner from the onset of loading, provided that at least one of the principal strains is extensional. The model is initially isotropic, but becomes

anisotropic if damage develops in specific directions. Through a clever formulation, general anisotropy is handled through the use of second order tensors, and thus does not require the use of fourth-order tensors, as do most such models. It appears that the model can describe the standard modes of cracking, as well as the so-called "splitting mode" under uniaxial compression, a mode which is beyond the scope of most existing fracture models. Details of the model, together with a number of applications, are given by Valanis (1985).

Recently, the above approach for describing damage and fracture of solids was extended by Valanis (1987, 1988) to plastic-damaging solids, with the result that a new endochronic-damaging model is now available which possesses all of the desirable features found in the earlier (no damage) model but can now treat cracking, anisotropy and dilatancy. The key concept behind the theory is a mapping which transforms the current, damaged and generally anisotropic state of a material into an isotropic, undamaged state. The model describes both stiffness degradation and yield limit degradation due to developing damage, as well as dilatancy, and contains, as special cases, several models that are noteworthy, including the classical elastic-fracturing model. The model has been successfully applied to recent data on the response of plain concrete to simple tension (Read, 1988)*** . For further details of the model and its application to plain concrete, see Valanis and Read (1989).

In view of the Air Force's interest in shock loading of defense structures, and with the goal of eventually introducing strain-rate dependence into the endochronic concrete model, a comprehensive review of strain rate effects in plain concrete was conducted (Read, 1985; Hegemier and Read, 1985). In particular, we sought an answer to the following question: Does the existing data on strain rate effects in plain concrete realistically reflect the true rate dependence of this material, or are the inferred rate effects the result of spurious system effects, inhomogeneous deformation or poor methods of data interpretation? In view of the importance of strategic structure response to this study, the review was focussed on the strain rate range from 10^{-1} to 10^{2} sec^{-1}, where almost all of the data comes from drop hammer devices. From the review, it was concluded that considerable caution should be exercised in using such data to develop rate-dependent constitutive models. The responses of test specimens in such devices are complicated by a number of factors, including inhomogeneous deformation, non-ideal boundary conditions and complex stress-wave fields. For further details, the works by Read (1985) and Hegemier and Read (1986) should be consulted.

*** See Appendix B.

Concrete, as well as rocks and dense soils, when compressed at constant axial strain rate under conditions of either uniaxial stress or triaxial compression, exhibit a phenomenon called "strain softening". Materials which exhibit such softening are characterized by a constitutive response in the axial direction in which the stress rises monotonically with strain to a peak, and then decreases with further increases in strain.

In the past, strain softening has been generally viewed as a true continuum material property and routinely incorporated into constitutive models. As a result, the literature abounds with advanced, complex constitutive models for materials such as concrete, rock and soil which are designed to simulate strain softening. Recently, however, both numerical and analytical difficulties have surfaced concerning the solution of certain wave propagation problems in strain softening materials. As examples, it is noted that strain softening can lead to mesh dependence from the numerical viewpoint and loss of hyperbolicity from the analytical standpoint.

In view of these difficulties, and because plain concrete is a strain softening material (at least for pressures below the brittle-ductile transition), an extensive study of strain softening, including experimental, theoretical and numerical issues, was conducted. The results from this study are given in the works by Read and Hegemier (1984), Hegemier and Read (1984), and Hegemier and Read (1985). In essence, it was found that without exception the initiation of strain softening corresponds to the transition of the test specimen from a continuum to a structure and/or to significant geometrical changes in the specimen's minimum cross-sectional area. It was concluded that strain softening, as inferred in the usual manner from conventional laboratory tests, is <u>not a material property</u> and therefore should not be incorporated into the usual (local) types of constitutive equations. This conclusion has been reaffirmed by subsequent investigators.

During the present reporting period, there has been considerable activity directed toward developing and applying non-local models of strain softening. Virtually all of this activity has focussed on the case of softening under tension, and a measure of success has been achieved. The more difficult case of softening in compression has received little attention and continues to be an unresolved problem. Further research is needed to develop a general approach which can deal with softening under both tensile and compressive loading conditions.

Finally, the types of experimental data normally used to develop constitutive models for plain concrete were critically assessed as part of this study (Hegemier and Read, 1985). Various issues pertaining to strain softening, strain hardening, failure states, failure modes and strain rate effects were considered. Particular attention was given to the effects of different boundary conditions and different test devices on the resulting data. Also, the manner of defining failure was explored. It was found that failure modes are strongly influenced by a number of factors, perhaps the most important being the test boundary conditions. Considerable scatter in data was found with respect to failure modes, especially at low confining pressures.

3.3 FUTURE STUDIES.

In order to complete the research undertaken in this task, and to accomplish the ultimate goal of developing a constitutive model of plain concrete that is capable of describing the response of this material to shock loading, including damage and fracture, the following tasks are recommended in a future effort:

- In view of the very encouraging progress made in this study toward developing a theory for the plasticity and fracture of concrete, further effort should be undertaken to explore and validate the theory under more general loading conditions, such as uniaxial compression and triaxial compression. These cases involve cracking patterns that are considerably more complex than those which occur under simple tension, and thus should provide insight for further model development.

- The success of the new endochronic plastic-fracturing model in describing real physical phenomena depends strongly on the ability of the damage evolution equation to reflect the underlying micromechanical damage processes. Additional effort, therefore, needs to be devoted to setting the damage evolution equation on a firm micromechanical foundation.

- Further investigate the still unresolved question of strain-rate dependence of concrete, with particular attention on the critical assessment of experimental techniques developed by the defense community during the past several years.

- If the issue of rate-dependence can be resolved, introduce strain-rate effects into the endochronic plastic fracturing model. Validate model against appropriate strain-rate data not used in calibrating the model.

- While considerable progress has been made recently in understanding "strain softening", there are still many outstanding questions. Most importantly, there is still no generally accepted method for taking strain softening into account under general loading conditions. This area is in need of immediate attention.

Section 4
PUBLICATIONS

The publications which resulted from the research conducted under this contract are listed below.

Hageman, L. J., H. Murakami and G. A. Hegemier (1986), "On Simulating Steel-Concrete Interaction in Reinforced Concrete. Part II: Validation Studies," *Mechanics of Materials*, Vol. 5, 187.

Hegemier, G. A., and H. E. Read (1984), "Strain Softening" (Discussion), Theoretical Foundations for Large-Scale Computations for Nonlinear Material Behavior, edited by S. Nemat-Nasser, R. J. Asaro and G. A. Hegemier, Martinus Nijhoff, Publ.

Hegemier, G. A., H. Murakami and L. J. Hageman (1984), "On Tension Stiffening in Reinforced Concrete," *Mechanics of Materials*, Vol. 4(2), 161.

Hegemier, G. A., and H. E. Read (1985), "On Deformation and Failure of Brittle Solids: Some Outstanding Issues," *Mechanics of Materials*, Vol. 4(3), 215.

Hegemier, G. A., and H. Murakami (1985), "A Nonlinear Theory for Reinforced Concrete," Proc. Second Symposium on the Interaction of Non-Nuclear Munitions with Structures, Panama City, FLA.

Hegemier, G. A., and H. Murakami (1986), "On Simulating the Nonlinear Planar Hysteretic Response of Reinforced Concrete and Concrete Masonry," Third ASCE/EMD Specialty Conference on Dynamics of Structures, UCLA, Los Angeles, California.

Hegemier, G. A., H. Murakami, and K. Sweet, (1988), "Influence of Steel-Concrete Bond Characteristics on Stiffness Degradation, Ductility, and Failure conditions in Reinforced Concrete," In preparation.

Murakami, H., and G. A. Hegemier (1986), "On Simulating Steel-Concrete Interaction in Reinforced Concrete. Part I: Theoretical Development," *Mechanics of Materials*, Vol. 5, 171.

Murakami, H., and G. A. Hegemier (1986), "A Nonlinear Dowel Action Model," submitted to *Intl. J. Solids and Structures*.

Read, H. E. and G. A. Hegemier (1984), "Strain Softening of Rock, Soil and Concrete," *Mechanics of Materials*, Vol. 3, 271.

Read, H. E. (1985), "Strain-Rate Effects in Concrete: A Review of Experimental Data and Methods," S-CUBED, La Jolla, Calif. Report No. SSS-R-85-6081.

Read, H. E., (1988), "Endochronic Plastic-Fracturing Theory with Application to Plain Concrete," S-CUBED La Jolla, CA ., Technical Report SSS-R-89-9848, December.

Valanis, K. C., (1985), "A Theory of Fracture for Brittle Solids," S-CUBED, La Jolla, Calif. Internal Report.

Valanis, K. C., and H. E. Read (1986), "An Endochronic Plasticity Theory for Concrete," *Mechanics of Materials*, Vol. 5, 277.

Valanis, K. C., (1987), ENDOCHRONICS, INC., Private Communication.

Valanis, K. C., (1988), "An Internal Variable Theory of Plasticity and Fracture," ENDOCHRONICS, INC., Vancouver, WA., Private Communication, February.

Valanis, K. C., and H. E. Read (1989), "An Internal Variable Theory for Plastic-Fracturing Solids," to be submitted for publication.

Annual Reports

Hegemier, G. A., H. E. Read, K. C. Valanis and H. Murakami, (1985) "Development of Advanced Constitutive Models for Plain and Reinforced Concretes," S-CUBED, La Jolla, CA., 1st Annual Report, SSS-R-85-7150, April.

Hegemier, G. A., H. E. Read, K. C. Valanis and H. Murakami, (1986), "Development of Advanced Constitutive Models for Plain and Reinforced Concretes," S-CUBED, La Jolla, CA., 2nd Annual Report, SSS-R-86-7914, April.

Hegemier, G. A., H. E. Read, K. C. Valanis and H. Murakami, (1987), "Development of Advanced Constitutive Models for Plain and Reinforced Concretes," S-CUBED, La Jolla, CA., 3rd Annual Report, SSS-R-87-8454, March.

APPENDIX A
SSS-DFR-89-10119

ON MIXTURE MODELS WITH MICROSTRUCTURE FOR REINFORCED CONCRETE

G. A. Hegemier
H. Murakami
K. Sweet

Technical Report

Prepared for

Air Force Office of Scientific Research
Bolling AFB, D.C. 20332

AFOSR Contract No. F49620-84-C-0029

December 31, 1988

ABSTRACT

This report describes an effort to develop continuum mixture models with microstructure for reinforced concrete with unidirectional or bidirectional steel reinforcement layouts. In addition to model construction, analytical and numerical examples are presented in an effort to demonstrate the capability of the theory to simulate stiffness degradation, ductility, and failure conditions. The theory incorporates progressive concrete cracking, steel-concrete bond slip, and yielding of the steel.

TABLE OF CONTENTS

Section			Page
1	INTRODUCTION		5
2	FORMULATION OF THE LINEAR PROBLEM		6
3.	HOMOGENIZATION PROCEDURE		9
	3.1	Scaling	9
	3.2	Microcoordinates	11
	3.3	Synthesized Field Equations	11
	3.4	Local Periodicity Condition	11
	3.5	Weighted Residual Procedure	13
	3.6	Trial Functions	16
4.	DEVELOPMENT OF 3D MIXTURE MODEL FOR R/C		19
5.	DEVELOPMENT OF 2D MIXTURE MODEL FOR R/C PANELS		23
	5.1	Plane Stress Constraints	23
	5.2	Constitutive Relations	23
	5.3	Equilibrium Equations	27
	5.4	Boundary Conditions	27
	5.5	Principle of Virtual Work	28
	5.6	Summary of Basic Equations in Material Coordinates	28
	5.7	Basic Equations in General Coordinates	30
6.	MODIFICATION FOR INTERFACE SLIP		34
7.	MODIFICATION FOR REBAR YIELD		36
8.	BASIC EQUATIONS FOR UNIAXIAL DEFORMATION		37
9.	STIFFNESS DEGRADATION, DUCTILITY, FAILURE: UNIAXIAL DEFORMATION IN DIRECTION OF STEEL (ϕ=0).		40
	9.1	Formulation of the Problem	40
	9.2	Solution for Field Variables	46
	9.3	Fracture Criteria and Sequence	49
	9.4	Stiffness Degradation	51
		9.4.1 Influence of Bond Strength	51
		9.4.2 Influence of Steel Volume Fraction	55

TABLE OF CONTENTS (Concluded)

Section			Page
	9.5	Ductility and Failure	55
		9.5.1 Definition of Ductility	57
		9.5.2 Influence of Bond Strength	57
		9.5.3 Influence of Concrete Tensile Strength	57
		9.5.4 Influence of Rebar Strain Hardening	57
		9.5.5 Ductility vs. Dimensionless Bond Strength	64
10.		EXTENSION TO OBLIQUE STEEL	70
	10.1	Basic Equations and Solution	70
	10.2	Fracture Criterion and Sequence	73
	10.3	Stiffness Degradation	73
11.		EXTENSION OF MIXTURE MODEL TO ORTHOGONAL BI-DIRECTIONAL REBAR LAYOUTS	78
	11.1	A 3D Cell for Two Rebar Systems	78
	11.2	Scaling and Microcoordinates	78
	11.3	Multi-variable Field Representation and ξ^*-Periodicity Condition	80
	11.4	Trial Displacement Field	80
	11.5	Principle of Virtual Work for Synthesized Field	84
	11.6	Mixture Equations of Equilibrium	85
	11.7	Mixture constitutive Relations	88
12.		LIST OF REFERENCES	93

SECTION 1

INTRODUCTION

This report deals with microstructural mixture models for reinforced concrete systems with unidirectional and bidirectional steel layouts. Sections 2 - 7 concern the development of models for 3D reinforced concrete elements and 2D reinforced concrete panels -- all with unidirectional rebar layouts. These models are examined from the standpoint of simulation capability in Sections 8-10. Included here are discussions of stiffness degradation, ductility, and failure conditions. In Section 11, the modeling effort is expanded to include rebar layouts which are bidirectional.

The models developed incorporate progressive concrete cracking, steel-concrete bond slip, and yielding of the reinforcement. The models are nonphenomenological in that all model parameters are defined once the properties and geometries of the material components are defined.

Section 2

FORMULATION OF THE LINEAR PROBLEM

Consider a reinforced concrete element with a uniaxial, periodic steel layout. At time t in the loading process, let this element consist of a collection of intact subelements. Let $\bar{V}$ and $\partial\bar{V}$, respectively, denote the volume and boundary surface of a typical sub-element. Thus, if crack surfaces penetrate the element, they are confined to $\partial\bar{V}$.

For reference, let rectangular Cartesian material coordinates $\bar{x}_1$, $\bar{x}_2$, $\bar{x}_3$ be selected with $\bar{x}_1$ in the axial direction; Figure 2.1. For notational convenience, $(\ )^{\alpha}$, $\alpha = 1,2$, will denote quantities associated with material α with $\alpha = 1$ denoting steel and $\alpha = 2$ denoting concrete. In addition, the notations $(\bar{\ })_{,i} \equiv \partial(\bar{\ })/\partial\bar{x}_i$ will be employed. The usual Cartesian indicial notation will be adopted in which Latin indices range from 1 to 3, and repeated indices imply the summation convention unless otherwise stated. Quantities of the form $(\bar{\ })$ and $(\ )$ denote dimensional and nondimensional variables, respectively.

Under the premise of small deformations and linear elastic, isotropic component response, the basic governing relations for the components and the component interfaces are:

(a) Equilibrium equations

$$\bar{\sigma}^{(\alpha)}_{ji,j} + \bar{f}^{(\alpha)}_{i} = 0 \quad \text{on } \bar{V}^{(\alpha)} \tag{2.1}$$

where $\bar{\sigma}_{ij}$ denotes the stress tensor, $\bar{f}^{(\alpha)}_i$ represents a body force per unit volume, and $\bar{V}^{(\alpha)}$ is the volume occupied by material α;

(b) Constitutive relations

$$\bar{\sigma}^{(\alpha)}_{ij} = \bar{\lambda}^{(\alpha)}\delta_{ij}e^{(\alpha)}_{kk} + 2\bar{\mu}^{(\alpha)}e^{(\alpha)}_{ij} \quad \text{on } \bar{V}^{(\alpha)} \tag{2.2}$$

where $\bar{\lambda}^{(\alpha)}$, $\bar{\mu}^{(\alpha)}$ are Lamé's constants, δ_{ij} is the Kronecker delta, and e_{ij} is the infinitesimal strain tensor;

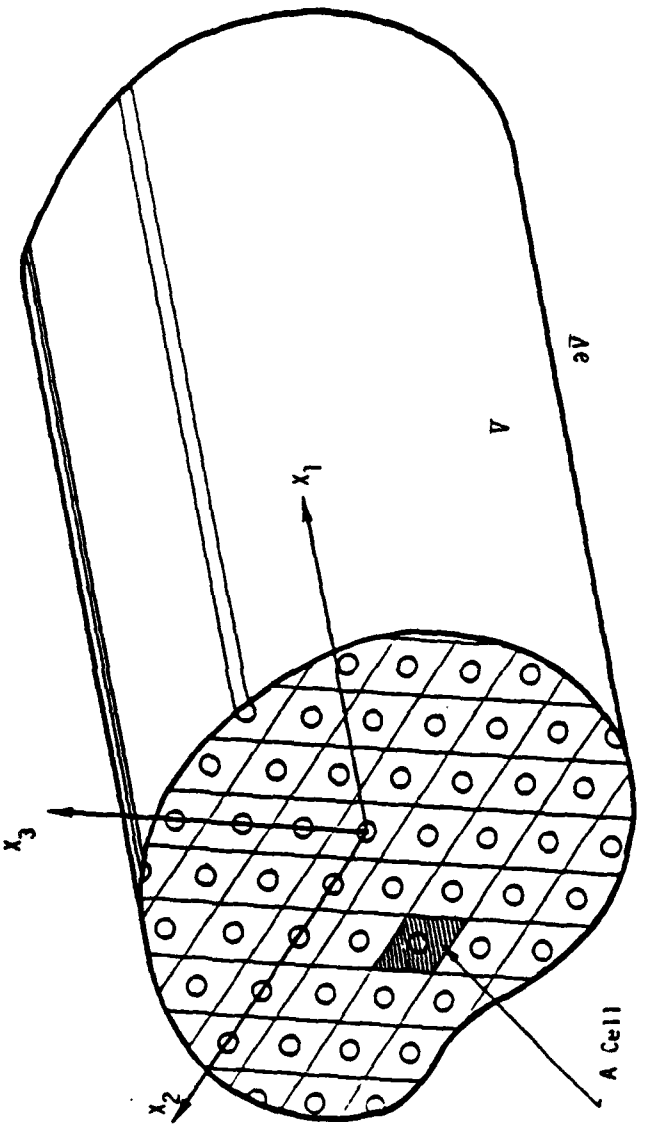

Figure 2.1. Reinforced concrete subelement.

(c) Strain-displacement relations

$$e_{ij}^{(\alpha)} = \frac{1}{2}\left(\bar{u}_{i,j}^{(\alpha)} + \bar{u}_{j,i}^{(\alpha)}\right) \text{ on } \bar{V}^{(\alpha)} \; ; \tag{2.3}$$

(d) Interface continuity conditions

$$\bar{u}_i^{(1)} = \bar{u}_i^{(2)} \; , \; \bar{\sigma}_{ij}^{(1)} \nu_j^{(1)} = \bar{\sigma}_{ji}^{(2)} \nu_j^{(1)} \text{ on } \bar{\delta} \tag{2.4}$$

where $\bar{\delta}$ denotes the interface between the two constituents and $\nu_j^{(1)}$ is the unit outward normal to material 1 on $\bar{\delta}$, which satisfies $\nu_1^{(1)} = 0$;

(e) Appropriate boundary conditions on $\partial\bar{V}$.

Conditions (a) - (e) define a well-posed boundary value problem. However, a direct solution of this problem for the stress and deformation fields on an element domain $\bar{V}$ is rendered virtually intractable for most cases by the many interfaces $\bar{\delta}$ and the three-dimensional aspect of the problem. A primary objective of the work to follow is to alleviate this difficulty by a process of homogenization or smoothing of the original heterogeneous material in $\bar{V}$.

Section 3

HOMOGENIZATION PROCEDURE

3.1 SCALING.

The homogenization process begins with a simple scaling of both dependent and independent variables. This step is facilitated by the introduction of the following nondimensional quantities:

$$
\begin{aligned}
x_i &= \bar{x}_i/\bar{\Lambda} \ , \\
u_i^{(\alpha)} &= \bar{u}_i^{(\alpha)}/\bar{\Lambda} \\
\sigma_{ij}^{(\alpha)} &= \bar{\sigma}_{ij}^{(\alpha)}/\bar{E}_{(m)} , \\
f_i^{(\alpha)} &= \bar{f}_i^{(\alpha)}\bar{\Lambda}/\bar{E}_{(m)} \ , \\
(\lambda,\mu)^{(\alpha)} &= (\bar{\lambda},\bar{\mu})^{(\alpha)}/\bar{E}_{(m)} ,
\end{aligned}
\tag{3.1}
$$

where $\bar{\Lambda}$ denotes a reference macro length and $\bar{E}_{(m)}$ is a reference composite elastic modulus. Under (3.1), equations (2.1) - (2.4) become

$$\sigma_{ji,j}^{(\alpha)} + f_i^{(\alpha)} = 0 \text{ on } V^{(\alpha)} \ , \tag{3.2}$$

$$\sigma_{ij}^{(\alpha)} = \lambda^{(\alpha)}\delta_{ij}e_{kk}^{(\alpha)} + 2\mu e_{ij}^{(\alpha)} \text{ on } V^{(\alpha)} , \tag{3.3}$$

$$e_{ij}^{(\alpha)} = \frac{1}{2}\left[u_{i,j}^{(\alpha)} + u_{j,i}^{(\alpha)}\right] \text{ on } V^{(\alpha)} \ , \tag{3.4}$$

$$u_i^{(1)} = u_i^{(2)} \ , \ \sigma_{ji}^{(1)}\nu_j^{(1)} = \sigma_{ji}^{(2)}\nu_j^{(1)} \text{ on } \partial \ , \tag{3.5}$$

where $V^{(\alpha)} = \bar{V}^{(\alpha)}/\Lambda^3$ and ∂ is again the component interface.

3.2 MICROCOORDINATES.

It is expected that the stress and deformation fields will vary significantly with respect to two basic length scales: (1) a "macro" length typical of the body size or loading condition; and (2) a "micro" length typical of a "cell" planar dimensions as depicted in Figure 2.1. These macro and micro scales will be associated with the variables $\bar{\Lambda}$ and $\bar{\Delta}$, respectively. Further, it is expected that these scales will differ by at least one order of magnitude in most cases. This suggests the use of multivariable asymptotic techniques, Hegemier, *et al* (1979). This approach commences by introducing new independent variables according

$$\begin{aligned} x^*_\gamma &= \phi^{-1}(\epsilon)x_\gamma,\ \phi(\epsilon) \to 0 \text{ as } \epsilon \to 0 \quad , \\ \tilde{x}_\gamma &= \psi(\epsilon)x_\gamma,\ \psi(\epsilon) \to 1 \text{ as } \epsilon \to 0 \ , \end{aligned} \tag{3.6a}$$

where $\gamma = 2,3$ and

$$\epsilon \equiv \bar{\Delta}/\bar{\Lambda} \quad . \tag{3.6b}$$

For the present analysis, it will suffice to set

$$\phi(\epsilon) = \epsilon \ , \ \psi(\epsilon) = 1 \quad . \tag{3.7}$$

Thus, all field variables $f(x_i,t)$ are now functions of the "microcoordinates" x^*_γ as well as the "macrocoordinates" $\tilde{x}_\gamma \equiv x_\gamma$, i.e.,

$$f(x_i) = F(x_i ; x^*_\gamma ; \epsilon) \quad . \tag{3.8}$$

Spatial derivatives of a function $f(x_i)$ then take the form

$$f_{,i} = F_{,i} + \epsilon^{-1}F_{,i^*} \tag{3.9}$$

where $()_{,i} \equiv \partial(\ )/\partial x_i$ and $(\ )_{,i^*} \equiv \partial(\ )/\partial x^*_1$ with $(\ )_{,1^*} \equiv \partial()/\partial x^*_1 = 0$. For notational convenience, the functions f and F will both be written as f in the following.

3.3 SYNTHESIZED FIELD EQUATIONS.

The operations (3.8) and (3.9), when applied to all field variables, lead to the following synthesized governing field equations in nondimensional form:

$$\sigma^{(\alpha)}_{ji,j} + \frac{1}{\epsilon}\sigma^{(\alpha)}_{ji,j^*} + f^{(\alpha)}_i = 0 \tag{3.10}$$

$$\sigma^{(\alpha)}_{ij} = \lambda^{(\alpha)}\delta_{ij}e^{(\alpha)}_{kk} + 2\mu e^{(\alpha)}_{ij} \quad , \tag{3.11}$$

$$e^{(\alpha)}_{ij} = \frac{1}{2}\left\{\left[u^{(\alpha)}_{i,j} + u^{(\alpha)}_{j,i}\right] + \frac{1}{\epsilon}\left[u^{(\alpha)}_{i,j^*} + u^{(\alpha)}_{j,i^*}\right]\right\}, \tag{3.12}$$

$$u^{(1)}_i = u^{(2)}_i, \ \sigma^{(1)}_{ji}\nu^{(1)}_j = \sigma^{(2)}_{ji}\nu^{(1)}_j \equiv T^*_i \text{ on } \partial \tag{3.13}$$

3.4 LOCAL PERIODICITY CONDITION.

An important premise, called the local periodicity condition, is now introduced. This condition consists of the assumption that <u>local</u> periodicity in the microvariables x^*_γ, $\gamma = 2,3$, may be invoked for all field variables. This premise allows one to analyze a single cell in an effort to determine the distribution of any field variable with respect to the coordinates x^*_γ. A typical such cell is illustrated in Figure 3.1. The local periodicity premise is suggested by the Floquet Theory associated with linear differential equations with periodic coefficients, the set of relations (3.10) - (3.12) can be reformulated as such a set of differential equations.

The local periodicity condition implies that all field variables $f(x_k;x^*_\gamma)$ satisfy

$$f\left[x_k;\ \hat{x}^*_2,\hat{x}^*_3;\epsilon\right] = f\left[x_k;\ -\hat{x}^*_2,-\hat{x}^*_3;\epsilon\right] \tag{3.14}$$

where $(\hat{x}^*_2,\hat{x}^*_3)$ and $(-\hat{x}^*_2,-\hat{x}^*_3)$ denote reflected points on the boundary $\partial\Omega$ of a typical cell with area $\Omega = A^{(1)} \cup A^{(2)}$.

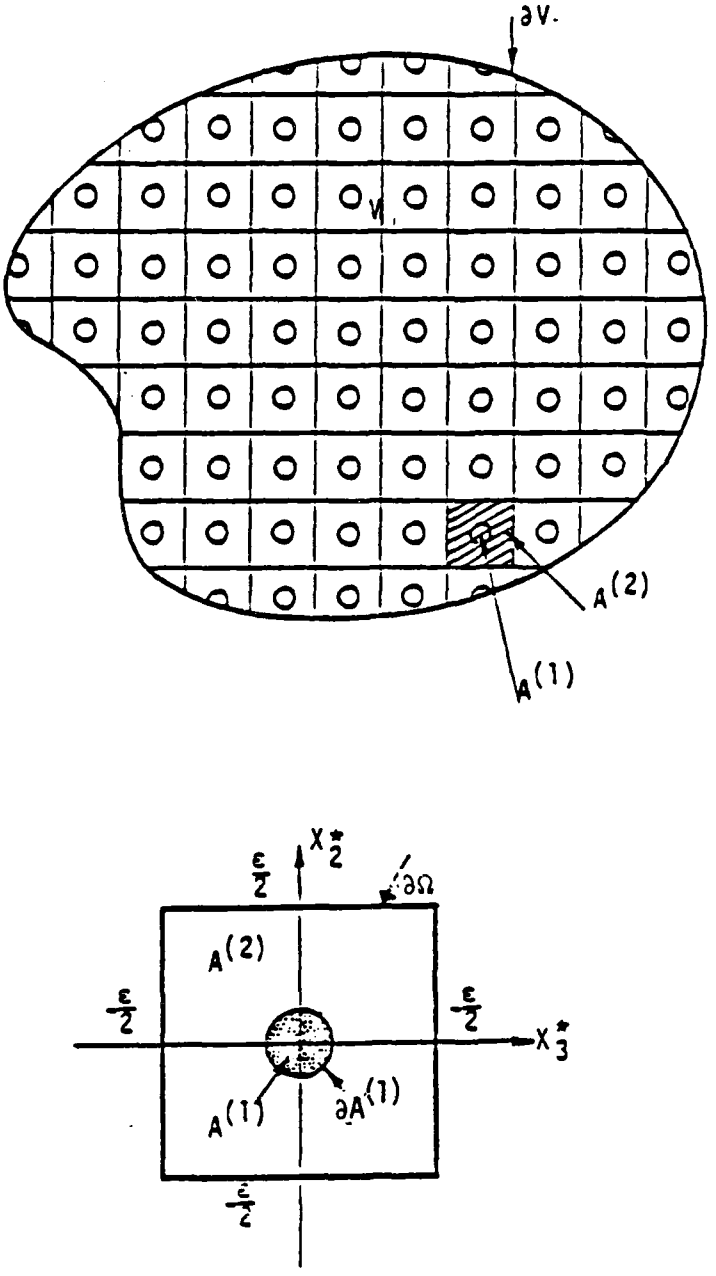

Figure 3.1. Typical cell.

Now, on the boundary $\partial\Omega$, it is evident that $\nu_i^{(2)}(\hat{x}_2^*,\hat{x}_3^*) = -\nu_i^{(2)}(-\hat{x}_2^*,-\hat{x}_3^*)$. Thus, x_γ^* - periodicity implies that

$$\int_{\partial\Omega} f\left(x_k;x_\gamma^*;\epsilon\right)\nu_i^{(2)}\,d(\partial\Omega) = 0 \qquad (3.15)$$

for any field variable f. The property (3.15) will be useful later.

3.5 WEIGHTED RESIDUAL PROCEDURE.

In this subsection, a weighted residual procedure is introduced. This procedure will be subsequently used to eliminate the microcoordinates $x_\gamma^*(\gamma = 2,3)$ from all field variables through an averaging operation, and to establish appropriate field equations for the resulting averaged fields.

To begin, let ϕ denote the space of all H^1-functions $f(x_k;x_\gamma^*)$ on V with respect to $x_k(k = 1\text{-}3)$ and on Ω with respect to x_γ^* $(\gamma = 2,3)$ that are x_γ^* -periodic according to subsection 3.4. Any function $u_i \in \phi$ with $u_i = \hat{u}_i$ on ∂V_u, where $\hat{u}_i$ is the specified displacement, will be called an admissible trial displacement. Any function $\delta u_i \in \phi$ with $\delta u_i = 0$ on δV_u will be called a weighting function or are admissible variation (of u_i). In addition, let $\tilde{\phi}$ denote the space of all L^2-functions $h(x_k;x_\gamma^*)$ on V with respect to $x_k(k = 1\text{-}3)$ and on Ω with respect to x_γ^* $(\gamma = 2,3)$ that are x_γ^*-periodic. Any function $\sigma_{ij} \in \tilde{\phi}$ with $\sigma_{ji}\nu_j = \hat{T}_i$ on δV_T, where $\hat{T}_i$ is the specified traction, will be called an admissible trial stress. Any function $\delta\sigma_{ij} \in \tilde{\phi}$ with $\delta\sigma_{ij} = 0$ on δV_T will be called a weighting function or an admissible variation (of σ_{ij}). In the above, it has been tacitly assumed for convenience that the boundary data on δV is of the non-mixed type, i.e., that u_i is specified on δV_u while $\hat{T}_i$ is specified on δV_T with $\delta V = \delta V_u \cup \partial V_T$ and $\delta V_u \cap \partial V_T = 0$ (generalization to the mixed case does not represent a significant problem).

Next, consider the weighted residual R defined by

$$R \equiv \iiint_V \left\{ \sum_{\alpha=1}^{2} \iint_{A^{(\alpha)}} \delta u_i^{(\alpha)} \left[\sigma_{ji,j} + \frac{1}{\epsilon} \sigma_{ji,j^*} + f_i \right]^{(\alpha)} dA^{(\alpha)} \right\} dV$$

$$+ \iiint_V \left\{ \sum_{\alpha=1}^{2} \iint_{A^{(\alpha)}} \delta \sigma_{ij}^{(\alpha)} \left[e_{ij}(\bullet\bullet\bullet) - e_{ij} \right]^{(\alpha)} dA^{(\alpha)} \right\} dV$$

$$+ \iiint_V \left\{ \oint_{\partial} \frac{1}{\epsilon} \delta T_i^* \left[u_i^{(1)} - u_i^{(2)} \right] ds^* \right\} dV + \iint_{\partial V} \left\{ \sum_{\alpha=1}^{2} \iint_{A^{(\alpha)}} \left[\Psi_i - \sigma_{ij} \nu_j \right]^{(\alpha)} \delta u_i^{(\alpha)} dA^{(\alpha)} \right\} dS \qquad (3.16)$$

$$+ \iiint_V \left\{ \sum_{\alpha=1}^{2} \oint_{\partial} \frac{1}{\epsilon} \left[\Psi_i - \sigma_{ji} \nu_j \right]^{(\alpha)} \delta u_i^{(\alpha)} ds^* \right\} dV + \iiint_V \left\{ \oint_{\partial\Omega} \frac{1}{\epsilon} \left[-\sigma_{ji}^{(2)} \nu_j^{(2)} \right] \delta u_i^{(2)} d(\partial\Omega) \right\} dV$$

where $dV = dx_1 dx_2 dx_3$; $dA^{(\alpha)} = dx_2^* dx_3^*$; ds^* is a differential element of $\partial \equiv \partial A^{(1)}$, dS is a differential element of ∂V; $\partial\Omega$ denotes the outer cell boundary; $T_i^* \equiv \sigma_{ij}^{(1)} \nu_j^{(1)}$ on ∂; for a given trial displacement $u_i^{(\alpha)}$, $e_{ij}^{(\alpha)}$ is computed according to (3.12); and the notation $e_{ij}^{(\alpha)}(\bullet\bullet\bullet)$ denotes the inverse of (3.11) which is to be computed given a trial stress σ_{ij}, i.e.,

$$e_{ij}^{(\alpha)}(\bullet\bullet\bullet) = \frac{1 + \nu^{(\alpha)}}{E^{(\alpha)}} \sigma_{ij}^{(\alpha)} - \frac{\nu^{(\alpha)}}{E^{(\alpha)}} \sigma_{kk}^{(\alpha)} \delta_{ij} \quad . \qquad (3.17a)$$

where

$$E^{(\alpha)} \equiv \frac{\mu^{(\alpha)}(3\lambda + 2\mu)^{(\alpha)}}{(\lambda + 2\mu)^{(\alpha)}}, \qquad \nu^{(\alpha)} \equiv \frac{\lambda^{(\alpha)}}{2(\lambda + \mu)^{(\alpha)}} \quad . \qquad (3.17b)$$

In (3.16), the integrations with respect to the macrocoordinates are carried out over the entire domain V while those with respect to the microcoordinates x_γ^* are performed over a typical cell.

Now, if R =0 is satisfied for: (1) all admissible $\delta u_i^{(\alpha)}$ which are arbitrary over V and $A^{(\alpha)}$, and on ∂V_T and $A^{(\alpha)}$; (2) all admissible $\delta \sigma_{ij}^{(\alpha)}$ which are arbitrary over V

and $A^{(\alpha)}$, and on δV_u and $A^{(\alpha)}$; and (3) all admissible $\delta \overset{\psi^*}{T}_i$ which are arbitrary over V and ∂, then the first five integrals must vanish independently and it is evident that weak solutions of the local field equations have been generated that satisfy the equilibrium equations (3.10) (first integral), the constitutive relations (3.11) (second integral), the interface displacement continuity (3.13) (third integral), the specified traction on ∂V (fourth integral), and the traction continuity on ∂ (fifth integral). The kinematic condition (3.12) is satisfied identically since e_{ij} is computed from u_i via (3.12). The last (sixth) integral vanishes if the stresses are required to be in a $\tilde{\psi}$-solution set; otherwise the vanishing of this integral imposes the x^*_γ-periodicity condition on the transverse stresses σ_{ij} (i,j ≠ 1) (note that $\nu_1^{(2)} \equiv 0^\gamma$ on the cell boundary $\partial\Omega$).

If R = 0 is satisfied for all admissible δu_i in a subspace of ψ, and for all admissible $\delta\sigma_{ij}$ in a subspace of $\tilde{\psi}$, then the field equations (3.10)- (3.13) are satisfied in a weighted residual (approximate) sense.

From (3.16) with R = 0, Gauss' Theorem, and the x^*_γ-periodicity condition, one obtains

$$\iiint_V \left\{ \sum_{\alpha=1}^{2} \iint_{A^{(\alpha)}} \left[\sigma_{ij}^{(\alpha)} \delta e_{ij}^{(\alpha)} + \delta\sigma_{ij}^{(\alpha)} \left(e_{ij}^{(\alpha)} - e_{ij}^{(\alpha)}(\bullet\bullet\bullet) \right] dx_2^* dx_3^* \right.$$

$$\left. + \frac{1}{\epsilon} \oint_{\partial} \left[T_i^* \left(\delta u_i^{(2)} - \delta u_i^{(1)} \right) + \delta T_i^* \left(u_i^{(2)} - u_i^{(1)} \right) \right] ds^* \right\} dx_1 dx_2 dx_3$$

$$= \iiint_V \left\{ \sum_{\alpha=1}^{2} \iint_{A^{(\alpha)}} f_i^{(\alpha)} \delta u_i^{(\alpha)} dx_2^* dx_3^* \right\} dx_1 dx_2 dx_3$$

$$+ \iiint_{\delta V_T} \left\{ \sum_{\alpha=1}^{2} \iint_{A^{(\alpha)}} t_i^{(\alpha)} \delta u_i^{(\alpha)} dx_2^* dx_3^* \right\} dS \quad , \tag{3.18}$$

where

$$\delta e_{ij} \equiv \frac{1}{2}\left\{ \delta u_{i,j} + \delta u_{j,i} + \frac{1}{\epsilon}\left(\delta u_{i,j}^* + \delta u_{j,i}^* \right) \right\} \quad . \tag{3.19}$$

Equation (3.18) is similar to Reissner's mixed variational principle (1984,1986) in which variations of the stresses are considered along with variations of the displacements. The terms of (3.17) involving $\delta\sigma_{ij}^{(\alpha)}$ and δT_i^* are constraint conditions that reflect satisfaction of the material constitutive relations and the interface displacement continuity conditions, respectively. Consequently, (3.18) can be envisaged as the principle of virtual work for the synthesized fields with constraint conditions; here $\delta\sigma_{ij}$ and δT_i^* play the role of Lagrangian multipliers. In what follows, only variations in the transverse stresses $\sigma_{ij}(i,j\neq 1,1)$ will be considered, i.e., $\delta\sigma_{11} \equiv 0$.

3.6 TRIAL FUNCTIONS.

As indicated in the previous subsection, the weighted residual procedure (3.18) will be subsequently employed to eliminate the x_γ^*-dependence (i.e., the dependence on the microcoordinates) from all field variables, and to establish field equations for the x_γ^*-averaged (i.e., cell-averaged) fields. To accomplish this task, however, appropriate trial functions $u_i^{(\alpha)} \in \mathcal{V}$ and $\sigma_{ij}^{(\alpha)} \in \tilde{\mathcal{V}}$ must be postulated or constructed. In particular, it will be necessary to exhibit an explicit x_γ^*-dependence of <u>all</u> displacements $u_i^{(\alpha)}$ and the <u>transverse</u> stress components $\sigma_{ij}^{(\alpha)}$ $(i,j \neq 1,1)$.

The required x_γ^*-dependence of the displacements and the transverse stresses can be obtained by application of an asymptotic procedure developed by Hegemier (1974) and Murakami, Maewal and Hegemier (1981) (see Murakami and Hegemier (1986) for application to a similar problem). This procedure is as follows: The premise that

the ratio of micro-to-macrodimensions is small, $\epsilon << 1$, and the form of the synthesized equations (3.10) - (3.17), suggest an expansion of the dependent variables in the asymptotic series

$$\left\{u_i,\ \sigma_{ij}\right\}^{(\alpha)}\left(x_k;x^*_\gamma;\epsilon\right) = \sum_{n=0}^{\infty} \epsilon^n \left\{u_{i\,(n)},\sigma_{ij\,(n)}\right\}^{(\alpha)}\left(x_k;x^*_\gamma\right) . \tag{3.20}$$

If (3.20) is substituted into (3.10) - (3.13), and the coefficients of different powers of ϵ are equated to zero in the usual manner, a sequence of boundary value problems (called microboundary value problems or MBVP's) are defined on the cell. In general, solution of this sequence is difficult. However, for those cases where a circular cylinder approximation of the cell boundary $\delta\Omega$ is appropriate (i.e., where the cell aspect ratio is approximately unity), consideration of this sequence to $O(\epsilon)$ motivates the following form for the trial fields:

(a) Displacement trial functions

$$u_i^{(\alpha)}\left(x_k;x^*_\gamma;\epsilon\right) = U_i^{(\alpha)}\left(x_k\right) + \epsilon \overset{2}{S}_i\left(x_k\right) g^{(\alpha)}(r)\cos\theta + \epsilon\, \overset{3}{S}_i\left(x_k\right) g^{(\alpha)}(r)\sin\theta + O\left(\epsilon^2\right), \tag{3.21a}$$

where

$$\overset{3}{S}_2 = \overset{2}{S}_3 , \tag{3.21b}$$

$$g^{(1)}(r) = \frac{r}{n^{(1)}} , \quad g^{(2)}(r) = \frac{1}{n^{(2)}}\left[-r + \frac{1}{r}\right] , \tag{3.21c}$$

$$x^*_2 = r\cos\theta, \quad x^*_3 = r\sin\theta \tag{3.21d}$$

and where $n^{(\alpha)}$ denote volume fractions, i.e., $n^{(\alpha)} = A^{(\alpha)}/A$ where $A \equiv A^{(1)} \cup A^{(2)} = \Omega$ is the total cell area.

(b) Transverse stress trial functions

$$\begin{bmatrix}\sigma_{22}\\ \sigma_{33}\\ \sigma_{23}\end{bmatrix}^{(a)}(x_k;x_\gamma^*;\epsilon) = \begin{bmatrix}\tau_{22}\\ \tau_{33}\\ \tau_{23}\end{bmatrix}^{(a)}(x_k) + \frac{\delta_{a2}}{r^2}\left\{ t_{22}^{(2)}(x_k)\begin{bmatrix}\cos2\theta\\ \cos2\theta\\ 0\end{bmatrix}\right.$$

$$\left. + t_{33}^{(2)}(x_k)\begin{bmatrix}\cos2\theta\\ -\cos2\theta\\ \sin2\theta\end{bmatrix} + t_{23}^{(2)}(x_k)\begin{bmatrix}\sin2\theta\\ \sin2\theta\\ 0\end{bmatrix}\right\}$$

$$+ \frac{\epsilon}{4}P_2(x_k)g^{(a)}(r)\begin{bmatrix}3\cos\theta\\ \cos\theta\\ \sin\theta\end{bmatrix} + \frac{\epsilon}{4}P_3(x_k)g^{(a)}(r)\begin{bmatrix}\sin\theta\\ 3\sin\theta\\ \cos\theta\end{bmatrix} + O(\epsilon^2)\ ; \qquad (3.22a)$$

$$\begin{bmatrix}\sigma_{31}\\ \\ \sigma_{12}\end{bmatrix}^{(a)}(x_k;x_\gamma^*;\epsilon) = \begin{bmatrix}\tau_{31}\\ \\ \tau_{12}\end{bmatrix}^{(a)}(x_k) + \frac{\delta_{a2}}{r^2}\left\{ t_{12}^{(2)}(x_k)\begin{bmatrix}\sin2\theta\\ \\ \cos2\theta\end{bmatrix}\right.$$

$$\left. + t_{31}^{(2)}(x_k)\begin{bmatrix}\cos2\theta\\ \\ -\sin2\theta\end{bmatrix}\right\} + \frac{\epsilon P_1}{2}(x_k)g^{(a)}(r)\begin{bmatrix}\sin\theta\\ \\ \cos\theta\end{bmatrix} + O(\epsilon^2). \qquad (3.22b)$$

SECTION 4

DEVELOPMENT OF 3D MIXTURE MODEL FOR R/C

Following substitution of the trial fields (3.21) and (3.22) into the variational principle (3.18), integration over x_γ^*, and appropriate integrations by parts, one obtains the Euler-Lagrange equations of the variational principle in the form:

(a) Mixture Equilibrium

$$n^{(\alpha)}\sigma_{ji,j}^{(\alpha a)} + (-1)^{\alpha+1} P_i + n^{(\alpha)} f_i^{(\alpha)} = 0 \qquad (i = 1\text{-}3) \tag{4.1a}$$

where

$$\sigma_{ij}^{(\alpha a)} \equiv \frac{1}{A} \iint_{A^{(\alpha)}} \sigma_{ij}^{(\alpha)} dx_2^* dx_3^* \ , \tag{4.1b}$$

$$P_i \equiv \frac{1}{\epsilon A} \oint_{\partial} T_i^* ds^* = \frac{1}{\epsilon A} \oint_{\partial} \sigma_{ji}^{(1)} \nu_j^{(1)} \ ds^* \ . \tag{4.1c}$$

In (4.1a), $\sigma_{ij}^{(\alpha a)}$ is a cell-averaged stress tensor and P_i represents an effective interaction body force due to the transfer of the stress vector across the interface ∂. For the circular cylinders approximation, $A = \pi$.

(b) Mixture Equilibrium - stress moments

$$\sigma_{22}^{(1a)} - \sigma_{22}^{(2a)} - \frac{1}{2n^{(1)}}\left[t_{22}^{(2)} + 2t_{33}^{(2)}\right] = 0 \ , \tag{4.2a}$$

$$\sigma_{33}^{(1a)} - \sigma_{33}^{(2a)} + \frac{1}{2n^{(1)}}\left[t_{22}^{(2)} - 2t_{33}^{(2)}\right] = 0 \ , \tag{4.2b}$$

$$\sigma_{23}^{(1a)} - \sigma_{23}^{(2a)} - \frac{1}{2n^{(1)}} t_{23}^{(2)} = 0 \quad , \tag{4.2c}$$

$$\sigma_{31}^{(1a)} - \sigma_{31}^{(2a)} + \frac{1}{n^{(1)}} t_{31}^{(2)} = 0, \tag{4.2d}$$

$$\sigma_{12}^{(1a)} - \sigma_{12}^{(2a)} - \frac{1}{n^{(1)}} t_{12}^{(2)} = 0 \quad , \tag{4.2e}$$

(c) Constitutive Relations - transverse stress averages

$$\left[\frac{\lambda + 2\mu}{\hat{\lambda}^2}\right]^{(\alpha)} \sigma_{22}^{(\alpha a)} - \left[\frac{\lambda}{\hat{\lambda}^2}\right]^{(\alpha)} \sigma_{33}^{(\alpha a)} = U_{2,2}^{(\alpha)} + \left[\frac{2\lambda\mu}{\hat{\lambda}^2}\right]^{(\alpha)} U_{1,1}^{(\alpha)} + \frac{(-1)^{\alpha+1}}{n^{(\alpha)}} \overset{2}{S}_2 \ , \tag{4.3a}$$

$$\left[\frac{\lambda + 2\mu}{\hat{\lambda}^2}\right]^{(\alpha)} \sigma_{33}^{(\alpha a)} - \left[\frac{\lambda}{\hat{\lambda}^2}\right]^{(\alpha)} \sigma_{22}^{(\alpha a)} = U_{3,3}^{(\alpha)} + \left[\frac{2\lambda\mu}{\hat{\lambda}^2}\right]^{(\alpha)} U_{1,1}^{(\alpha)} + \frac{(-1)^{\alpha+1}}{n^{(\alpha)}} \overset{3}{S}_3 , \tag{4.3b}$$

$$\frac{1}{\mu^{(\alpha)}} \sigma_{23}^{(\alpha a)} = U_{2,3}^{(\alpha)} + U_{3,2}^{(\alpha)} + 2 \frac{(-1)^{\alpha+1}}{n^{(\alpha)}} \overset{3}{S}_2 \quad , \tag{4.3c}$$

$$\frac{1}{\mu^{(\alpha)}} \sigma_{31}^{(\alpha a)} = U_{3,1}^{(\alpha)} + U_{1,3}^{(\alpha)} + \frac{(-1)^{\alpha+1}}{n^{(\alpha)}} \overset{3}{S}_1 \ , \tag{4.3d}$$

$$\frac{1}{\mu^{(\alpha)}} \sigma_{12}^{(\alpha a)} = U_{1,2}^{(\alpha)} + U_{2,1}^{(\alpha)} + \frac{(-1)^{\alpha+1}}{n^{(\alpha)}} \overset{2}{S}_1 \ . \tag{4.3e}$$

In the derivation of (4.3), use was made of the equality $\sigma_{ij}^{(\alpha a)} = \tau_{ij}^{(\alpha)}$ for $(i,j) \neq (1,1)$. In addition, the parameter $\hat{\lambda}$ above is defined by

$$\hat{\lambda} \equiv 4\mu(\lambda + \mu) . \tag{4.3f}$$

(d) Constitutive Relations - transverse stress moments

$$t_{22}^{(2)} = - \frac{(\lambda + \mu)^{(2)}}{n^{(2)}} \left[\overset{2}{S}_2 - \overset{3}{S}_3\right] \ , \tag{4.4a}$$

$$t_{33}^{(2)} = - \frac{\mu^{(2)}}{n^{(2)}} \left[{}^{2}S_2 + {}^{3}S_3 \right] \quad , \tag{4.4b}$$

$$t_{23}^{(2)} = - \frac{(\lambda + \mu)^{(2)}}{n^{(2)}} \left[{}^{3}S_2 + {}^{2}S_3 \right] = - \frac{2(\lambda + \mu)^{(2)}}{n^{(2)}} {}^{3}S_2 , \tag{4.4c}$$

$$t_{12}^{(2)} = - \frac{\mu^{(2)}}{n^{(2)}} {}^{2}S_1 \tag{4.4d}$$

$$t_{31}^{(2)} = \frac{\mu^{(2)}}{n^{(2)}} {}^{3}S_1 \quad . \tag{4.4e}$$

(e) Constitutive Relations - Interaction terms

$$P_1 = \beta_{(1)} \frac{\left[U_1^{(2)} - U_1^{(1)} \right]}{\epsilon^2} \quad , \tag{4.5a}$$

$$P_2 = \beta_{(2)} \frac{\left[U_2^{(2)} - U_2^{(1)} \right]}{\epsilon^2} \quad , \tag{4.5b}$$

$$P_3 = \beta_{(3)} \frac{\left[U_3^{(2)} - U_3^{(1)} \right]}{\epsilon^2} \quad , \tag{4.5c}$$

where

$$\beta_{(1)}^{-1} \equiv \frac{1}{2} \sum_{\alpha=1}^{2} \left(h^{(\alpha)} / \mu^{(\alpha)} \right) \quad , \tag{4.5d}$$

$$\beta_{(2)}^{-1} = \beta_{(3)}^{-1} = \sum_{\alpha=1}^{2} \frac{h^{(\alpha)} (\lambda + 3\mu)^{(\alpha)}}{8\mu^{(\alpha)} (\lambda + \mu)^{(\alpha)}} \quad , \tag{4.5e}$$

and where

$$h^{(1)} = \frac{1}{4} \quad , \quad h^{(2)} = \frac{-1}{4n^{(2)}} \left[2 + n^{(2)} + \frac{2}{n^{(2)}} \ell n \; n^{(1)} \right] \quad . \tag{4.5f}$$

(f) Constitutive Relations - Axial stresses

$$\sigma_{11}^{(\alpha a)} = \left\{(\lambda + 2\mu) - \frac{\lambda^2}{(\lambda + \mu)}\right\}^{(\alpha)} U_{1,1}^{(\alpha)} + \left\{\frac{\lambda}{2(\lambda + \mu)}\right\}^{(\alpha)} \left[\sigma_{22}^{(\alpha a)} + \sigma_{33}^{(\alpha a)}\right]. \quad (4.6)$$

(g) Boundary Conditions

The appropriate boundary conditions for (4.1a) are

$$\text{either } \delta U_i^{(\alpha)} = 0 \text{ or } \overset{*}{T}{}_i^{(\alpha p)} = n^{(\alpha)} \sigma_{ji}^{(\alpha a)} \nu_j \quad (4.7a)$$

on δV, where

$$\overset{*}{T}{}_i^{(\alpha p)} \equiv \frac{1}{A} \iint_{A^{(\alpha)}} \overset{*}{T}{}_i dx_2^* dx_3^* = \frac{1}{\pi} \iint_{A^{(\alpha)}} \overset{*}{T}{}_i dx_2^* dx_3^* . \quad (4.7b)$$

The relations (4.1a), (4.2a-e), (4.3a-e), (4.4a-e), (4.5a-c), (4.6), and (4.7a) constitute a complete continuum mixture model for the case of fully three-dimensional fields.

SECTION 5

DEVELOPMENT OF 2D MIXTURE MODEL FOR R/C PANELS

In this section, the 3D mixture model of Section 4 is specialized for the case of plane stress. The resulting equations constitute a model for the in-plane deformation of reinforced concrete panels. The (material) reference coordinate system associated with such a panel is depicted in Figure 5.1.

5.1 PLANE STRESS CONSTRAINTS.

The following constraints are deemed to be appropriate for the planar deformation of a reinforced concrete panel:

$$\sigma_{33}^{(\alpha a)} = \sigma_{32}^{(\alpha a)} = \sigma_{31}^{(\alpha a)} \equiv 0. \tag{5.1a}$$

$$(\,)_{,3} \equiv 0 \quad , \quad U_3^{(\alpha)} \equiv 0 \quad . \tag{5.1b}$$

Equations (5.1a) and (4.2b-d) furnish

$$t_{31}^{(2)} = t_{32}^{(2)} \equiv 0 \quad , \tag{5.2a}$$

$$t_{22}^{(2)} = 2t_{33}^{(2)} \quad . \tag{5.2b}$$

The relations (5.2), when combined with (4.4) yield

$$\overset{3}{S}_1 = \overset{3}{S}_2 \equiv 0 \quad , \tag{5.3a}$$

$$\overset{3}{S}_3 = \left(\frac{\lambda - \mu}{\lambda + 3\mu}\right)^{(2)} \overset{2}{S}_2 \quad , \tag{5.3b}$$

$$\sigma_{22}^{(1a)} - \sigma_{22}^{(2a)} = t_{22}^{(2)}/n^{(1)} \tag{5.3c}$$

5.2 CONSTITUTIVE RELATIONS.

Under the constraint (5.1a), and upon noting that

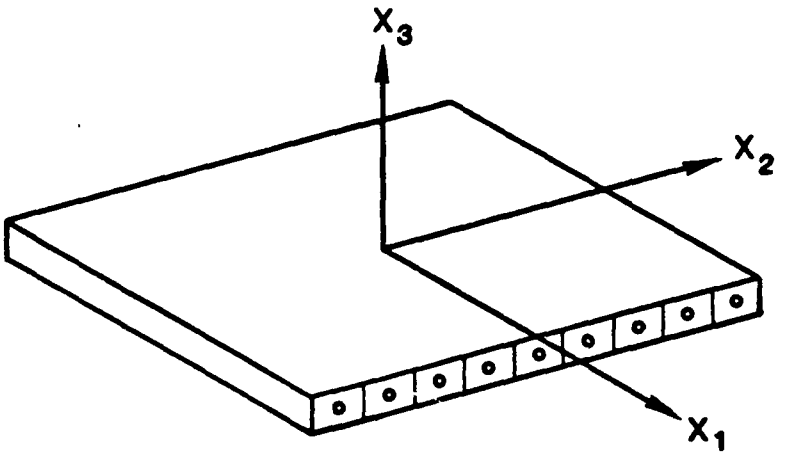

Figure 5.1. Material coordinate system.

$$\frac{4\mu(\lambda + \mu)}{\lambda + 2\mu} = \frac{E}{1 - \nu^2} \, , \quad \frac{2\lambda\mu}{\lambda + 2\mu} = \frac{\nu E}{1 - \nu^2} \, , \quad \mu = \frac{E}{2(1 + \nu)} \tag{5.4}$$

one obtains from (4.3a), (4.3e), and (4.6)

$$\sigma_{22}^{(\alpha a)} = \left[\frac{E}{1 - \nu^2}\right]^{(\alpha)} \left[U_{2,2}^{(\alpha)} + \frac{(-1)^{\alpha+1}}{n^{(\alpha)}} \overset{2}{S}_2 + \nu^{(\alpha)} U_{1,1}^{(\alpha)}\right] \, , \tag{5.5a}$$

$$\sigma_{12}^{(\alpha a)} = \left[\frac{E}{2(1 + \nu)}\right]^{(\alpha)} \left[U_{1,2}^{(\alpha)} + U_{2,1}^{(\alpha)} + \frac{(-1)^{\alpha+1}}{n^{(\alpha)}} \overset{2}{S}_1\right] \, . \tag{5.5b}$$

$$\sigma_{11}^{(\alpha a)} = \left[\frac{E}{1 - \nu^2}\right]^{(\alpha)} \left[U_{1,1}^{(\alpha)} + \nu^{(\alpha)} \left[U_{2,2}^{(\alpha)} + \frac{(-1)^{\alpha+1}}{n^{(\alpha)}} \overset{2}{S}_2\right]\right] \, . \tag{5.5c}$$

The expressions (5.5a-c) can be written entirely in terms of $U_1^{(\alpha)}$ and $U_2^{(\alpha)}$ as follows. First, the quantity $\overset{2}{S}_2$ can be determined in terms of $U_1^{(\alpha)}$ and $U_2^{(\alpha)}$ by substitution of (5.5a,c) into (5.3c) and use of (4.4a) and (5.3b); the result of this operation is

$$\begin{aligned} \overset{2}{S}_2 = & - \left[\frac{\gamma\nu E}{1 - \nu^2}\right]^{(1)} U_{1,1}^{(1)} + \left[\frac{\gamma\nu E}{1 - \nu^2}\right]^{(2)} U_{1,1}^{(2)} - \left[\frac{\gamma E}{1 - \nu^2}\right]^{(1)} U_{2,2}^{(1)} \\ & + \left[\frac{\gamma E}{1 - \nu^2}\right]^{(2)} U_{2,2}^{(2)} \end{aligned} \tag{5.7a}$$

where

$$\gamma^{-1} \equiv \frac{1}{n^{(1)}} \left[\frac{E}{1 - \nu^2}\right]^{(1)} + \frac{1}{n^{(2)}} \left[\frac{E}{1 - \nu^2}\right]^{(2)} + \frac{2E^{(2)}}{n^{(1)} n^{(2)} \left[1 + \nu^{(2)}\right] \left[3 - 4\nu^{(2)}\right]} \, . \tag{5.7b}$$

Next, substitution of (5.5b) and (4.4d) into (4.2e) yields

$$\overset{2}{S}_1 = - \frac{\gamma^{(s)}}{2} \left[\frac{E}{1 + \nu}\right]^{(1)} \left[U_{1,2}^{(1)} + U_{2,1}^{(1)}\right] + \frac{\gamma^{(s)}}{2} \left[\frac{E}{1 + \nu}\right]^{(2)} \left[U_{1,2}^{(2)} + U_{2,1}^{(2)}\right] , \tag{5.8a}$$

where

$$\gamma_{(s)}^{-1} \equiv \frac{E^{(1)}}{2n^{(1)}\left[1 + \nu^{(1)}\right]} + \frac{E^{(2)}\left[1 + n^{(1)}\right]}{2n^{(1)}n^{(2)}\left[1 + \nu^{(2)}\right]} \quad . \tag{5.8b}$$

Finally, upon substitution of (5.7a) and (5.8a) into (5.5a-c), one obtains the desired constitutive relations; these can be expressed in matrix form as

$$\{\sigma\} = [C]\{e\} \tag{5.9a}$$

where

$$\{\sigma\} \equiv \left\{n^{(1)}\sigma_{11}^{(1a)},\ n^{(2)}\sigma_{11}^{(2a)},\ n^{(1)}\sigma_{22}^{(1a)},\ n^{(2)}\sigma_{22}^{(2a)},\ n^{(1)}\sigma_{12}^{(1a)},\ n^{(2)}\sigma_{12}^{(2a)}\right\}^T,$$

$$\{e\} \equiv \left\{U_{1,1}^{(1)},\ U_{1,1}^{(2)},\ U_{2,2}^{(1)}, U_{2,2}^{(2)},\ U_{1,2}^{(1)} + U_{2,1}^{(1)},\ U_{1,2}^{(2)} + U_{2,1}^{(2)}\right\}^T ,$$

$$[C] \equiv [C_{kl}] \ , \ k,l = 1 \text{ to } 6 \text{ with } C_{kl} = C_{lk} \text{ and}$$

$$C_{kl} = 0 \text{ for } k = 5,6 \text{ and } l = 1 \text{ to } 4; \tag{5.9b}$$

and where

$$C_{11} = \left[n^{(1)} - \gamma\nu^{(1)^2}D^{(1)}\right]D^{(1)} \ , \quad C_{12} = \gamma\nu^{(1)}\nu^{(2)}D^{(1)}D^{(2)} = \nu^{(1)}\nu^{(2)}C_{43},$$

$$C_{22} = \left[n^{(2)} - \gamma\nu^{(2)^2}D^{(2)}\right]D^{(2)} \ , \ C_{13} = \left[n^{(1)} - \gamma\, D^{(1)}\right]\nu^{(1)}D^{(1)},$$

$$C_{14} = \gamma D^{(1)}D^{(2)}\nu^{(1)} = \nu^{(1)}C_{34} \ , \ C_{23} = \gamma D^{(1)}D^{(2)}\nu^{(2)} = \nu^{(2)}C_{34} \ ,$$

$$C_{24} = \left[n^{(2)} - \gamma D^{(2)}\right]D^{(2)}\nu^{(2)} \ , \ C_{34} = \gamma D^{(1)}D^{(2)} \ ,$$

$$C_{55} = n^{(1)}\mu^{(1)}\left[1 - \gamma_{(s)}\frac{\mu^{(1)}}{n^{(1)}}\right], \ C_{66} = n^{(2)}\mu^{(2)}\left[1 - \frac{\gamma_{(s)}}{n^{(2)}}\mu^{(2)}\right] \ ,$$

$$C_{56} = \gamma_{(s)}\mu^{(1)}\mu^{(2)} \ , \ C_{66} = n^{(2)}\mu^{(2)}\left[1 - \gamma_{(s)}\frac{\mu^{(2)}}{n^{(2)}}\right] \ . \tag{5.9c}$$

In the above,

$$D^{(\alpha)} \equiv \frac{E^{(\alpha)}}{1 - \nu^{(\alpha)2}} \ , \ \mu^{(\alpha)} = \frac{E^{(\alpha)}}{2\left(1 + \nu^{(\alpha)}\right)} \ . \tag{5.9d}$$

In addition to the material constitutive equations (5.9a), the interaction "constitutive relations" are, from (4.5a,b):

$$P_1 = \beta_{(1)} \frac{\left[U_1^{(2)} - U_1^{(1)}\right]}{\epsilon^2} \ , \ P_2 = \beta_{(2)} \frac{\left[U_2^{(2)} - U_2^{(1)}\right]}{\epsilon^2} \tag{5.10a}$$

where $\beta_{(1)}, \beta_{(2)}$ can be expressed in terms of E, ν by

$$\beta_{(1)}^{-1} = \sum_{\alpha=1}^{2} \frac{h^{(\alpha)}(1 + \nu)^{(\alpha)}}{E^{(\alpha)}} \ , \ \beta_{(2)}^{-1} = \sum_{\alpha=1}^{2} \frac{h^{(\alpha)}(1 + \nu)^{(\alpha)}(3 - 4\nu)^{(\alpha)}}{4E^{(\alpha)}} \ . \tag{5.10b}$$

5.3 EQUILIBRIUM EQUATIONS.

The appropriate equilibrium equations for the 2D model can be obtained directly from (4.1a) together with the plane stress condition (5.1a); this yields

$$n^{(\alpha)} \sigma^{(\alpha a)}_{\beta\gamma,\beta} + (-1)^{\alpha+1} P_\gamma + n^{(\alpha)} f^{(\alpha)}_\gamma = 0 \tag{5.11}$$

where $\beta, \gamma = 1,2$.

5.4 BOUNDARY CONDITIONS.

The theory is completed by specification of the boundary conditions on ∂V; these are, from (4.7) given by

$$\text{either } \delta U^{(\alpha)}_\beta = 0 \text{ or } n^{(\alpha)} \sigma^{(\alpha a)}_{\beta\gamma} \nu_\gamma = \Psi^{(\alpha p)}_\beta \tag{5.12}$$

where, again, $\beta, \gamma = 1,2$.

5.5 PRINCIPLE OF VIRTUAL WORK.

For purposes of numerical computations, it is instructive to note the form of the principle of virtual work for the plane stress problem under discussion. This form is

$$\iiint_V [\{\sigma\}^T \delta\{e\} + \{F\}^T \delta\{U\}]\, dV = \iint_{\partial V_T} \{T\}^T \delta\{U\}\, dS \tag{5.13}$$

where

$$\{U\} \equiv \left\{U_1^{(1)}, U_1^{(2)}, U_2^{(1)}, U_2^{(2)}\right\}^T ,$$

$$\{F\} \equiv \left\{-P_1 + n^{(1)} f_1^{(1)},\ P_1 + n^{(2)} f_1^{(2)},\ -P_2 + n^{(1)} f_2^{(1)},\ P_2 + n^{(2)} f_2^{(2)}\right\}^T ,$$

$$\{T\} \equiv \left\{\psi_1^{(1p)},\ \psi_1^{(2p)},\ \psi_2^{(1p)},\ \psi_2^{(2p)}\right\}^T$$

and where $\{e\}$, $\{\sigma\}$ are given by (5.9b).

5.6 SUMMARY OF BASIC EQUATIONS IN MATERIAL COORDINATES.

The basic equations that govern the linear planar response of a R/C panel with a unidirectional steel layout are summarized below. Use of these equations require that the reference coordinates be material coordinates, i.e., that the x_1-axis be aligned with the steel as depicted in Figure 5.1.

(a) Equilibrium Equations

$$\sigma_{\gamma\delta,\gamma}^{(\alpha p)} + (-1)^{\alpha+1} p_\delta + f_\delta^{(\alpha p)} = 0 \tag{5.14}$$

where $\alpha = 1,2$; $\delta,\gamma = 1,2$.

(b) Material Constitutive Relations

$$\sigma_{11}^{(\alpha p)} = n^{(\alpha)} D^{(\alpha)} \left[U_{1,1}^{(\alpha)} + \nu^{(\alpha)} \left(U_{2,2}^{(\alpha)} + (-1)^{\alpha+1} \frac{S_2^2}{n^{(\alpha)}} \right) \right] ,$$

$$\sigma_{12}^{(\alpha p)} = n^{(\alpha)}\mu^{(\alpha)}\left[U_{1,2}^{(\alpha)} + U_{2,1}^{(\alpha)} + (-1)^{\alpha+1}\frac{S_1^2}{n^{(\alpha)}}\right]$$

$$\sigma_{22}^{(\alpha p)} = n^{(\alpha)}D^{(\alpha)}\left[U_{2,2}^{(\alpha)} + (-1)^{\alpha+1}\frac{S_2^2}{n^{(\alpha)}} + \nu^{(\alpha)}U_{1,1}^{(\alpha)}\right] \quad . \tag{5.15}$$

(c) Interactive constitutive Relations for P_δ

$$P_\delta = \beta_{(\delta)}\left[U_\delta^{(2)} - U_\delta^{(1)}\right] \tag{5.16}$$

where $\delta = 1,2$; no sum on δ.

(d) Interaction Constitutive Relations for S_γ^δ

$$S_2^2 = \gamma D^{(2)}\left[U_{2,2} + \nu U_{1,1}\right]^{(2)} - \gamma D^{(1)}\left[U_{2,2} + \nu U_{1,1}\right]^{(1)} ,$$

$$S_1^2 = \gamma^*\mu^{(2)}\left[U_{1,2} + U_{2,1}\right]^{(2)} - \gamma^*\mu^{(1)}\left[U_{1,2} + U_{2,1}\right]^{(1)} \quad . \tag{5.17}$$

(e) Parameters

$$D^{(\alpha)} = E^{(\alpha)}/\left[1 - \nu^2\right]^{(\alpha)} \quad , \quad \mu^{(\alpha)} = E^{(\alpha)}/2(1 + \nu)^{(\alpha)} \quad ,$$

$$\beta_{(1)}^{-1} = \frac{1}{2}\sum_{\alpha=1}^{2}\left[h^{(\alpha)}/\mu^{(\alpha)}\right] \quad , \quad \beta_{(2)}^{-1} = \sum_{\alpha=1}^{2} h^{(\alpha)}(3 - 4\nu)^{(\alpha)}/8\mu^{(\alpha)} \quad ,$$

$$h^{(1)} = \frac{1}{4} \quad , \quad h^{(2)} = -\frac{1}{4n^{(2)}}\left[2 + n^{(2)} + \frac{2}{n^{(2)}}\ell n\, n^{(1)}\right] ,$$

$$\gamma^{-1} = \frac{D^{(1)}}{n^{(1)}} + \frac{D^{(2)}}{n^{(2)}} + \frac{4\mu^{(2)}}{n^{(2)}}\left[\frac{1}{n^{(1)}\left[3 - 4\nu^{(2)}\right]}\right] ,$$

$$\gamma^{*-1} = \frac{\mu^{(1)}}{n^{(1)}} + \frac{\mu^{(2)}}{n^{(2)}}\left[\frac{1 + n^{(1)}}{n^{(1)}}\right] \quad . \tag{5.18}$$

(f) *Partial Stresses, body forces*

$$\sigma_{\delta\gamma}^{(\alpha p)} \equiv n^{(\alpha)}\sigma_{\delta\gamma}^{(\alpha a)} \quad , \quad f_{\delta}^{(\alpha p)} \equiv n^{(\alpha)} f_{\delta}^{(\alpha)} \tag{5.19}$$

where $\alpha = 1,2$; $\delta,\gamma = 1,2$.

(g) Alternate Form of Material Constitutive Relations

$$\{\sigma\} = [C]\{e\} \tag{5.20}$$

where $\{\sigma\}$, $\{e\}$, and $[C]$ are defined by (5.9).

5.7 BASIC EQUATIONS IN GENERAL COORDINATES.

For some applications, it may prove convenient to utilize reference coordinates which are rotated with respect to the material coordinates as shown in Figure 5.2. The basic equations can be rewritten when referenced to such coordinates as follows:

Let x_1, x_2 *denote the material coordinates and* let $\hat{x}_1, \hat{x}_2$ be defined according to

$$\begin{aligned} x_1 &= \hat{x}_1 \cos\phi - \hat{x}_2 \sin\phi \quad , \\ x_2 &= \hat{x}_1 \sin\phi + x_2^* \cos\phi \quad , \\ x_3 &= \hat{x}_3 \quad . \end{aligned} \tag{5.21}$$

Then, it is easily demonstrated that the stress, strain components in the new coordinate system are given by

$$\begin{aligned} s_{11} &= \cos^2\phi\, \hat{s}_{11} + \sin^2\phi\, \hat{s}_{22} - 2\sin\phi\cos\phi\, \hat{s}_{12} \, , \\ s_{22} &= \sin^2\phi\, \hat{s}_{11} + \cos^2\phi \hat{s}_{22} + 2\sin\phi\cos\phi\, \hat{s}_{12} \\ s_{12} &= \left(\cos^2\phi - \sin^2\phi\right)\hat{s}_{12} + \sin\phi\cos\phi\left(\hat{s}_{11} - \hat{s}_{22}\right) \, , \end{aligned} \tag{5.22a}$$

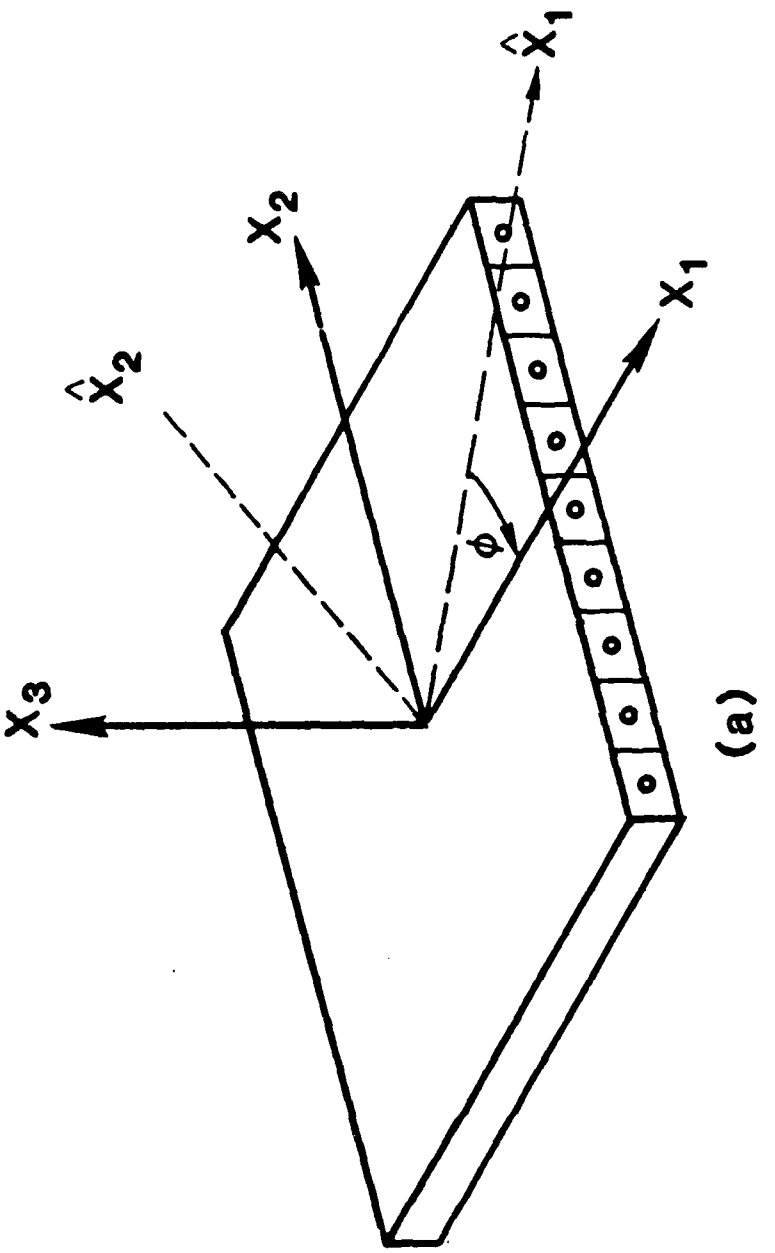

Figure 5.2. General coordinate system.

where $s_{\gamma\delta}$ represents $(\sigma_{\phi\delta})^{(\alpha a)}$ or $(e_{\gamma\delta})^{(\alpha)}$; the latter are given by

$$2e^{(\alpha)}_{\gamma\delta} \equiv U^{(\alpha)}_{\gamma,\delta} + U^{(\alpha)}_{\delta,\gamma} \quad (\delta,\gamma = 1,2). \tag{5.22b}$$

In addition, it can be shown that

$$\begin{aligned} t_1 &= \hat{t}_1 \cos\phi - \hat{t}_2 \sin\phi \quad , \\ t_2 &= \hat{t}_1 \sin\phi + \hat{t}_2 \cos\phi \quad , \end{aligned} \tag{5.22c}$$

where t_γ represents S^2_γ, $U^{(\alpha)}_\gamma$, $f^{(\alpha)}_\gamma$, or P_γ.

Substitution of (5.22a) - (5.22c) into the basic relations of subsection 5.6, and with use of (5.21) to evaluate derivatives with respect to x_1,x_2 in terms of derivatives with respect to $\hat{x}_1,\hat{x}_2$, one obtains

(a) Equilibrium Equations

$$\hat{\sigma}^{(\alpha p)}_{\gamma\delta,\gamma} + (-1)^{\alpha+1} \hat{P}_\delta + \hat{f}^{(\alpha p)}_\delta = 0 \tag{5.23}$$

where $\alpha = 1,2$ and $\delta,\gamma = 1,2$.

(b) Material Constitutive Relations

$$\{\hat{\sigma}\} = [\hat{C}]\{\hat{e}\} \tag{5.24a}$$

where

$$[\hat{C}] = [T][C][T]^T \quad ; \tag{5.24b}$$

$$[T] = \begin{bmatrix} \cos^2\phi & 0 & \sin^2\phi & 0 & 2\sin\phi\cos\phi & 0 \\ 0 & \cos^2\phi & 0 & \sin^2\phi & 0 & 2\sin\phi\cos\phi \\ \sin^2\phi & 0 & \cos^2\phi & 0 & -2\sin\phi\cos\phi & 0 \\ 0 & \sin^2\phi & 0 & \cos^2\phi & 0 & -2\sin\phi\cos\phi \\ -\sin\phi\cos\phi & 0 & \sin\phi\cos\phi & o & \cos^2\phi-\sin^2\phi & 0 \\ 0 & -\sin\phi\cos\phi & 0 & \sin\phi\cos\phi & 0 & \cos^2\phi-\sin^2\phi \end{bmatrix} \tag{5.24c}$$

The 6x6 matrix [C] is defined by (5.9b,c).

(c) Interaction Terms

$$\hat{P}_1 = \hat{\beta}_{11}\left[\hat{U}_1^{(2)} - \hat{U}_1^{(1)}\right] + \hat{\beta}_{12}\left[\hat{U}_2^{(2)} - \hat{U}_2^{(1)}\right] \ ,$$

$$\hat{P}_2 = \hat{\beta}_{22}\left[\hat{U}_2^{(2)} - \hat{U}_2^{(1)}\right] + \hat{\beta}_{21}\left[\hat{U}_1^{(2)} - \hat{U}_1^{(1)}\right] \ , \tag{5.25a}$$

where

$$\hat{\beta}_{11} \equiv \beta_{(1)}\cos^2\phi + \beta_{(2)}\sin^2\phi \ ,$$

$$\hat{\beta}_{22} = \beta_{(2)}\cos^2\phi + \beta_{(1)}\sin^2\phi \ ,$$

$$\hat{\beta}_{12} = -\hat{\beta}_{21} = \left(\beta_{(1)} - \beta_{(2)}\right)\sin\phi\cos\phi. \tag{5.25b}$$

SECTION 6

MODIFICATION FOR INTERFACE SLIP

The 2D and 3D models of the previous sections are subject to the restriction of a perfect steel-concrete interface bond. This restriction is removed in this section.

Virtually all rebar in use today in the United States is deformed. Consequently, the geometry of the actual steel-concrete interface is complex. For modeling purposes, it is conventional to replace this surface by an artificial mean surface. In the present analysis, this is the surface $\bar{\partial}$ in dimensional form and ∂ in nondimensional form.

Given the mean surface ∂, the actual steel-concrete interaction is approximated by specifying an interface constitutive law between the traction T_i^* on ∂ and the relative slip $[u_i] \equiv u_i^{(2)} - u_i^{(1)}$ across ∂. This law must reflect local damage to the concrete in the form of crushing and microcracking.

For most practical problems, it is sufficient to incorporate axial slip only. The constitutive law associated with such slip can be expressed generally in the form

$$T_1^* = F([u_1]) \tag{6.1}$$

where F is a functional of the entire slip history. A subset of (6.1) which has been previously used by a number of researchers consists of a slip initiation criterion and a slip rule; these are similar to the yield criterion and flow rule of incremental plasticity theory. Application of incremental plasticity theory to slip phenomena has been suggested by Drucker and Prager (1952), and employed by Seguchi *et al.* (1974), Bazant and Gambarova (1980), and Bazant and Tsubaki (1980).

With little loss of generality, one may assume that the slip is axisymmetric; see Murakami and Hegemier (1986). For axisymmetric axial slip, and an incremental slip law, the phenomena of "slip" may be incorporated into the previously derived 2D and 3D models by replacing the constitutive relation for P_1 in all equations with a relation of the form

$$\dot{P}_1 = K_{(1)}\left[\dot{U}_2^{(2)} - \dot{U}_1^{(1)}\right] \tag{6.2}$$

where $(\dot{}) \equiv \partial()/\partial t$, t denotes (nondimensional) "bookkeeping" time, and $K_{(1)}$ is a tangent modulus which may depend on the field variables.

As an example, the following slip law has been frequently employed for cases in which reversed slip does not occur:

$$\begin{aligned} &\dot{P}_1 = \beta_{(1)}\left[\dot{U}_1^{(2)} - \dot{U}_1^{(1)}\right] \quad \text{if} \quad |P_1| < P_{(cr)} \ , \\ &P_1 = P_{(cr)}\,\mathrm{sgn}\left[\dot{U}_1^{(2)} - \dot{U}_1^{(1)}\right] \quad \text{if} \quad |P_1| = P_{(cr)} \end{aligned} \tag{6.3a}$$

In the above,

$$P_{(cr)} = 2\sqrt{n^{(1)}}\,\sigma_{(cr)}/\epsilon \tag{6.3b}$$

where $\sigma_{(cr)} > 0$ is the (idealized) local critical bond stress. The law (6.3a) corresponds to a local rigid-plastic bond law of the form

$$\begin{aligned} &[\dot{u}_1] = 0 \quad \text{if} \quad |T^*_1| < \sigma_{(cr)} \ , \\ &[\dot{u}_1] \neq 0, \quad T^*_1 = \sigma_{(cr)}\,\mathrm{sgn}[u_1] \quad \text{if} \quad |T^*_1| = \sigma_{(cr)} \end{aligned} \tag{6.3c}$$

where, again, $[u_1] = u_1^{(2)} - u_1^{(1)}$ represents the local interface slip across ∂ in the axial direction.

It should be recalled at this point that the quantitites $[u_i]$ and $[U_i]$ measure different phenomena. The former on ∂ means local slip across ∂. The latter (see (3.21a)) is a measure of the difference between the average steel and concrete displacements over the cell. Consequently, $[U_i]$ includes both elastic deformation and slip; the quantity $\beta_{(1)}$ is a measure of this elastic deformation.

SECTION 7

MODIFICATION FOR REBAR YIELD

When rebar yield occurs, the constitutive relations (5.9a) must be revised. If incremental plasticity is utilized to describe the rebar response, then (5.9a) must be replaced by an incremental relation of the form

$$\{\dot{\sigma}\} = [D]\{\dot{e}\} \quad . \tag{7.1}$$

The matrix [D] represents a tangent modulus matrix whose coefficients may depend on the plastic component of {e}.

SECTION 8

BASIC EQUATIONS FOR UNIAXIAL DEFORMATION

A problem of considerable importance concerns the simulated behavior of a R/C panel when the latter is subjected to uniaxial deformation. The relevance of this problem stems from the ability to conduct laboratory experiments on R/C panels under uniaxial deformation and hence to validate the developed model by comparison of simulated and measured response.

The uniaxial problem is depicted in Fig 8.1. The panel deformation is constrained to the $\hat{x}_1$-direction. The rebar layout makes an angle ϕ with this direction. The governing equations for the R/C panel are obtained from (5.23), (5.24a) with $\hat{C}$, C replaced by $\hat{D}$,D; and (5.25a) with $\beta_{(1)}$ replaced by $K_{(1)}$. The appropriate constraints are

$$\hat{U}_2^{(\alpha)} \equiv 0 \quad , \alpha = 1,2 \quad . \tag{8.1}$$

Under (8.1), the relevant governing equations reduce to

(a) Equilibrium

$$\begin{aligned} &\hat{\sigma}_{11,1}^{(1p)} + \hat{P}_1 = 0 \ , \\ &\hat{\sigma}_{11,1}^{(2p)} - \hat{P}_1 = 0 \ ; \end{aligned} \tag{8.2}$$

where $(\hat{\ })_{,1} \equiv d(\hat{\ })/d\hat{x}_1$;

(b) Interaction

$$\overset{*}{\hat{P}}_1 = \hat{\beta}_{11}\left[\overset{*}{\hat{U}}_1^{(2)} - \overset{*}{\hat{U}}_1^{(1)}\right] \ , \tag{8.3}$$

$$\hat{\beta}_{11} = K_{(1)} \cos^2\phi + \beta_{(2)} \sin^2\phi \ ;$$

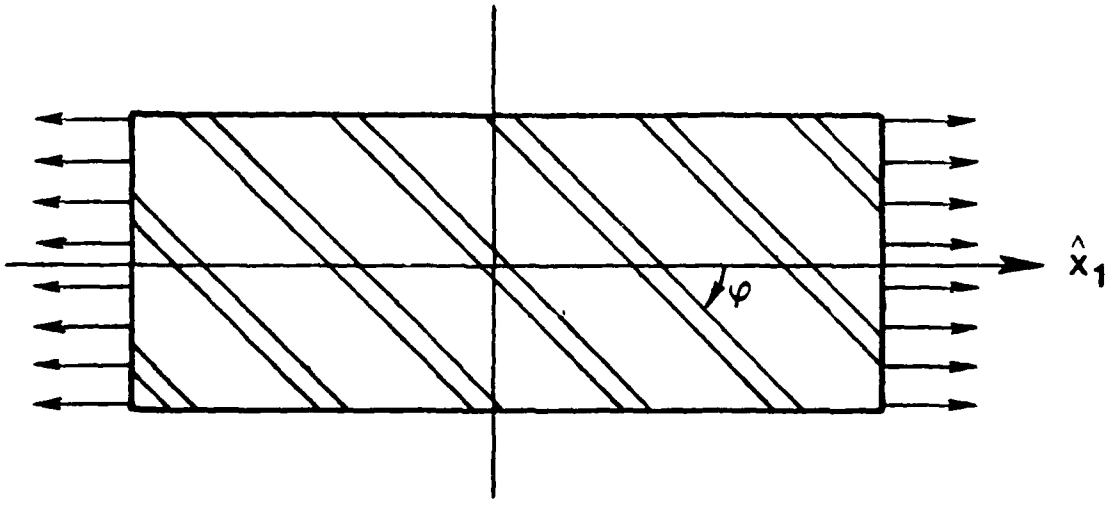

Figure 8.1. Uniaxial problem.

(c) Constitutive

$$\overset{\bullet}{\sigma}{}^{(1p)}_{11} = \hat{D}_{11}\overset{\bullet}{U}{}^{(1)}_{1,1} + \hat{D}_{12}\overset{\bullet}{U}{}^{(2)}_{1,1}$$

(8.4)

$$\overset{\bullet}{\sigma}{}^{(2p)}_{11} = \hat{D}_{12}\overset{\bullet}{U}{}^{(1)}_{1,1} + \hat{D}_{22}\overset{\bullet}{U}{}^{(2)}_{1,1} \quad .$$

The equations (8.2) - (8.4) are employed in detailed studies of simulation response characteristics in the following two sections.

SECTION 9

STIFFNESS DEGRADATION, DUCTILITY, FAILURE: UNIAXIAL DEFORMATION IN DIRECTION OF STEEL ($\phi = 0$)

In this section, the nonlinear response of a R/C panel is examined in detail for the case of monotonic uniaxial deformation and for $\phi = 0$. The latter condition implies that the steel is aligned with the direction of deformation; see Fig 8.1. Using an elastic-brittle fracture model for the concrete, an elastic plastic model for the steel, and an elastic-perfectly plastic description of the steel-concrete interface, response characteristics are examined that relate to global stiffness degradation of the R/C panel under extension, ductility of the R/C panel, and failure conditions. The associated analysis incorporates progressive concrete cracking, steel-concrete slip, and yielding of the rebar. Of particular interest is the influence of bond strength and concrete cracking on the overall panel response.

9.1 FORMULATION OF THE PROBLEM.

The formulation begins by considering an initially unloaded R/C panel with two starting cracks located at the panel termini as depicted in Fig. 9.1. The initial crack spacing is 2ℓ. The panel loading condition corresponds to the following boundary conditions:

$$\bar{U}_1^{(1)} = \bar{u}_o \quad , \quad \bar{\sigma}_{11}^{(2a)} = 0 \quad \text{at } \bar{x}_1 = \ell$$

$$\bar{U}_1^{(1)} = -\bar{u}_o \quad , \quad \bar{\sigma}_{11}^{(2a)} = 0 \quad \text{at } \bar{x}_1 = -\ell \tag{9.1}$$

where $u_o > 0$. The notation $(\bar{\ })$ above and in what follows indicates that the quantities are dimensional.

Due to the problem symmetry, one need only consider half the panel as indicated in Fig. 9.2. Upon shifting the $\bar{x}_1$-axis as shown, the appropriate boundary conditions are

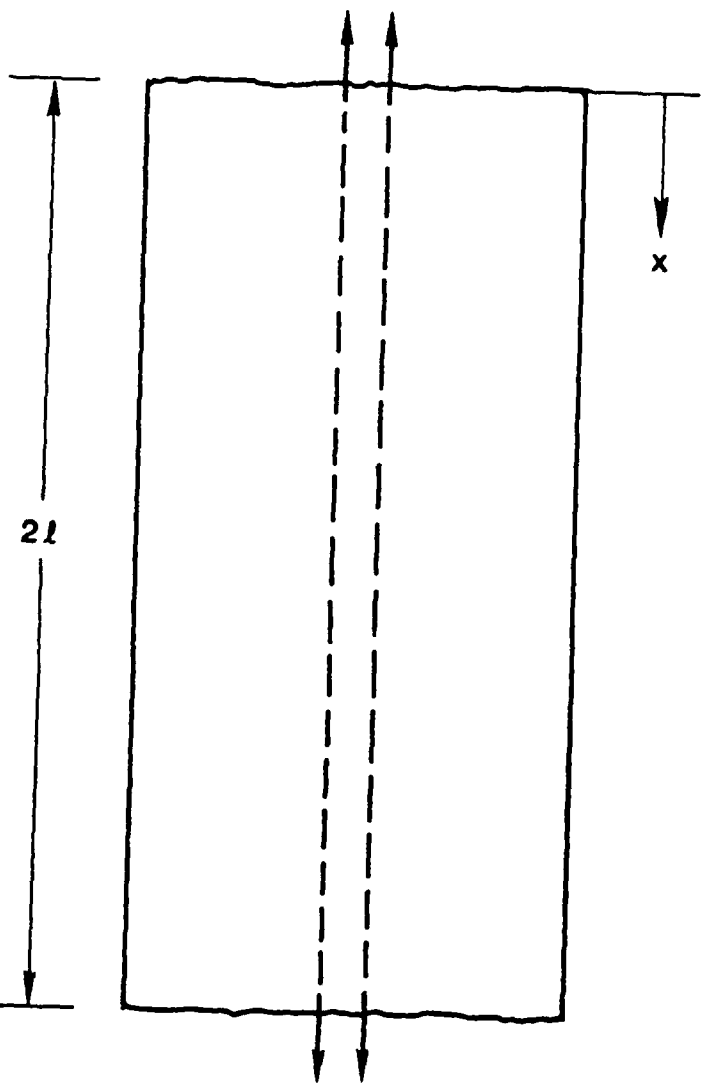

Figure 9.1. Initially unloaded R/C panel.

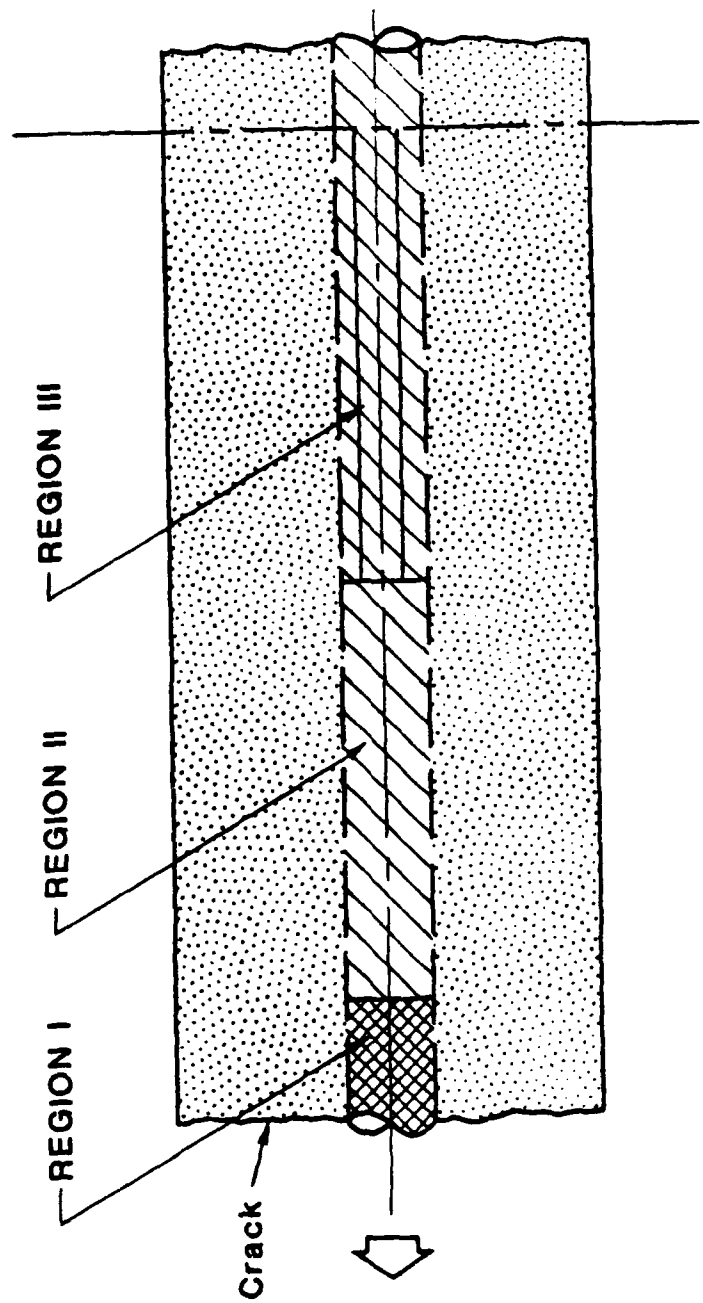

Figure 9.2. Partitioned subdomains on the interval $0 \geq \bar{x}_1 \geq \ell$

$$\bar{U}_1^{(1)} = -\bar{u}_o,\ \bar{\sigma}_{11}^{(2a)} = 0 \quad \text{at } \bar{x}_1 = 0 \quad ,$$

$$\bar{U}_1^{(1)} = \bar{U}_1^{(2)} = 0 \quad \text{at } \bar{x}_1 = \ell \ . \tag{9.2}$$

Given the boundary conditions (9.2), the governing equations (8.2) - (8.4) must be solved. Since the tangent moduli $\hat{\beta}_{11}$ and $\hat{D}_{kl}$ (k,ℓ = 1,2) depend on the field variables $\bar{U}_1^{(\alpha)}$ when bond slip and rebar yielding occur, the solution for a particular loading history $\bar{u}_o(t)$ must be, in general, obtained numerically. However, when $\bar{u}_o(t)$ is monotonically increasing, an analytical solution can be constructed. For this purpose, the domain $\bar{x}_1 \epsilon (0,\ell)$ must be partitioned into appropriate subdomains. The vast majority of the desired information concerning response characteristics can be obtained by consideration of three such domains as follows (see Fig.9.2):

Region I: Plastic debonded. In this interval the steel is plastic and the steel-concrete interface is debonded.

Region II: Elastic debonded. In this interval the steel is elastic but the steel-concrete interface is debonded.

Region III: Elastic bonded. - The steel is elastic and the interface is bonded in this interval.

Let us now assume that (1) the steel is elastoplastic with linear workhardening, Fig. 9.3; (2) the concrete is elastic-brittle fracture; and (3) the interface bond is rigid-perfectly plastic, Fig. 9.4. Further, in an attempt to simplify the analysis with little loss of pertinent information for $\phi = 0$, it will be assumed that $\hat{D}_{12} \simeq 0$ in (8.4). Under these conditions, the basic equations for each region are:

Region I $(0 < \bar{x}_1 < \bar{x}_p)$

$$\bar{\sigma}_{11,1}^{(1p)} + \bar{P}_{(cr)} = 0 \ , \quad \bar{\sigma}_{11,1}^{(2p)} - \bar{P}_{(cr)} = 0 \ .$$

$$\dot{\bar{\sigma}}_{11}^{(1p)} = n^{(1)}\bar{E}_{(p)}\dot{\bar{U}}_{1,1}^{(1)}, \qquad \dot{\bar{\sigma}}_{11}^{(2p)} = n^{(2)}\bar{E}^{(2)}\dot{\bar{U}}_{1,1}^{(2)} \tag{9.3}$$

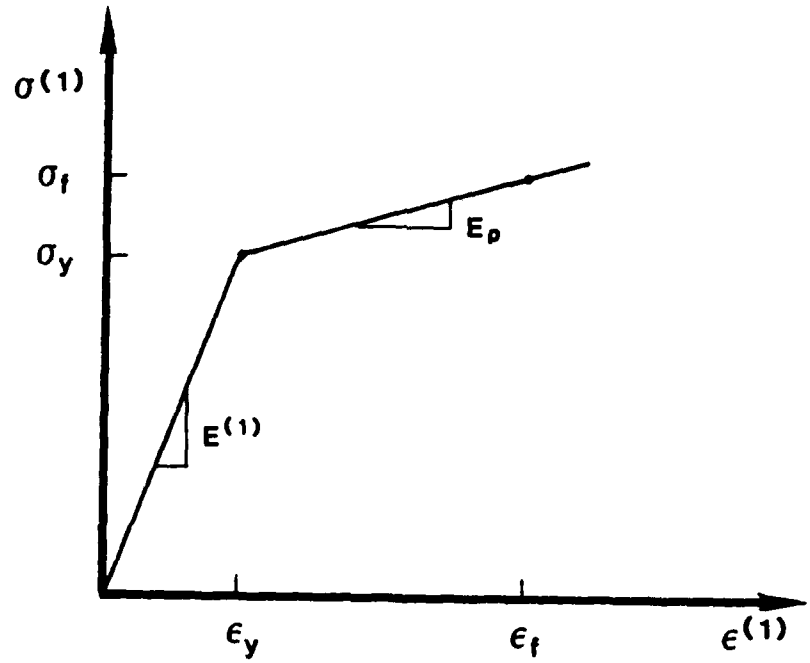

Figure 9.3. Rebar constitutive relation.

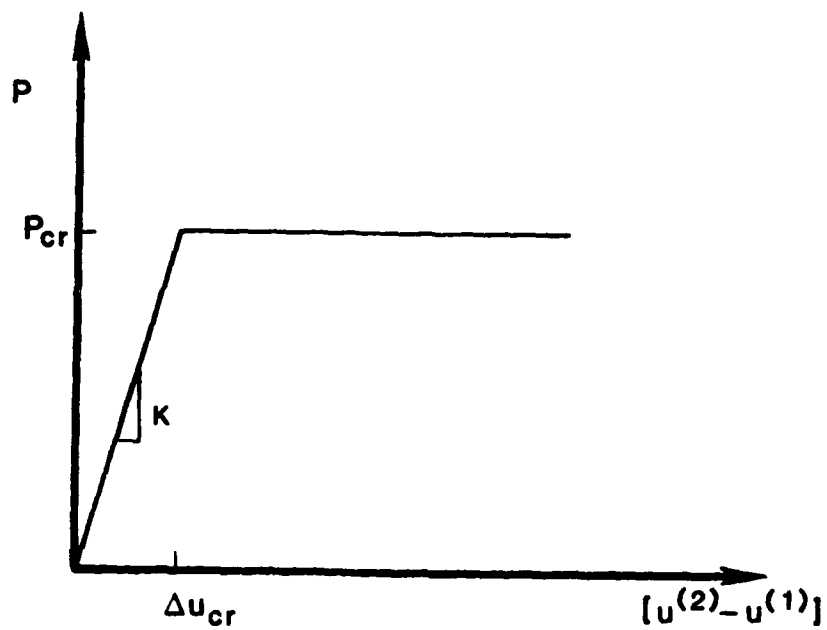

Figure 9.4. Bond-slip relation.

where $\bar{P}_{(cr)}$, $\bar{E}_{(p)}$, and $\bar{E}^{(2)}$ are constants;

Region II $(\bar{x}_p < \bar{x}_1 < \bar{x}_s)$

$$\bar{\sigma}^{(1p)}_{11,1} + \bar{P}_{(cr)} = 0 \ , \ \hat{\sigma}^{(2p)}_{11,1} - \bar{P}_{(cr)} = 0$$

$$\bar{\sigma}^{(1p)}_{11} = n^{(1)}\bar{E}^{(1)}\bar{U}^{(1)}_{1,1} \ , \ \bar{\sigma}^{(2p)}_{11} = n^{(2)}\bar{E}^{(2)}\bar{U}^{(2)}_{1,1} \qquad (9.4)$$

where $\bar{E}(1)$ is a constant.

Region III $(\bar{x}_s < \bar{x}_1 < 0)$

$$\bar{\sigma}^{(1p)}_{11,1} + \beta_{(1)}\left[\bar{U}^{(2)}_1 - \bar{U}^{(1)}_1\right] = 0 \ ,$$

$$\bar{\sigma}^{(2p)}_{11,1} - \beta_{(1)}\left[\bar{U}^{(2)}_1 - \bar{U}^{(1)}_1\right] = 0 \ , \qquad (9.5)$$

$$\bar{\sigma}^{(1p)}_{11} = n^{(1)}\bar{E}^{(1)}\bar{U}^{(1)}_{1,1} \ ,$$

$$\bar{\sigma}^{(2p)}_{11} = n^{(2)}\bar{E}^{(2)}\bar{U}^{(2)}_{1,1} \ .$$

9.2 SOLUTION FOR FIELD VARIABLES.

The solution of the governing differential equations (9.3) - (9.5) is easily obtained for each region. These solutions can then be pieced together at the region endpoints by imposing continuity of both displacements $\bar{U}^{(a)}_1$ and axial stresses $\bar{\sigma}^{(ap)}_{11}$. Finally, the solution is completed by satisfaction of the boundary conditions (9.2). The result is as follows:

Region I

$$\bar{\sigma}^{(1a)}_{11} = \bar{\sigma}_{(o)} - \frac{\bar{\sigma}_{(rx)}}{n^{(1)}}\tilde{x} \ ,$$

$$e_{11}^{(1)} = e_{(o)} - \frac{\bar{\sigma}_{(rx)}}{n^{(1)}\bar{E}_{(p)}} \tilde{x} \quad ,$$

$$\bar{\sigma}_{11}^{(2a)} = \frac{\bar{\sigma}_{(rx)}}{n^{(2)}} \tilde{x} \quad , \tag{9.6}$$

$$e_{11}^{(2)} = \frac{\bar{\sigma}_{(rx)}}{n^{(2)}\bar{E}^{(2)}} \tilde{x} \quad ,$$

$$\tilde{x}_{(p)} \equiv \bar{x}_{(p)}/\ell = \frac{n^{(1)}}{\bar{\sigma}_{(rx)}} \left[\sigma_{(o)} - \sigma_{(y)}\right]$$

Region II

$$\bar{\sigma}_{11}^{(1a)} = \bar{\sigma}_{(o)} - \frac{\bar{\sigma}_{(rx)}}{n^{(1)}} \tilde{x} \quad ,$$

$$e_{11}^{(1)} = \frac{\bar{\sigma}_{(o)}}{\bar{E}^{(1)}} - \frac{\bar{\sigma}_{(rx)}}{n^{(1)}\bar{E}^{(1)}} \tilde{x} \quad , \tag{9.7}$$

$$\bar{\sigma}_{11}^{(2a)} = \frac{\bar{\sigma}_{(rx)}}{n^{(2)}} \tilde{x} \quad ,$$

$$e_{11}^{(2)} = \frac{\bar{\sigma}_{(rx)}}{n^{(2)}\bar{E}^{(2)}} \tilde{x} \quad .$$

Region III

$$\bar{\sigma}_{11}^{(1a)} = \frac{\bar{E}_{(m)}}{n^{(2)}\bar{E}^{(2)}} \bar{\sigma}_{(o)} - \left[\bar{\sigma}_{(rx)} \tilde{x}_{(s)} - \frac{\bar{E}_{(m)}}{\bar{E}^{(1)}} \bar{\sigma}_{(o)}\right] \frac{\cosh \beta\ell(1 - \tilde{x})}{n^{(1)} \cosh \beta\ell \left[1 - \tilde{x}_{(s)}\right]} \quad ,$$

$$\bar{\sigma}_{11}^{(2a)} = \frac{\bar{E}_{(m)}}{n^{(2)}\bar{E}^{(1)}}\,\bar{\sigma}_{(o)} + \left[\bar{\sigma}_{(rx)}\tilde{x}_{(s)} - \frac{\bar{E}_{(m)}}{E^{(1)}}\,\bar{\sigma}_{(o)}\right]\frac{\cosh\beta\ell(1-\tilde{x})}{n^{(2)}\cosh\beta\ell\left[1-\tilde{x}_{(s)}\right]}\,,$$

$$e_{11}^{(1)} = \frac{\bar{E}_{(m)}\,\bar{\sigma}_{(o)}}{n^{(2)}\bar{E}^{(2)}\bar{E}^{(1)}} - \left[\bar{\sigma}_{(rx)}\tilde{x}_{(s)} - \frac{\bar{E}_{(m)}\bar{\sigma}_{(o)}}{\bar{E}^{(1)}}\right]\frac{\cosh\beta\ell(1-\tilde{x})}{n^{(1)}\bar{E}^{(1)}\cosh\,\beta\ell\left[1-\tilde{x}_{(s)}\right]}\,, \tag{9.8}$$

$$e_{11}^{(2)} = \frac{\bar{E}_{(m)}\bar{\sigma}_{(o)}}{n^{(2)}\bar{E}^{(2)}\bar{E}^{(1)}} + \left[\bar{\sigma}_{(rx)}\tilde{x}_{(s)} - \frac{\bar{E}_{(m)}}{\bar{E}^{(1)}}\,\bar{\sigma}_{(o)}\right]\frac{\cosh\beta\ell(1-\tilde{x})}{n^{(2)}\bar{E}^{(2)}\cosh\,\beta\ell\left[1-\tilde{x}_{(s)}\right]}\,.$$

In the above, the following variables have been used:

$$\tilde{x} \equiv \frac{\bar{x}}{\ell}\,,\quad \bar{\sigma}_{(rx)} \equiv \frac{2n^{(1)}\sigma^{(b)}_{(rx)}}{r^{(1)}/\ell}\,,$$

$$\bar{\sigma}_{(o)} \equiv \bar{\sigma}_{11}^{(1)}(0)\,,\quad \frac{1}{\bar{E}_{(m)}} \equiv \frac{1}{n^{(1)}\bar{E}^{(1)}} + \frac{1}{n^{(2)}\bar{E}^{(2)}}\,, \tag{9.9}$$

$$(\beta\ell)^2 \equiv K\ell^2/E_{(m)}\,,\quad \bar{E}_{(p)} = \text{plastic modulus}$$

$$K\ell^2 = \left[\frac{1}{r^{(2)}/\ell}\right]^2 \cdot \frac{8}{\left[\frac{1}{\mu^{(1)}} - \frac{\left[2 + n^{(2)} + \frac{2}{n^{(2)}}\,\ell n\, n^{(1)}\right]}{n^{(2)}\mu^{(2)}}\right]} \tag{9.10}$$

Further, the parameter $\tilde{x}_{(s)}$ is obtained by solution of the transcendental relation

$$\tilde{x}_{(s)} + \frac{1}{(\beta\ell)\tanh\left[\beta\ell\left[1-\tilde{x}_{(s)}\right]\right]} = \frac{\bar{E}_{(m)}}{\bar{E}^{(1)}}\,\frac{\bar{\sigma}_{(o)}}{\bar{\sigma}_{(rx)}}\,. \tag{9.11}$$

Overall Displacement.

In addition to stress and strain fields in each region, one can solve for the associated displacements $\bar{U}_1^{(\alpha)}$. Of particular interest is the displacement $\bar{u}_{(o)} \equiv -\bar{U}_1^{(1)}(0)$ which is given by

$$\bar{u}_{(o)} = \frac{\left[\bar{\sigma}_{(rx)}\tilde{x}_{(s)} - \frac{\bar{E}_{(m)}}{\bar{E}^{(1)}}\bar{\sigma}_{(o)}\right]}{n^{(1)}\bar{E}^{(1)}} \frac{\tanh\left[\beta\ell\left[1 - \tilde{x}_{(s)}\right]\right]}{\beta\ell} - \frac{\bar{E}_{(m)}\bar{\sigma}_{(o)}\left[1 - \tilde{x}_{(s)}\right]}{n^{(2)}\bar{E}^{(2)}\bar{E}^{(1)}}$$

(9.12)

$$+ \frac{\bar{\sigma}_{(rx)}}{2n^{(1)}\bar{E}^{(1)}}\left[\tilde{x}^2_{(s)} - \tilde{x}^2_{(p)}\right] - \frac{\bar{\sigma}_{(o)}}{\bar{E}^{(1)}}\left[\tilde{x}_{(s)} - \tilde{x}_{(p)}\right] + \frac{\bar{\sigma}_{rx}}{2n^{(1)}\bar{E}_{(p)}} - e_{(o)}\tilde{x}_{(p)} \cdot$$

where

$$e_{(o)} \equiv \frac{\sigma_{(y)}}{\bar{E}^{(1)}} + \frac{\left[\bar{\sigma}_{(o)} - \bar{\sigma}_{(y)}\right]}{\bar{E}_{(p)}} ,$$

(9.13)

$\bar{\sigma}_{(y)} \equiv$ Rebar initial yield stress.

9.3 FRACTURE CRITERION AND SEQUENCE.

The developed mixture model of reinforced concrete can simulate the cell-averaged fields $f^{(\alpha a)}(x_k)$ for each material. The model can also be used to estimate the local fields $f^{(\alpha)}(x_k; x^*_\gamma; \epsilon)$ within each material. Consequently, once an appropriate fracture criterion has been supplied, then one can proceed to examine a variety of possible fracture modes. A subset of such modes include primary (i.e., through) cracks, secondary (non-through) cracks, termini "cone" cracks, and axial splitting cracks. Although all such fracture modes are of interest, the present study will focus on the influence of primary cracks on the overall response characteristics of reinforced concrete.

An elementary, yet useful, criterion for the initiation of a primary crack can be postulated as follows:

$$\max \bar{\sigma}_{11}^{(2a)} = f_t^{(c)} \tag{9.14}$$

where $f_t^{(c)}$ measures the "tensile strength" of the concrete.

Examination of the stress field $\bar{\sigma}_{11}^{(2a)}$ in each of the foregoing regions reveals that the maximum average axial stress in the concrete, $\max \bar{\sigma}_{11}^{(2a)}$, occurs at $\bar{x}_1 = \ell$. Consequently in the absence of imposed statistical variations of $f_t^{(c)}$ with location, the first new crack (i.e., the first new crack system) will consist of a single crack located at the mid-point between the two initial *termini* cracks. The value of the applied stress $\bar{\sigma}_{(o)}$ when this first primary crack initiates is obtained from solving (9.8) with $\bar{\sigma}_{11}^{(2a)} = f_t^{(c)}$ and $\tilde{x} = 1$ together with (9.11). Using this value of $\bar{\sigma}_{(o)}$, the corresponding displacement $\bar{u}_{(o)}$ is obtained from (9.12). Immediately after fracture, the specimen suffers a stress drop at the same value of displacement $\bar{u}_{(o)}$. The new applied stress $\bar{\sigma}_{(o)}$ corresponding to this drop is obtained by replacing ℓ by $\ell/2$ in (9.12) and (9.11). It is noted that this leads to jumps in $\bar{\sigma}_{(rx)}$ and $\tilde{x}_{(s)}$, i.e., additional slip occurs during the fracture process.

Following the formation of the first new crack, the R/C element consists of two subelements, each of which is geometrically identical to the original element with one exception: The subelement length (or crack spacing) is now ℓ rather than 2ℓ. Each subelement is now extended monotonically from the value of the displacement corresponding to the initiation of the first fracture. The value of the applied stress $\bar{\sigma}_{(o)}$ at a given displacement for each subelement is given by (9.12), (9.11) with ℓ replaced by $\ell/2$. The value of $\bar{\sigma}_{(o)}$ corresponding to the initiation of a primary crack

within each subelement is obtained from (9.8), (9.11) with $\tilde{x} = 1$, ℓ replaced by $\ell/2$ and $\bar{\sigma}_{11}^{(2a)} = f_t^{(c)}$. The new applied stress $\bar{\sigma}_{(o)}$ corresponding to the stress drop subsequent to fracture is obtained by replacing ℓ by $\ell/4$ in (9.12) and (9.11).

Following the formation of the primary cracks in the above subelements, the R/C element consists of four subelements, each of which is geometrically identical to the original element except that the subelement length is now $\ell/2$ rather than ℓ. Each subelement is now extended monotonically from the value of the displacement corresponding to the initiation of the second crack system, and the entire process is repeated.

The foregoing algorithm leads to a crack sequence as depicted in Fig. 9.5. A typical corresponding stress-strain curve is depicted in Fig. 9.6; here $\sigma_{(e)} \equiv n^{(1)}\bar{\sigma}_{11}^{(1a)}(0)$ represents the overall applied stress based on the entire specimen cross-section and $e_{(e)} \equiv |\bar{u}(o)/(\ell/N)|$ is the overall strain (2ℓ = original specimen length, N = number of subelements).

9.4 STIFFNESS DEGRADATION.

With the aid of the crack evolution algorithm described in subsection 9.3, stiffness degradation during monotonic extension of a R/C specimen was examined in detail for the case $\phi = 0$, i.e., when the direction of loading was aligned with the rebar. The "stiffness" discussed refers to either the tangent or secant modulus associated with the overall stress ($\sigma_{(o)}$) versus the overall strain $e_{(e)}$; see subsection 9.3.

9.4.1 Influence of Bond Strength.

Bond strength was found to have a major influence on stiffness degradation. This influence can be observed in Fig. 9.7 which exhibits predicted relative tangent stiffness versus global strain for various values of steel-concrete bond strength ranging from 200 psi to ∞. In this example, the steel volume fraction $n^{(1)} = 0.01$ (1 percent), the concrete cover $r^{(2)}/\ell = 0.10$, the concrete tensile strength $f_t^{(c)} =$

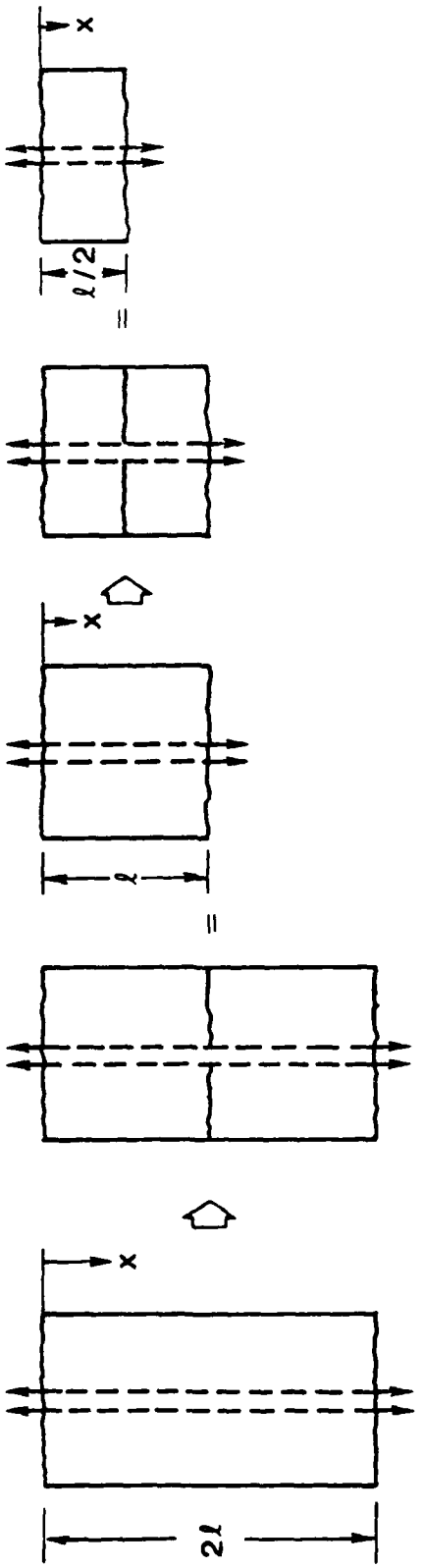

Figure 9.5. Crack sequence.

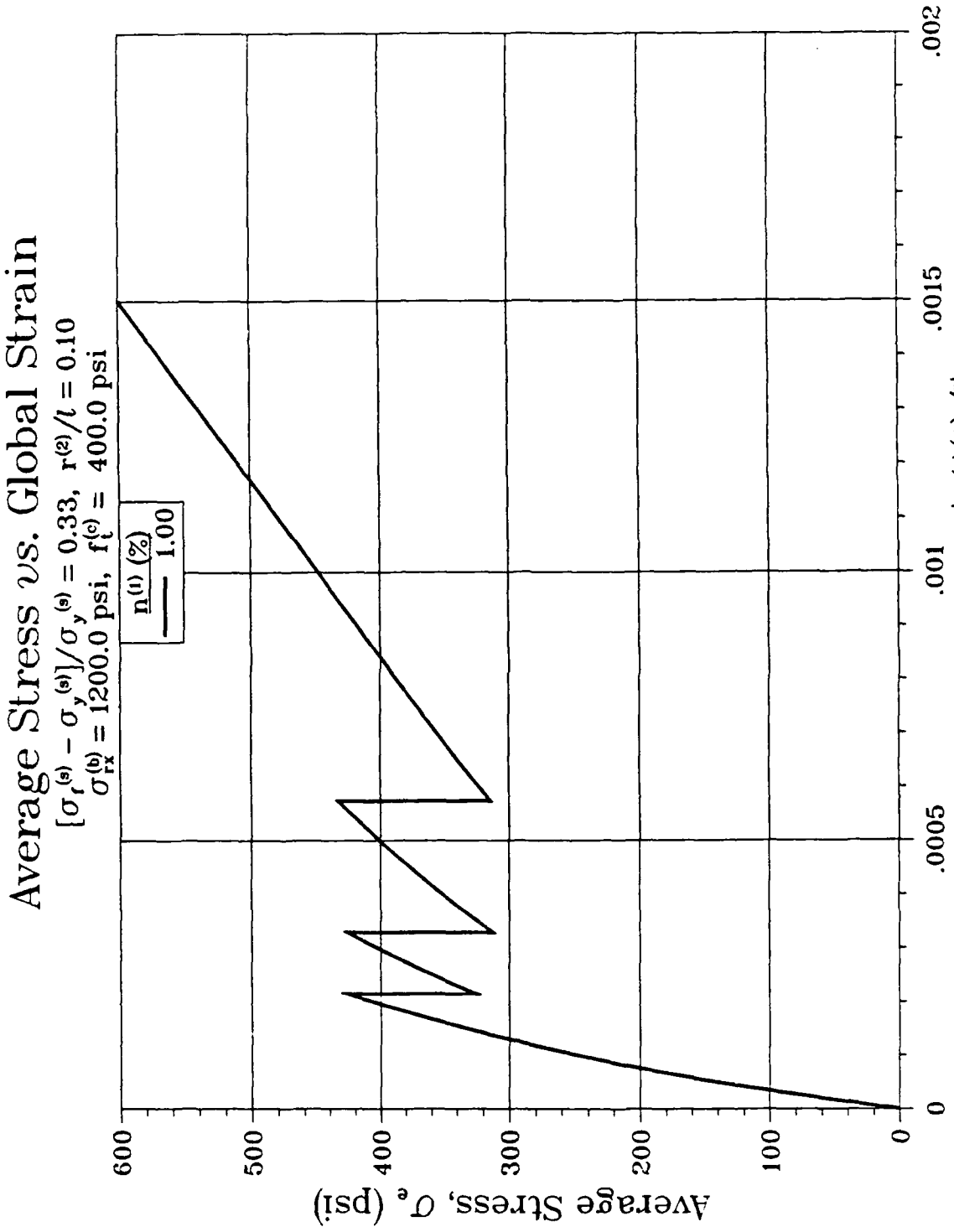

Figure 9.6. Typical stress-strain curve.

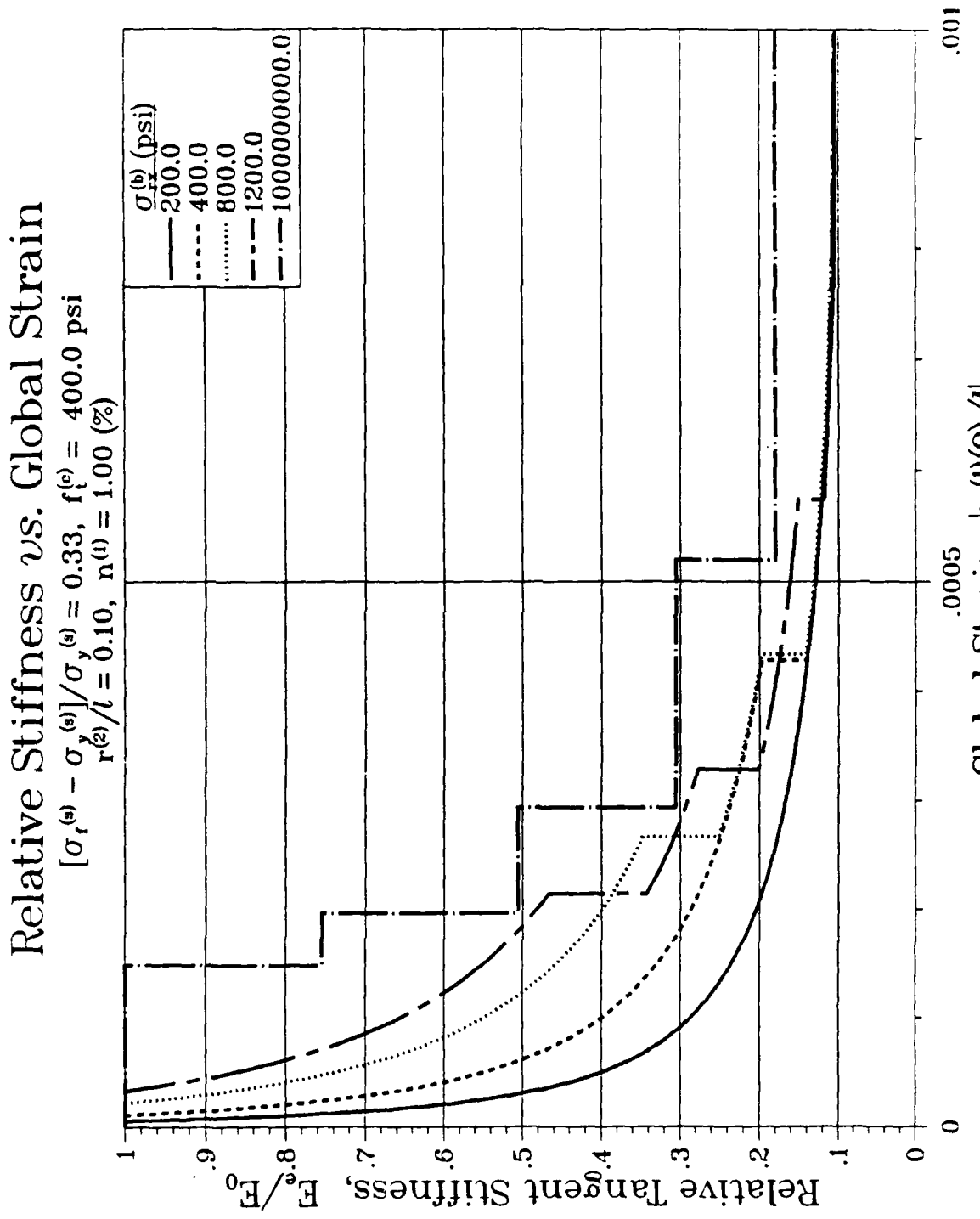

Figure 9.7. Influence of bond strength on stiffness degradation.

400 psi, and the rebar hardening characteristics are given by $(\sigma_f^{(s)} - \sigma_y^{(s)})/\sigma_y^{(s)} = 0.33$; the latter is perhaps typical of grade 60 rebar.

The two extreme cases in Fig. 9.7 correspond to a bond strength of ∞ and a bond strength of 200 psi (strengths in the range 600 - 800 psi are considered typical of many practical situations). In the former, stiffness degrades by cracking only i.e., in the absence of slip. In the latter, stiffness degradation is due to slip only. Intermediate cases involve both slip and cracking. It is evident that the rate of stiffness degradation increases rapidly with decreasing bond strength, i.e., increasing slip. It is also evident that tangent stiffness computed in the absence of slip (perfect steel-concrete interface bond) represents an upper bound.

9.4.2 Influence of Steel Volume Fraction.

The influence of steel volume fraction on stiffness degradation is seen by an examination of the 200 psi bond strength example in Figure 9.7 where stiffness degradation is influenced by slip only. The results, for steel volume fractions ranging from 2 to 0.1 percent, are given in Figure 9.8. The rate of stiffness degradation is shown to be greater for smaller steel volume fractions.

For cases involving both slip and cracking, the same trends are to be found (i.e., stiffness degradation occurs more rapidly for smaller steel volume fractions). It should be noted that the sharp decrease in overall tangent stiffness for steel volume fractions of 0.25 and 0.1 percent in Figure 9.8 is due to the rebar undergoing plastic deformation.

9.5 DUCTILITY AND FAILURE.

The developed mixture model of reinforced concrete provides stress and strain fields for each material component. Consequently, if the rebar failure condition is specified, then the mixture model can be applied to study the influence of various parameters such as bond strength, steel volume, concrete tensile strength, etc., on the overall ductility of the composite. Such a parametric study was conducted. The results, which appear to be entirely new, are presented below.

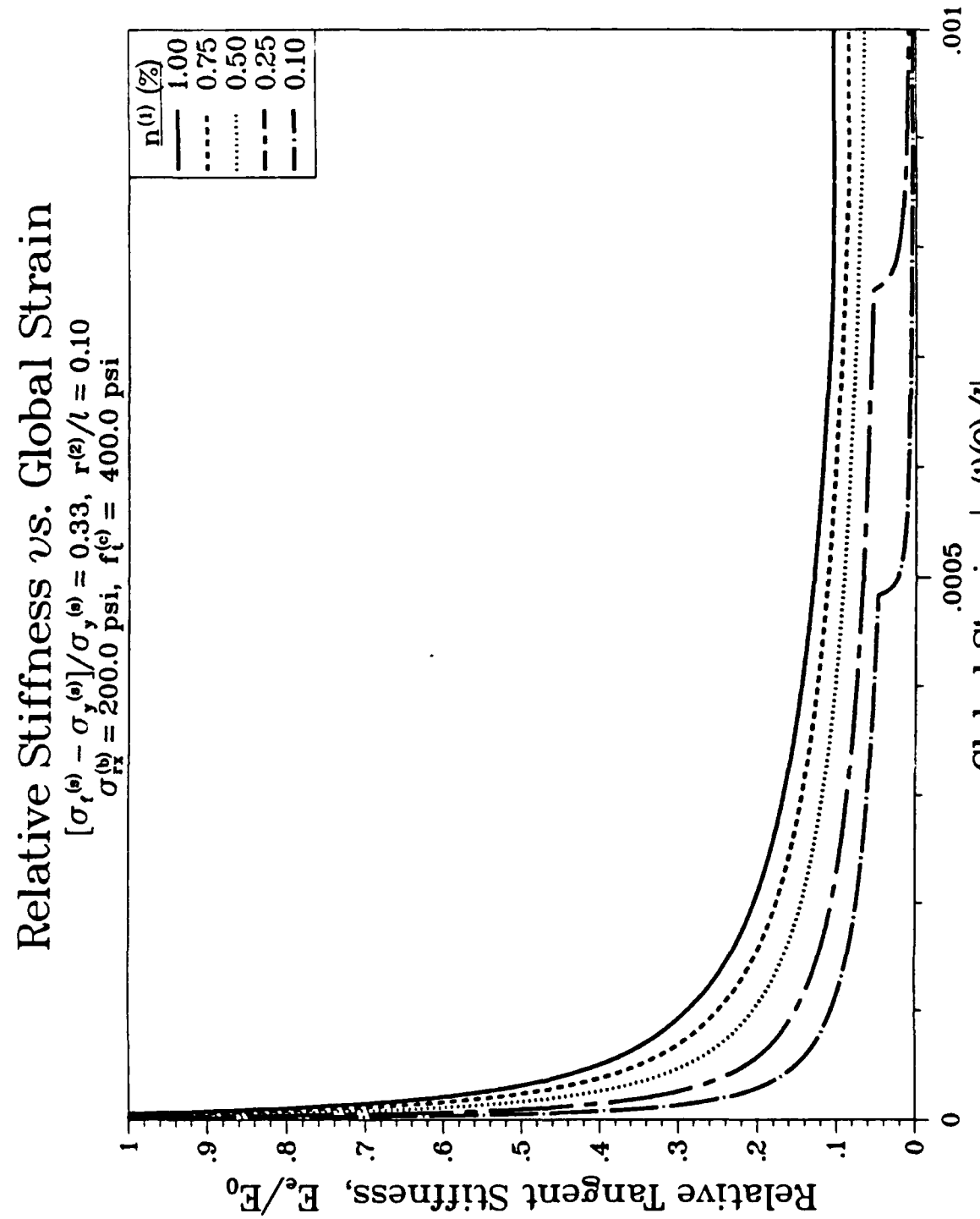

Figure 9.8. Influence of steel volume fraction on stiffness degradation.

9.5.1 Definition of Ductility.

For purposes of this study, a ductility measure $\mathscr{D}$ shall be defined according to

$$\mathscr{D} = e_f / e_f^{(s)} \tag{9.15}$$

where $e_f^{(s)}$ denotes the failure strain of the rebar alone, and e_f is the overall failure strain of the reinforced concrete composite. Consequently, $\mathscr{D} = 1$ for the rebar alone while $\mathscr{D} < 1$ for the composite.

It is noted that, for most practical situations, the strain field in the steel will be highly nonuniform. An example is depicted in Fig. 9.9. Consequently, $\mathscr{D}$ can be expected to be considerably less than unity for most cases of interest.

9.5.2 Influence of Bond Strength.

Bond strength exerts a major influence on overall specimen ductility. This influence is exemplified in Figure 9.10 for a range of steel percentages. The concrete tensile strength in this example is sufficiently high to preclude concrete cracking prior to failure of the rebar. As can be observed, the ductility reduces sharply from 1.0 as the bond strength is increased from zero. For bond strengths in excess of 600 psi, the ductility is generally less than 0.1 for a range of practical steel percentages -- in the absence of cracking.

9.5.3 Influence of Concrete Tensile Strength.

Concrete cracking -- or concrete tensile strength -- also plays a major role in overall specimen ductility. Figures 9.11 - 9.14 exhibit the influence of concrete cracking for a range of steel percentages. It is evident that the effect of progressive cracking is to dramatically increase the overall ductility. Cases where cracking occurs are indicated by the curves which show sudden changes in $\mathscr{D}$. A comparison of cases reveals that ductility in general increases as the concrete tensile strength decreases.

9.5.4 Influence of Rebar Strain Hardening.

The rebar in the current study was modeled as piecewise linear under monotonic extension with an elastic modulus of 3×10^7 psi and a plastic modulus, E_p, of

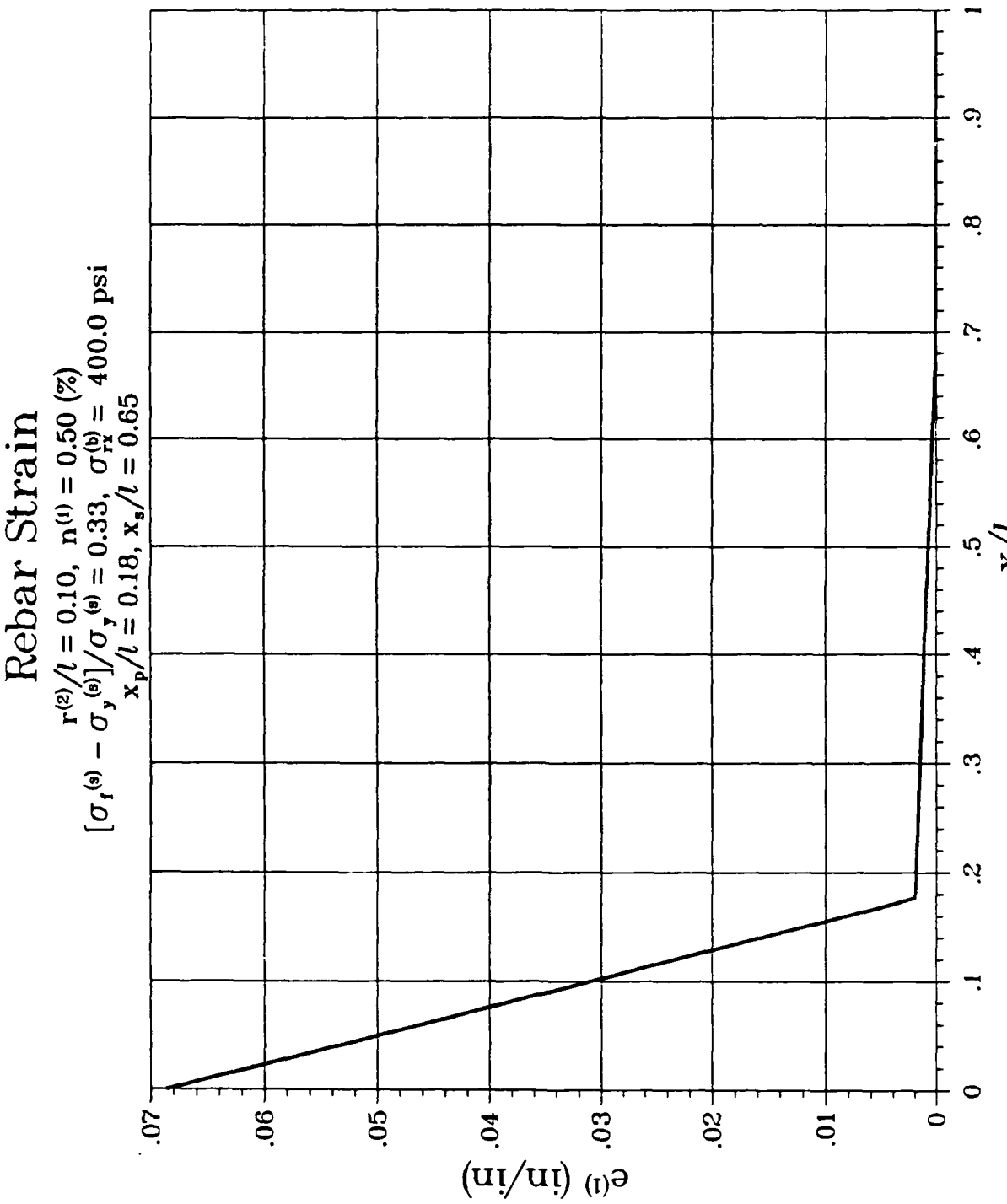

Figure 9.9. Typical nonuniform strain field in the steel.

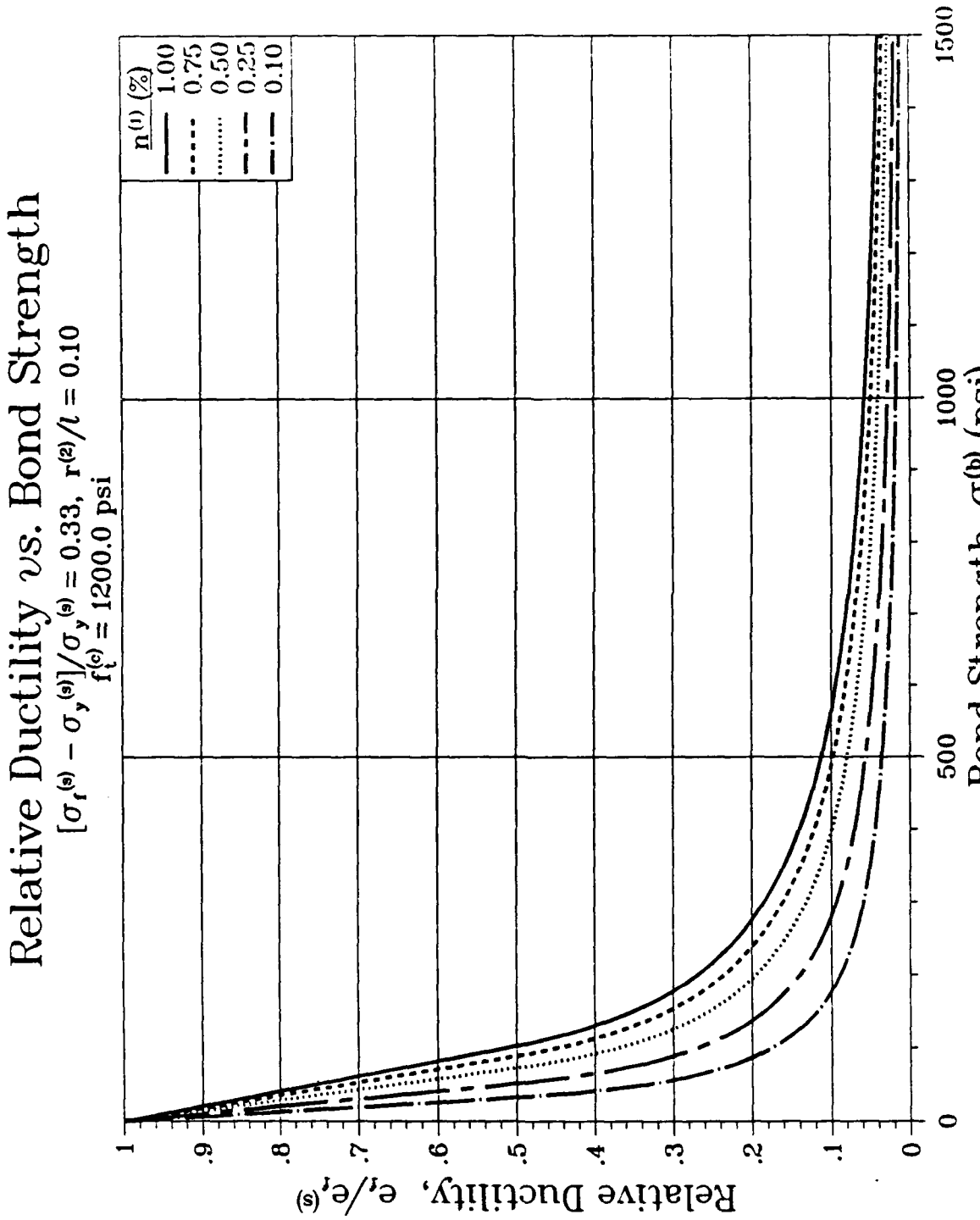

Figure 9.10. Influence of bond strength on specimen ductility.

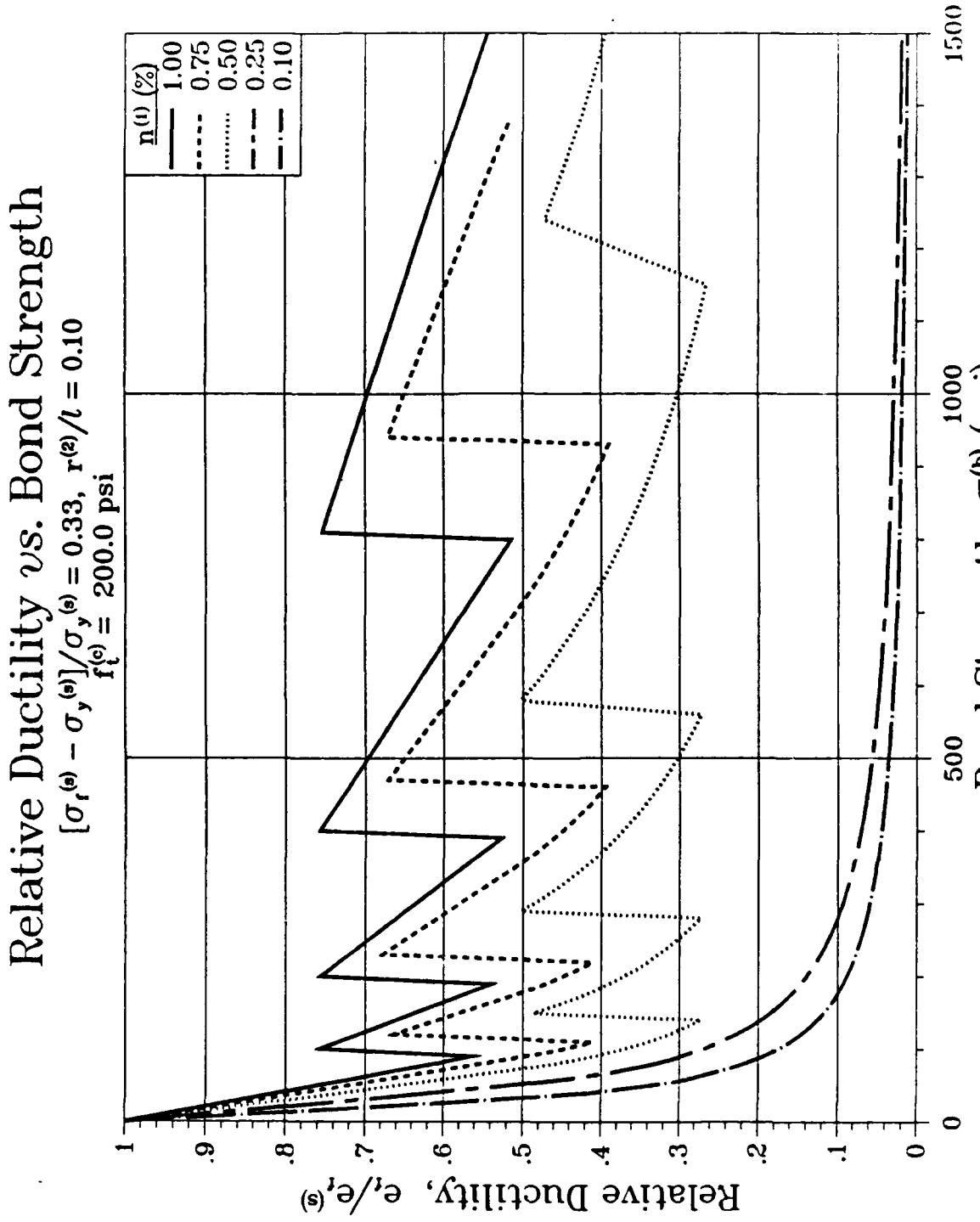

Figure 9.11. 200 psi concrete tensile strength.

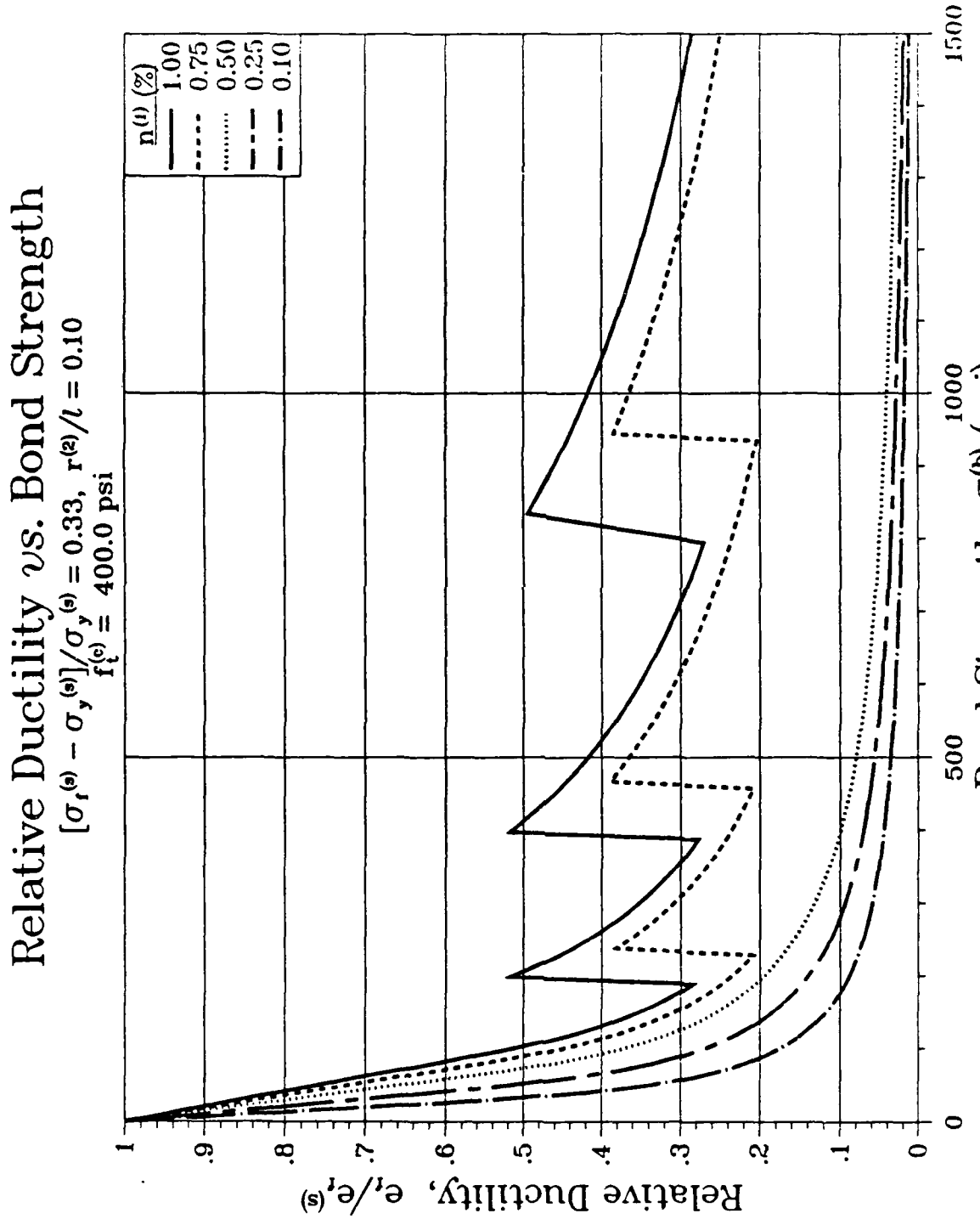

Figure 9.12. 400 psi concrete tensile strength.

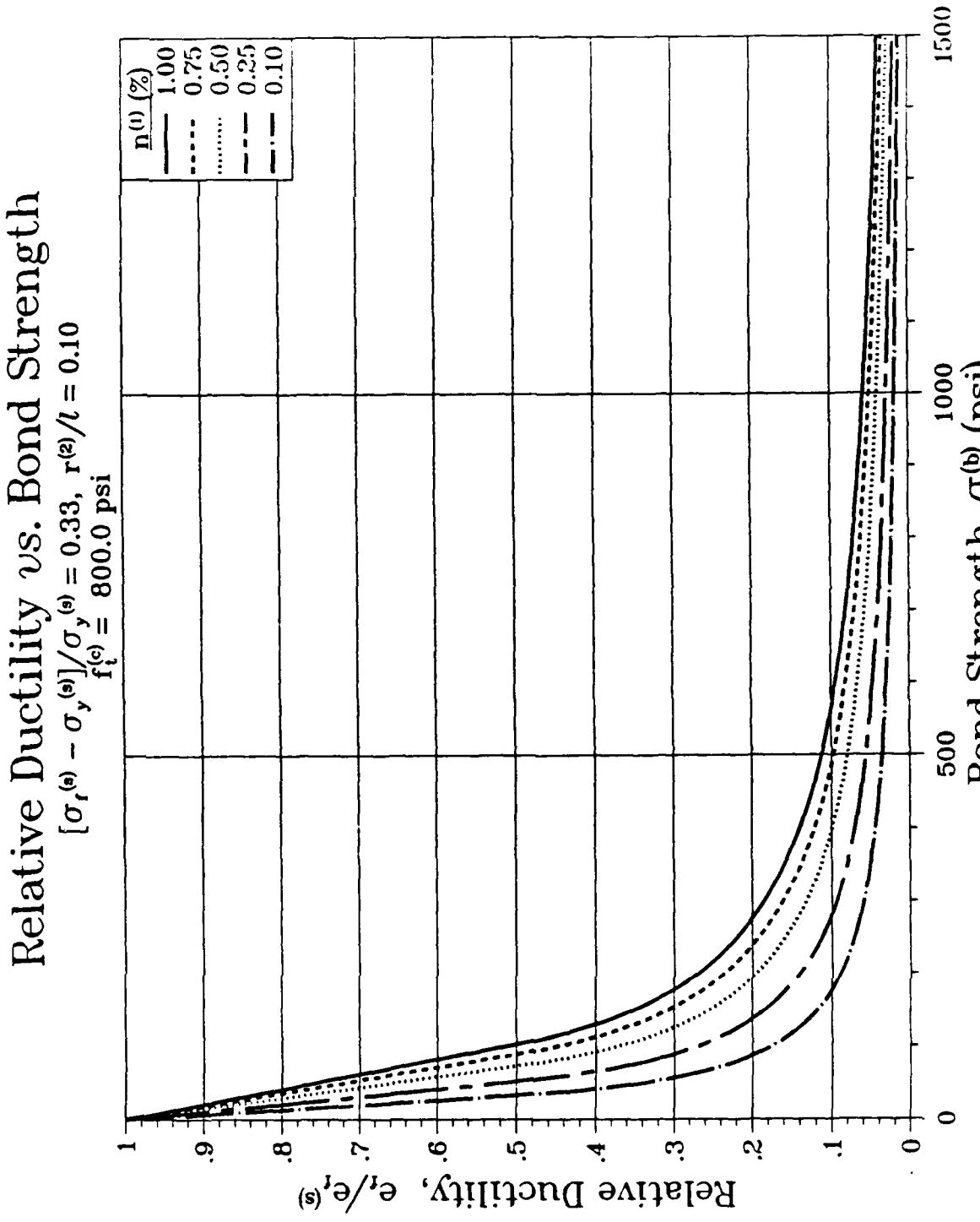

Figure 9.13. 800 psi concrete tensile strength.

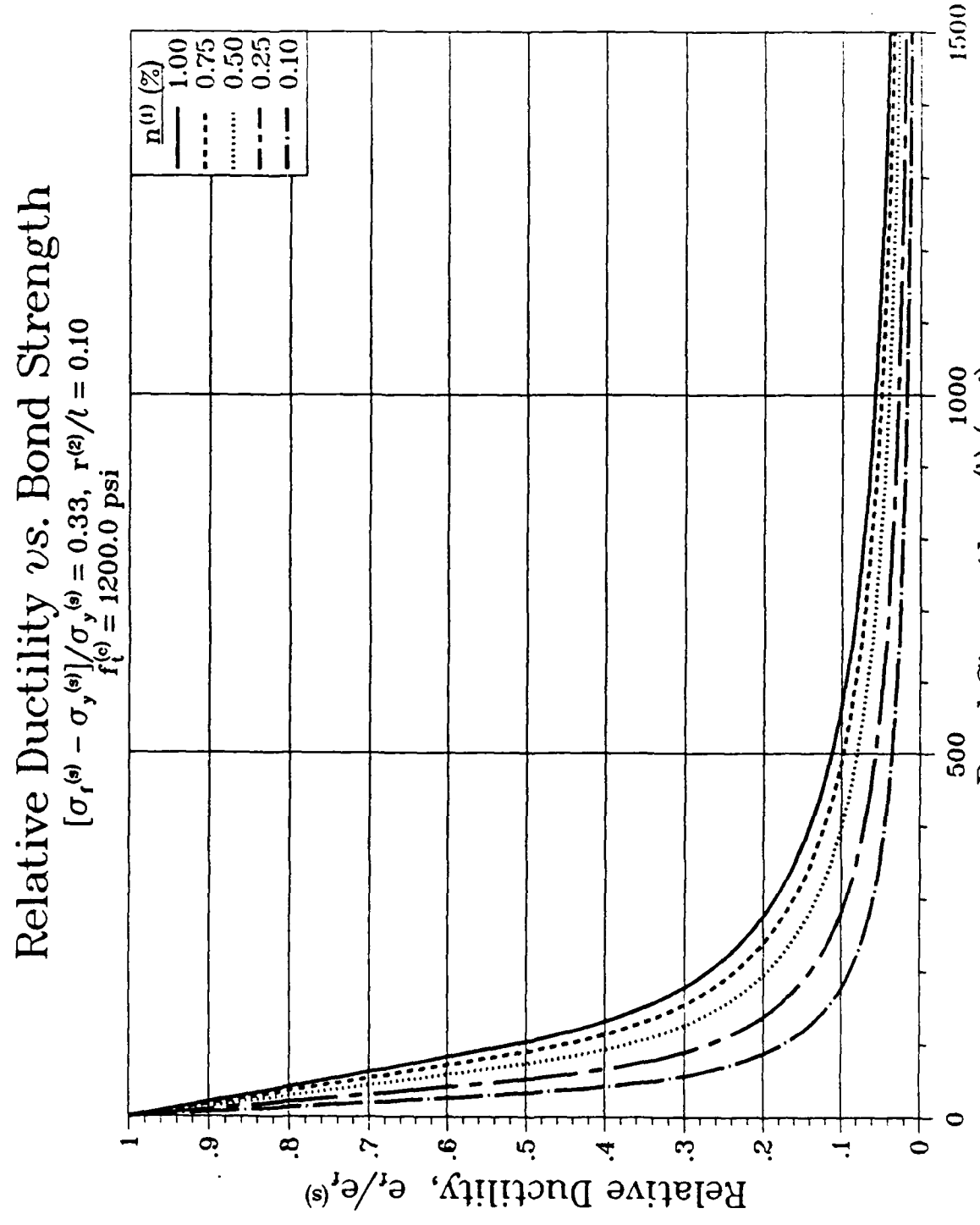

Figure 9.14. 1200 psi concrete tensile strength.

approximately 2-3 orders of magnitude less. Within the context of this description, the ductility was found to depend only weakly on the strain hardening modulus E_p. This weak dependence can be observed from Figures 9.15 - 9.18 wherein the modulus E_p varies from $E_p = 3 \times 10^4$ psi to $E_p = 6 \times 10^5$ psi.

9.5.5 Ductility versus Dimensionless Bond Strength.

In the process of conducting this study, it was discovered that one can collapse all ductility versus bond strength data by graphing that ductility versus a dimensionless bond strength defined according to $\bar{\sigma}_{rx}/E_m$ where $\bar{\sigma}_{rx}$ and E_m are given in (9.9). The resulting master curve is shown in Fig. 9.19. This curve applies for cases involving cracking as well as for those wherein no cracking occurs. When cracking occurs, 2ℓ represents the crack spacing. If slip only occurs, 2ℓ is the length of the specimen.

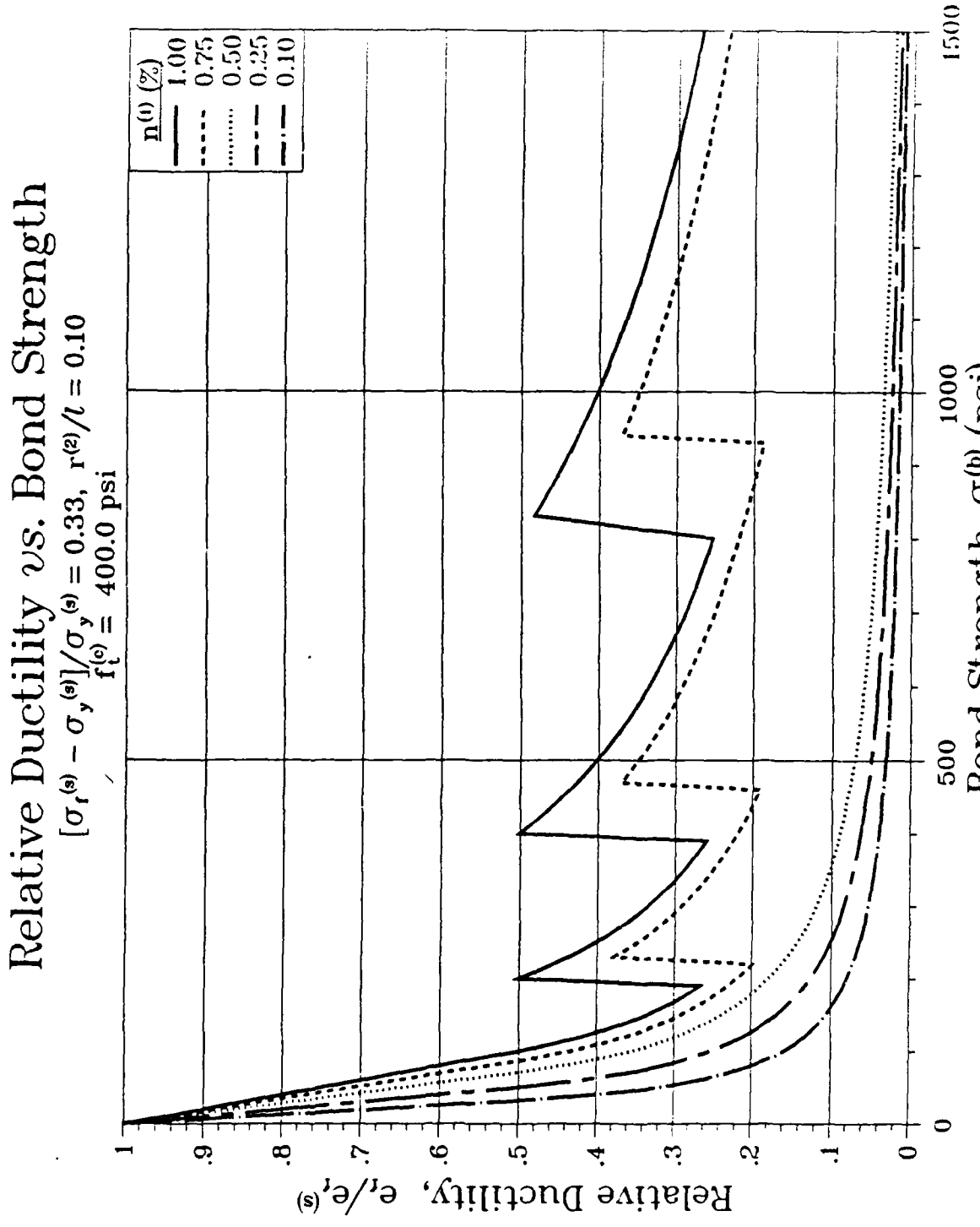

Figure 9.15. Rebar plastic modulus $E_p = 3 \times 10^4$ psi.

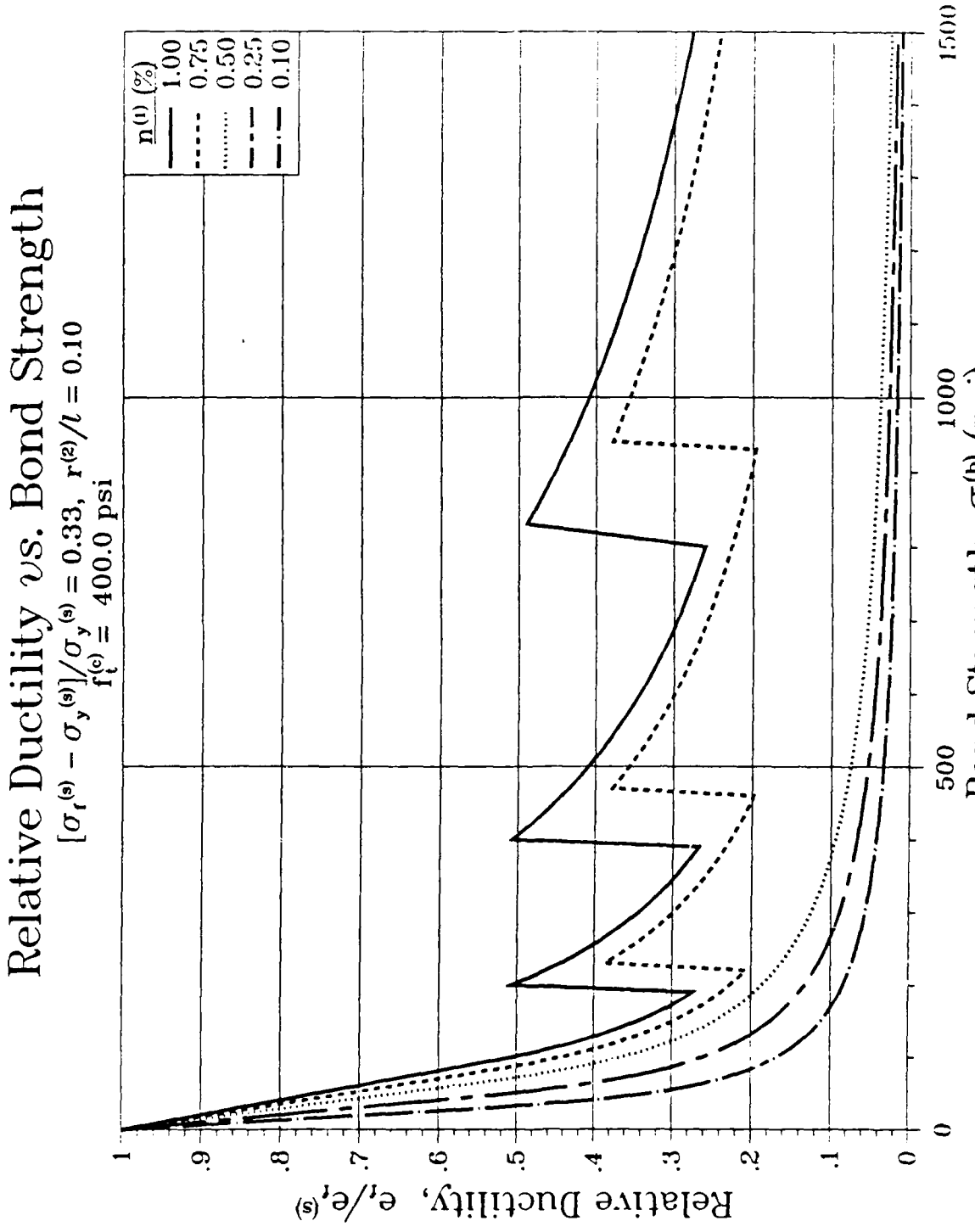

Figure 9.16. Rebar plastic modulus $E_\rho = 1.5 \times 10^5$ psi.

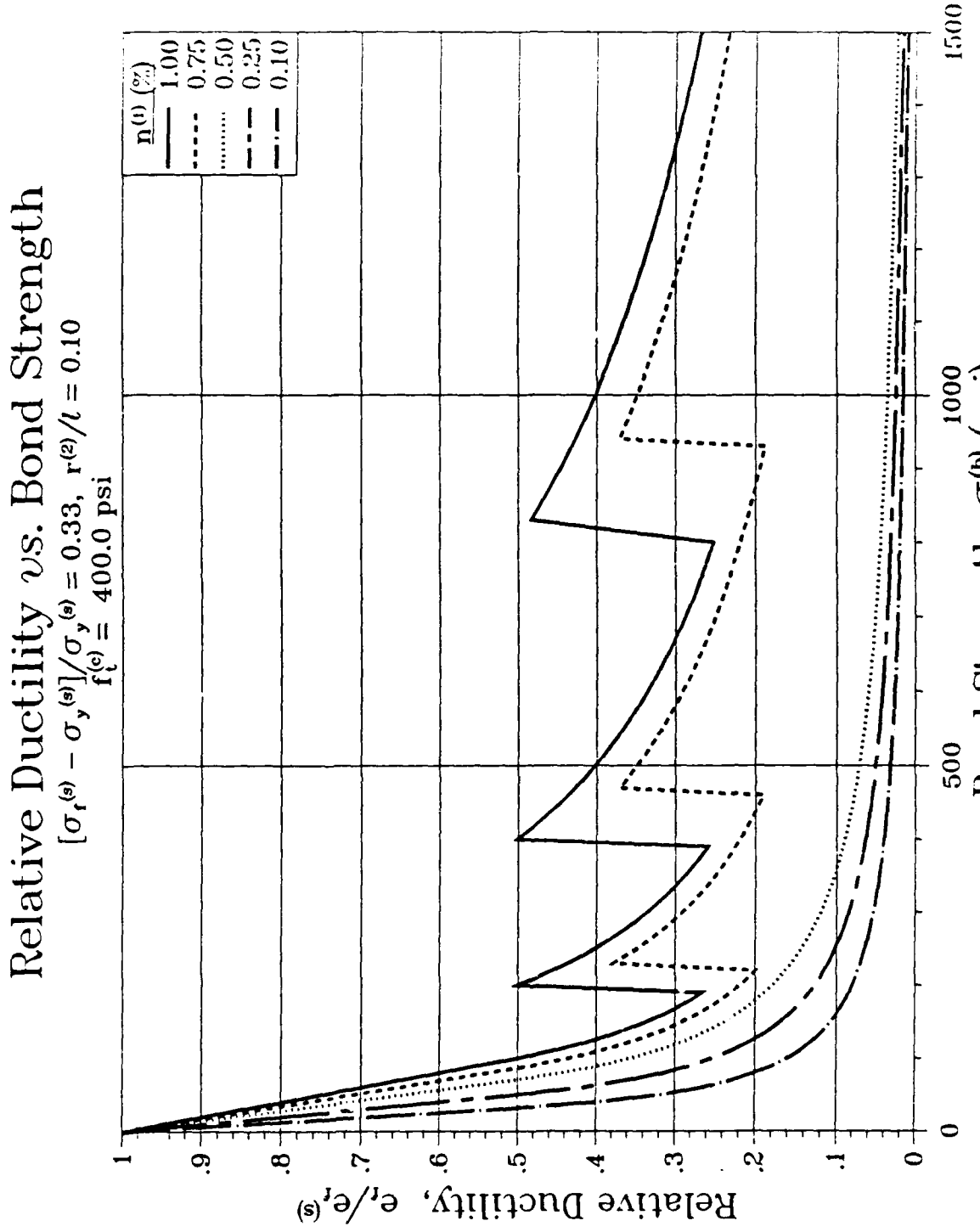

Figure 9.17. Rebar plastic modulus $E_p = 3 \times 10^5$ psi.

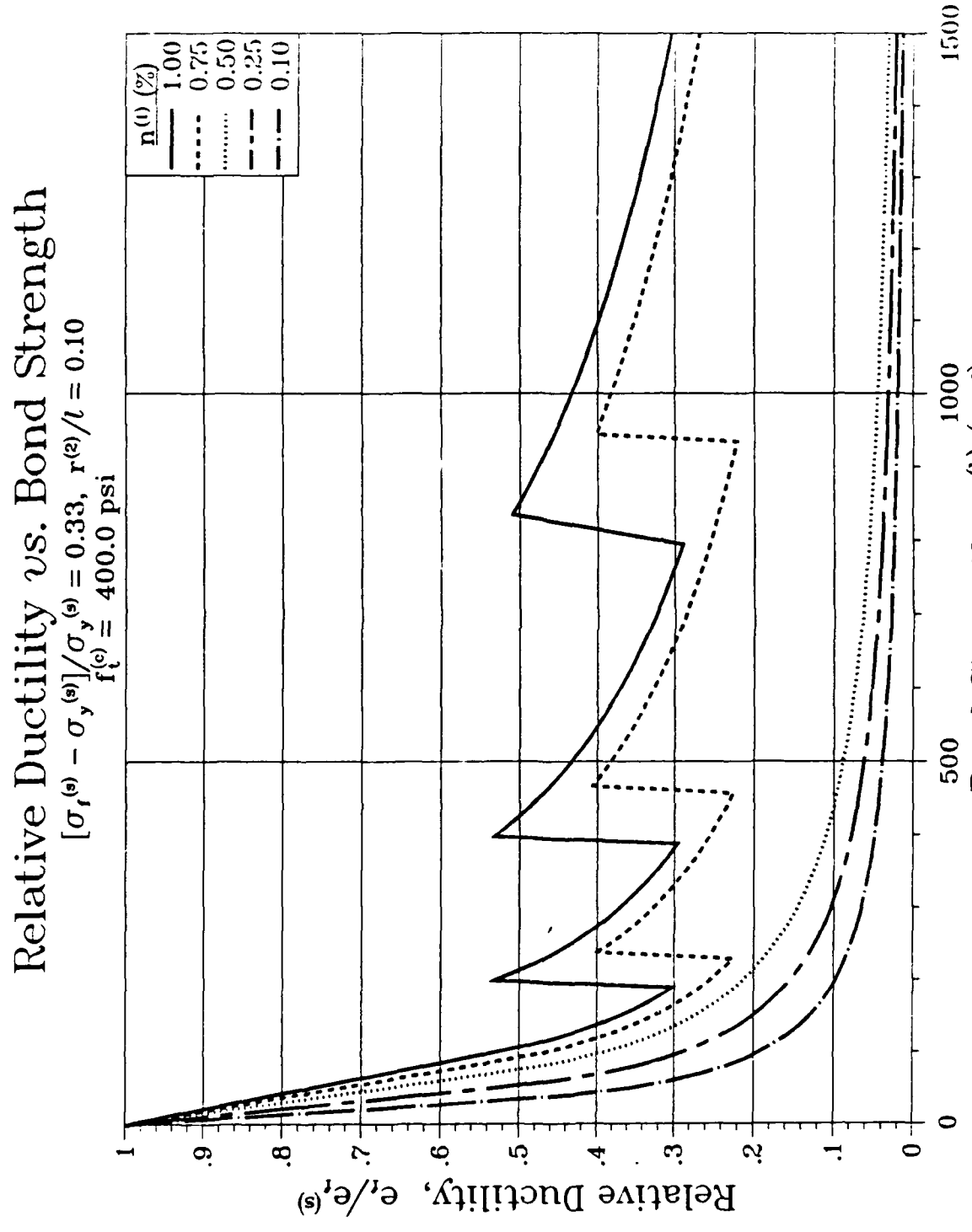

Figure 9.18. Rebar plastic modulus $E_p = 6 \times 10^5$ psi.

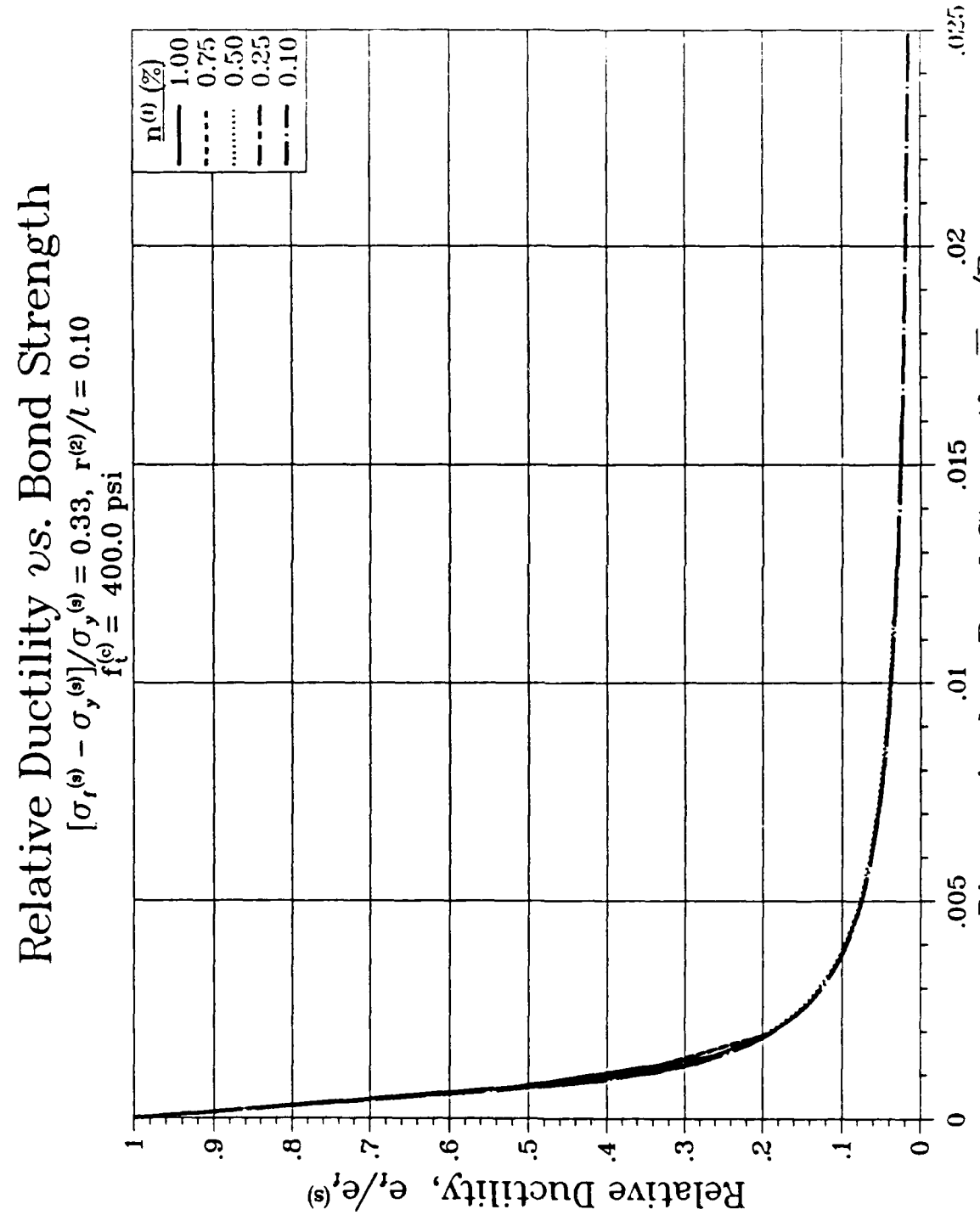

Figure 9.19. Collapsed ductility versus bond strength curve.

SECTION 10

EXTENSION OBLIQUE TO STEEL

In this section, the response of a R/C panel is examined for the case of monotonic extension in a direction which is oblique to the steel layout, Fig. 8.1. The focus of the presentation is on the influence of the angle ϕ on stiffness degradation. In the analysis to follow, the steel-concrete bond is assumed to be perfect.

10.1 BASIC EQUATIONS AND SOLUTION.

The governing equations for this case are

$$\hat{\sigma}^{(1p)}_{11,1} + \left[\beta_{(1)}\cos^2\phi + \beta_{(2)}\sin^2\phi\right]\left[\hat{U}^{(2)}_1 - \hat{U}^{(1)}_1\right] = 0 \ ,$$

$$\hat{\sigma}^{(2p)}_{11,1} - \left[\beta_{(1)}\cos^2\phi + \beta_{(2)}\sin^2\phi\right]\left[\hat{U}^{(2)}_1 - \hat{U}^{(1)}_1\right] = 0 \ ; \qquad (10.1)$$

$$\hat{\sigma}^{(1p)}_{11} = \hat{D}_{11}\hat{U}^{(1)}_{1,1} + \hat{D}_{12}\hat{U}^{(2)}_{1,1} \ ,$$

$$\hat{\sigma}^{(2p)}_{11} = \hat{D}_{12}\hat{U}^{(1)}_{1,1} + \hat{D}_{22}\hat{U}^{(2)}_{1,1} \ .$$

Substitution of (10.2) into (10.1) furnishes

$$\hat{D}_{11}\frac{d^2\hat{U}^{(1)}_1}{d\hat{x}^2_1} + \hat{D}_{12}\frac{d^2\hat{U}^{(2)}_1}{d\hat{x}^2_1} + \hat{\beta}^2_{11}\frac{\left[\hat{U}^{(2)}_1 - \hat{U}^{(1)}_1\right]}{\epsilon^2} = 0 \ ,$$

$$\hat{D}_{12}\frac{d^2\hat{U}^{(1)}_1}{d\hat{x}^2_1} + \hat{D}_{22}\frac{d^2\hat{U}^{(2)}_1}{d\hat{x}^2_2} - \hat{\beta}^2_{11}\frac{\left[\hat{U}^{(2)}_1 - \hat{U}^{(1)}_1\right]}{\epsilon^2} = 0 \ , \qquad (10.3)$$

where

$$\hat{\beta}_{11} \equiv \beta_{(1)}\cos^2\phi + \beta_{(2)}\sin^2\phi \qquad (10.4)$$

and where $\beta_{(1)}$, $\beta_{(2)}$ are given by (5.18).

The solution of (10.3) is readily obtained in the form

$$\hat{U}_1^{(1)} = A_1 e^{\lambda \hat{x}_1} + A_2 e^{-\lambda \hat{x}_1} + A_3 \hat{x}_1 + A_4 \quad ,$$

$$\hat{U}_1^{(2)} = - c\, A_1 e^{\lambda \hat{x}_1} - c A_2 e^{-\lambda \hat{x}_1} + A_3 \hat{x}_1 + A_4 \tag{10.5}$$

where

$$\lambda^2 \equiv \left[\frac{\hat{\beta}_{11}^2}{\epsilon^2}\right] \left[\frac{\hat{D}_{11} + \hat{D}_{22} + 2\hat{D}_{12}}{\hat{D}_{11}\hat{D}_{22} - \hat{D}_{12}^2}\right] \quad ,$$

$$c \equiv \frac{\hat{D}_{11}^2 + \hat{D}_{12}\left(2\hat{D}_{11} + \hat{D}_{12}\right)}{\left(\hat{D}_{11} + \hat{D}_{12}\right)\left(\hat{D}_{22} + \hat{D}_{12}\right)} = \frac{\left(\hat{D}_{11} + \hat{D}_{12}\right)}{\left(\hat{D}_{22} + \hat{D}_{12}\right)} \tag{10.6}$$

Equations (10.5) lead to the concrete stress:

$$\begin{aligned} \hat{\sigma}_{11}^{(2p)} &= n^{(2)} \hat{\sigma}_{11}^{(2a)} = \hat{D}_{12} \hat{U}_{1,1}^{(1)} + \hat{D}_{22} \hat{U}_{1,1}^{(2)} \\ &= A_1 e^{\lambda \hat{x}_1} \lambda \left(\hat{D}_{12} - \Delta \hat{D}_{22}\right) + A_2 e^{-\lambda \hat{x}_1} \lambda \left(- \hat{D}_{12} + \Delta \hat{D}_{22}\right) \\ &\quad + A_3 \left(\hat{D}_{12} + \hat{D}_{22}\right) \quad . \end{aligned} \tag{10.7}$$

The following boundary conditions are now specified:

$$\hat{U}_1^{(1)} = \hat{U}_1^{(2)} = 0 \quad \text{at } \hat{x}_1 = 0 \ ,$$

$$\hat{U}_1^{(1)} = \ell\,\bar{e} \text{ at } \hat{x}_1 = \ell \ , \quad (\bar{e} \text{ specified}) \tag{10.8}$$

$$\hat{\sigma}_{11}^{(2a)} = 0 \text{ at } \hat{x}_1 = \ell \ .$$

Substitution of (10.5) and (10.7) into (10.8) furnishes

$$A_1 = \frac{\bar{e}\ell}{\Delta}\left(\hat{D}_{12} + \hat{D}_{22}\right) = - A_2$$

$$A_3 = - \frac{2\bar{e}\,\ell\lambda}{\Delta}\left(\hat{D}_{12} - c\,\hat{D}_{22}\right) \cosh \lambda\ell \ . \tag{10.9}$$

$$A_4 = 0 \ ,$$

where

$$\Delta \equiv 2\left(\hat{D}_{12} + \hat{D}_{22}\right)\sinh \lambda\ell - 2\lambda\ell\left(\hat{D}_{12} - c\,\hat{D}_{22}\right)\cosh \lambda\ell \tag{10.10}$$

The solution of (10.3) subject to the boundary conditions (10.8) can now be written in the form

$$\hat{U}_1^{(1)} = \frac{2\bar{e}\ell}{\Delta}\left[\left(\hat{D}_{12} + \hat{D}_{22}\right)\sinh \lambda\hat{x}_1 - \lambda\left(\hat{D}_{12} - c\,\hat{D}_{22}\right)(\cosh \lambda\ell)\left(\hat{x}_1\right)\right]$$

(10.11)

$$\hat{U}_1^{(2)} = - \frac{2\bar{e}\ell}{\Delta}\left[c\,\left(\hat{D}_{12} + \hat{D}_{22}\right)\sinh \lambda\hat{x}_1 - \lambda\left(\hat{D}_{12} - c\,\hat{D}_{22}\right)(\cosh \lambda\ell)\left(\hat{x}_1\right)\right]$$

The displacements (10.11) furnish the stresses:

$$n^{(1)}\hat{\sigma}_{11}^{(1a)} = \frac{2\bar{e}\ell\lambda}{\Delta}\left[\left(\hat{D}_{12} + \hat{D}_{22}\right)\left(\hat{D}_{11} - c\,\hat{D}_{12}\right)\cosh \lambda\hat{x}_1\right.$$

$$\left. - \lambda\left(\hat{D}_{12} - c\,\hat{D}_{22}\right)\left(\hat{D}_{11} + \hat{D}_{12}\right)\cosh \lambda\ell\right] \ ,$$

(10.12)

$$n^{(2)}\hat{\sigma}_{11}^{(2a)} = \frac{2\bar{e}\ell\lambda}{\Delta}\left[\left(\hat{D}_{12} + \hat{D}_{22}\right)\left(\hat{D}_{12} - c\,\hat{D}_{22}\right)\cosh\lambda\hat{x}_1\right.$$

$$\left. - \lambda\left(\hat{D}_{12} - c\,\hat{D}_{22}\right)\left(\hat{D}_{12} + \hat{D}_{22}\right)\cosh\lambda\ell\right]$$

Examination of (10.12b) reveals that $\bar{\sigma}_{11}^{(2a)}$ attains a maximum at $\hat{x}_1 = 0$; the corresponding value of $\bar{\sigma}_{11}^{(2a)}$ is given by

$$n^{(2)}\hat{\sigma}_{11}^{(2a)}\left[\hat{x}_1 = 0\right] = \frac{2\bar{e}\ell\lambda}{\Delta}\left(\hat{D}_{12} + \hat{D}_{22}\right)\left(\hat{D}_{12} - c\,\hat{D}_{22}\right)(1 - \cosh\lambda\ell) \quad . \qquad (10.13)$$

Similarly, examination of (10.12a) reveals that max $\sigma_{11}^{(1a)}$ occurs at $\hat{x}_1 = \ell$ where

$$n^{(1)}\hat{\sigma}_{11}^{(1a)}\left[\hat{x}_1 = \ell\right] = \frac{2\bar{e}\ell\lambda}{\Delta}(1 + c)\left(\hat{D}_{11}\hat{D}_{22} - \hat{D}_{12}^2\right)\cosh\lambda\ell \quad . \qquad (10.14)$$

10.2 FRACTURE CRITERION AND SEQUENCE.

Consider now the problem of predicting the evolution of the primary crack field in the R/C specimen when the latter is subjected to monotonic extension. If condition (9.14) is again adopted as the criterion for primary crack initiation in the concrete then, since max $\hat{\sigma}_{11}^{(2a)}$ again occurs at the specimen center $\hat{x}_1 = 0$ (see (10.13)), the fracture sequence as well as the resulting overall stress-strain behavior can be computed using an algorithm similar to that outlined in Section 9.3.

10.3 STIFFNESS DEGRADATION.

Figure 10.1 shows the degradation of overall secant* stiffness with increasing overall specimen strain for rebar angles ranging from $\phi = 0°$ (rebar along loading direction) to $\phi = 60°$. Remarkably, the degradation curves fall into a reasonably thin band for the strain interval shown. However, while the stiffness "decay length" is similar for different rebar angles, major differences occur in both the "initial" stiffness

---

* Secant and tangent stiffness are equivalent when the interface bond is perfect and the rebar remains elastic.

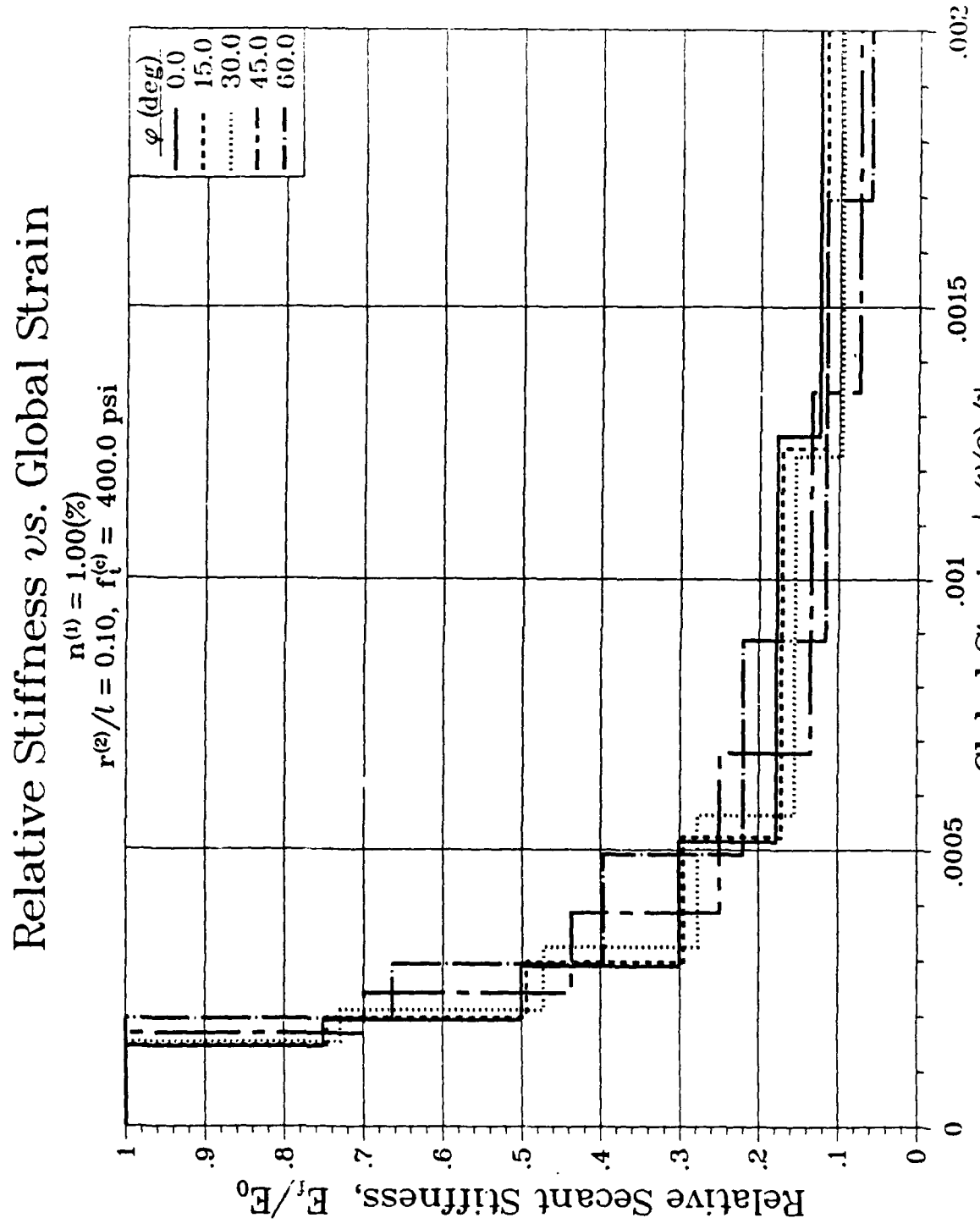

Figure 10.1. Degradation of overall secant stiffness.

(zero strain, E_o) and the "final" stiffness (∞ strain, $E_{f\infty}$). The variations in these initial and final stiffness with rebar angle are depicted in Figures 10.2 and 10.3 for steel volume fractions ranging from 0.1 to 1.0 percent. Variations in the final stiffness are masked in Figure 10.1 by the fact that they all tend to be approximately an order of magnitude smaller than the initial stiffness.

When reviewing the data depicted in Figure 10.1, it should be recalled that the steel-concrete interface bond has been assumed to be perfect, and the rebar has been taken as elastic. As can be observed in the examples cited for the case $\phi = 0°$, steel-concrete interface slip and rebar plasticity can be expected to alter the foregoing results to a significant degree in some cases.

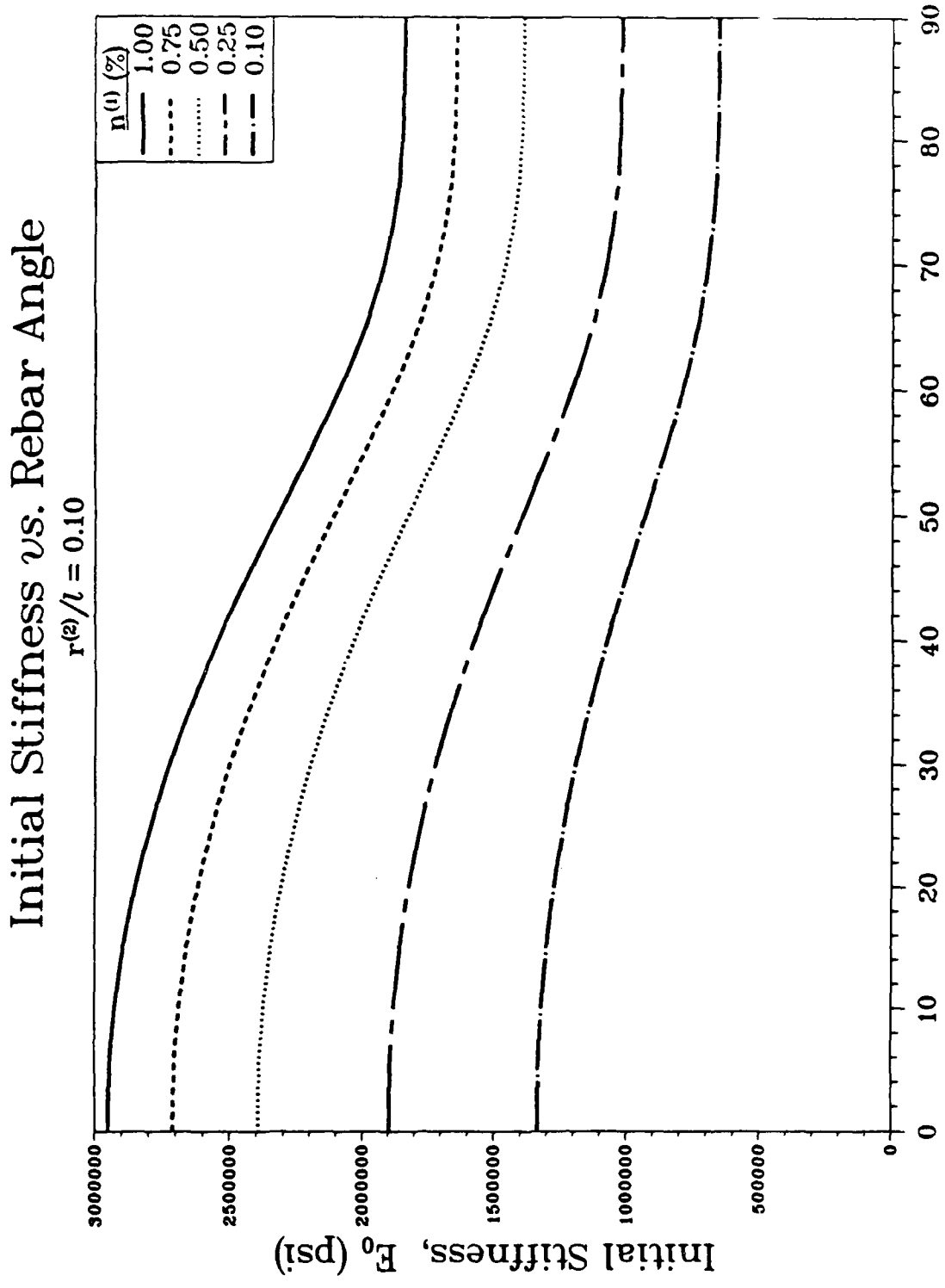

Figure 10.2. "Initial" (zero strain) stiffness.

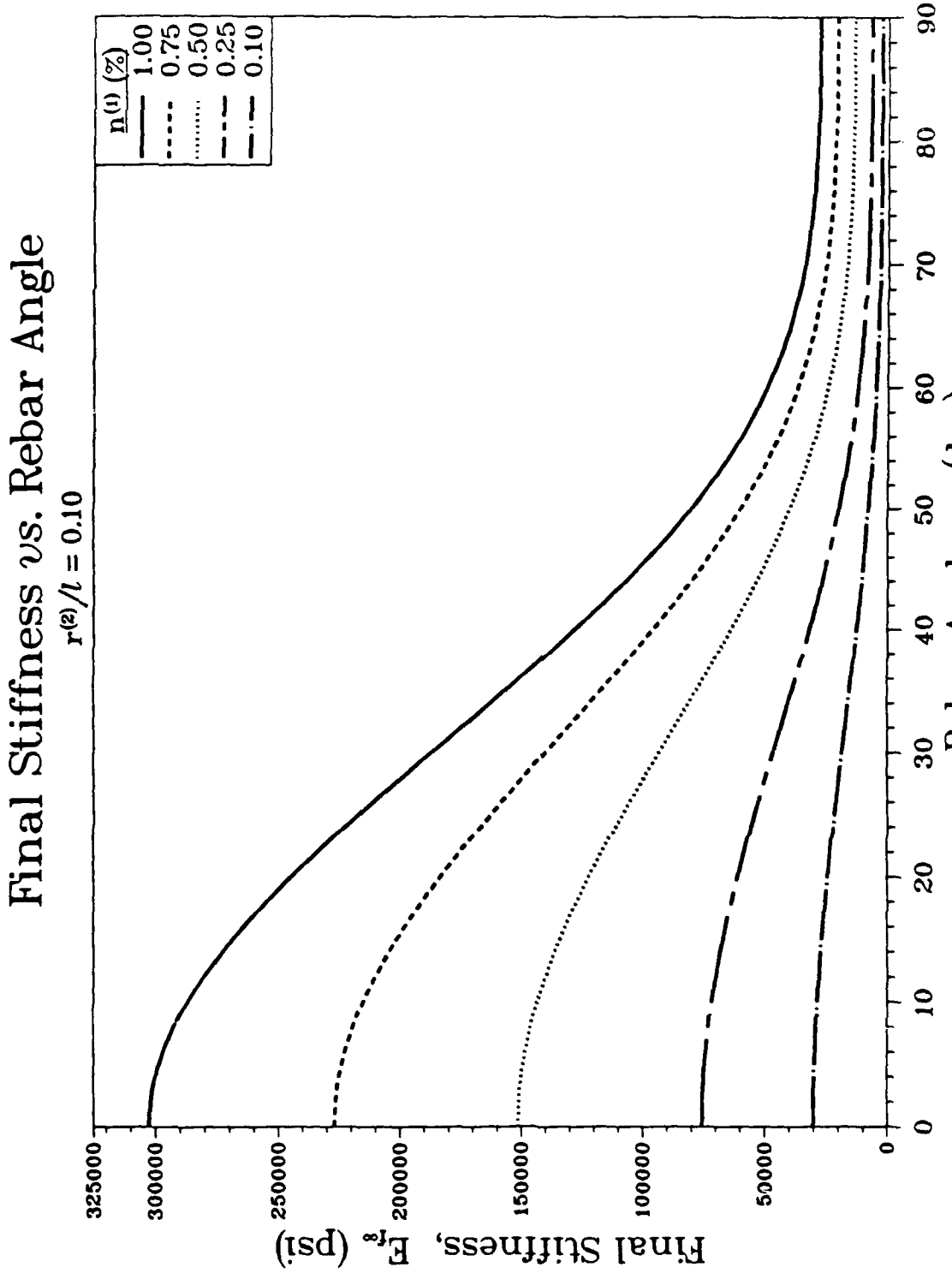

Figure 10.3. "Final" (∞ strain) stiffness.

SECTION 11

EXTENSION OF MIXTURE MODEL TO ORTHOGONAL BI-DIRECTIONAL REBAR LAYOUTS

The mixture models discussed in the preceding sections apply for uniaxial rebar layouts. Most practical cases,however, concern bi-directional or tri-directional layouts.

In what follows, the previous mixture theory is extended to include the case of bi-directional orthogonal rebar layouts. Both rebar plastic deformation and steel-concrete interface slip are included in the analysis.

11.1 A 3D CELL FOR TWO REBAR SYSTEMS.

The R/C material to be considered is depicted in Figure 11.1a. As indicated, two reinforcement systems are now involved. These are designated as Rebar System I and Rebar System II. Both systems are presumed to be periodic. This premise leads to the 3D cell illustrated in Figure 11.1. This cell is adopted as the basic building block in the following development.

11.2 SCALING AND MICROCOORDINATES.

With reference to Figure 11.1, the quantity

$$\bar{\Delta} \equiv \left(\bar{\Delta}_1\bar{\Delta}_2\bar{\Delta}_3\right)^{1/3}/\pi^{1/2} \tag{11.1}$$

is selected to represent the cell "size" and the parameter $\epsilon \equiv \bar{\Delta}/\bar{\Lambda}$ is adopted as the micro-to-macro dimension ratio where the meaning of $\bar{\Lambda}$ is as was indicated in Section 3.1, i.e., $\bar{\Lambda}$ is a reference macro length. Next, the space variables $\mathbf{x}$ and $\mathbf{x}^*$ are defined according to

$$\mathbf{x} = \bar{\mathbf{x}}\,/\bar{\Lambda} \quad , \quad \mathbf{x}^* = \bar{\mathbf{x}}\,/\bar{\Delta} \quad . \tag{11.2}$$

As in the previous analysis for the unidirectional steel layout, the components x_i and x^*_i represent "macro" and "micro" coordinates.

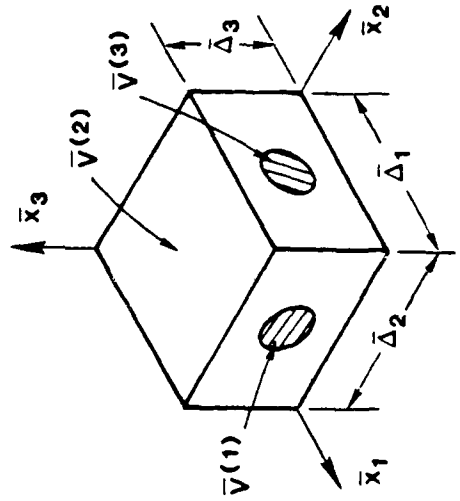

Figure 11.1b. Typical cell.

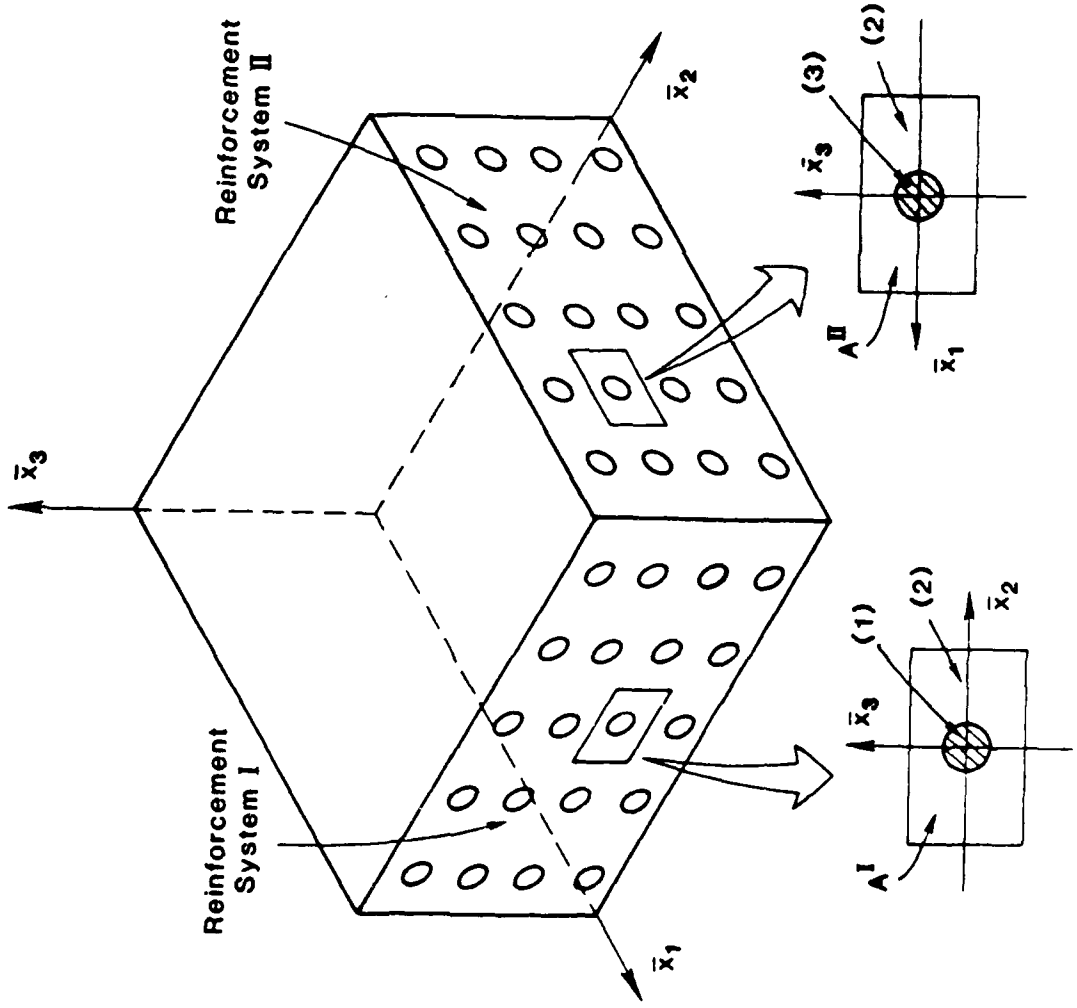

Figure 11.1a. Rebar geometry.

11.3 MULTIVARIABLE-FIELD REPRESENTATION AND x^*-PERIODICITY CONDITION.

For the case of bi-directional steel reinforcement, the x^*-periodicity condition is stated in the form

$$u_i^{(2)}\left[x,-\frac{\sqrt{\pi}\Delta_1}{2},x_2^*,x_3^*\right] = u_i^{(2)}\left[x,\frac{\sqrt{\pi}\Delta_1}{2},x_2^*,x_3^*\right],$$

$$u_1^{(2)}\left[x,x_1^*,-\frac{\sqrt{\pi}\Delta_2}{2},x_3^*\right] = u_i^{(2)}\left[x,x_1^*,\frac{\sqrt{\pi}\Delta_2}{2},x_3^*\right] \tag{11.3}$$

$$u_i^{(2)}\left[x,x_1^*,x_2^*,-\frac{\sqrt{\pi}\Delta_3}{2}\right] = u_i^{(2)}\left[x,x_1^*,x_2^*,\frac{\sqrt{\pi}\Delta_3}{2}\right]$$

11.4 TRIAL DISPLACEMENT FIELD (DISPLACEMENT MICROSTRUCTURE).

Two basic premises are now stated regarding the displacement microstructure. These are:

(1) The interaction between the two sets of rebar layouts which occupy the regions $A^{(1)}$ and $A^{(3)}$ are negligible (this implies that the interaction body force between $\mathbf{u}^{(1)}$ and $\mathbf{u}^{(3)}$ is negligible).

(2) The matrix displacement microstructure can be decomposed as follows:

$$u_i^{(2)}(x,x^*) = u_{i\,(o)}^{(2)}(x) + \epsilon\left[u_{i\,(1)}^{I\,(2)}\left[x,x_2^*,x_3^*\right] + u_{i\,(1)}^{II\,(2)}\left[x,x_3^*,x_1^*\right]\right] + 0(\epsilon^2). \tag{11.4}$$

where the superscripts I and II refer to rebar sets I and II (see Fig. 11.1).

Under the assumptions (1) and (2) above, the trial displacement fields for the rebar and concrete are stated in the form

Rebar Set I (material 1: $\alpha=1$)

$$u_i^{(1)}\left[x,x^*\right] = U_i^{(1)}(x) + \epsilon\left[S_i^{2I}(x)g^{I(1)}\left[x_2^*,x_3^*\right] + S_i^{3I}(x)h^{I(1)}\left[x_2^*,x_3^*\right]\right] \tag{11.5a}$$

Rebar Set II (material 3;α=3)

$$u_i^{(3)}\left[x,x^*\right] = U_i^{(3)}(x) + \epsilon\left[{}^{3II}_{S_i}(x)\,{}^{II}_{g}{}^{(3)}\left[x_3^*,x_1^*\right] + {}^{1II}_{S_i}(x)\,{}^{II}_{h}{}^{(3)}\left[x_3^*,x_1^*\right]\right] \quad (11.5b)$$

Concrete (material 2;α=2)

$$u_i^{(2)}\left[x,x^*\right] = U_i^{(2)}(x) + \epsilon\left[{}^{2I}_{S_i}(x)\,{}^{I}_{g}{}^{(2)}\left[x_2^*,x_3^*\right] + {}^{3I}_{S_i}(x)\,{}^{I}_{h}{}^{(2)}\left[x_2^*,x_3^*\right]\right.$$

$$\left. + {}^{3II}_{S_i}(x)\,{}^{II}_{g}{}^{(2)}\left[x_3^*,x_1^*\right] + {}^{1II}_{S_i}(x)\,{}^{II}_{h}{}^{(2)}\left[x_3^*,x_1^*\right]\right] \quad (11.5c)$$

where

$${}^{3I}_{S_2}(x) = {}^{2I}_{S_3}(x) \quad (11.6a)$$

$${}^{3II}_{S_1}(x) = {}^{1II}_{S_3}(x)\ . \quad (11.6b)$$

A typical cubic cell is now considered as illustrated in Fig. 11.2. Further, a multiple concentric cylinder's approximation for this cell is adapted as depicted in Fig. 11.2. (The length of this cell is adjusted to retain the original volume of the matrix). Within the context of the concentric cylinder's approximation, the trial displacements (11.5) are rewritten in the form

Rebar Set I

$$u_i^{(1)}\left[x,x^*\right] = U_i^{(1)}(x) + \epsilon\left[{}^{2I}_{S_i}(x)\,g^{(1)}(r_I)\cos\theta_I + {}^{3I}_{S_i}g^{(1)}(r_I)\sin\theta_I\right] + O(\epsilon^2)$$

$$= U_i^{(1)}(x) + \epsilon\left[{}^{2I}_{S_i}(x)\,\frac{x_2^*}{n^{(1)}} + {}^{3I}_{S_i}(x)\,\frac{x_3^*}{n^{(1)}}\right] + O(\epsilon^2) \quad (11.7a)$$

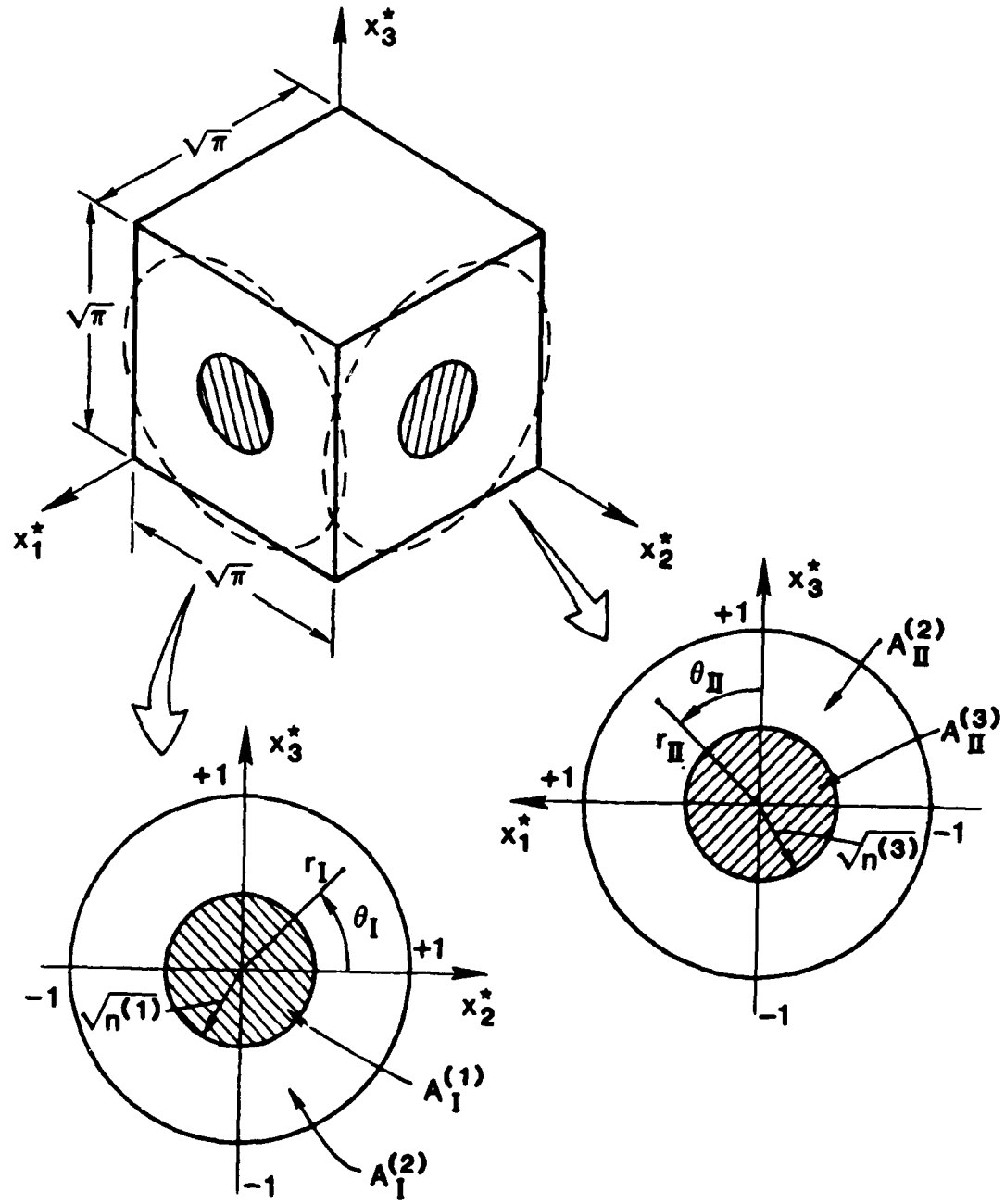

Figure 11.2. Cubic cell and circular cylinder approximation.

where

$$g^{(1)}(r_I) = \frac{r_I}{n^{(1)}} \tag{11.7b}$$

Rebar Set II

$$u_i^{(3)}(x,x^*) = U_i^{(3)}(x) + \epsilon\left[S_i^{3II}(x)h^{(3)}(r_{II})\cos\theta_{II} + S_i^{1II}(x)h^{(3)}(r_{II})\sin\theta_{II}\right] + O(\epsilon^2)$$

$$= U_i^{(3)}(x) + \epsilon\left[S_i^{3II}(x)\frac{x_3^*}{n^{(3)}} + S_i^{1II}(x)\frac{x_1^*}{n^{(3)}}\right] + O(\epsilon^2)\ , \tag{11.8a}$$

where

$$h^{(3)}(r_{II}) = \frac{r_{II}}{n^{(3)}} \tag{11.8b}$$

Concrete

$$u_i^{(2)}(x,x^*) = U_i^{(2)}(x) + \epsilon\left[S_i^{2I}(x)g^{(2)}(r_I)\cos\theta_I + S_i^{3I}(x)g^{(2)}(r_I)\sin\theta_I\right]$$

$$+ \epsilon\left[S_i^{3II}(x)h^{(2)}(r_{II})\cos\theta_{II} + S_i^{1II}(x)h^{(2)}(r_{II})\sin\theta_{II}\right]$$

$$+ O(\epsilon^2)$$

$$= U_i^{(2)}(x) + \epsilon\left[S_i^{2I}(x)\left(\frac{1}{1-n^{(1)}}\right)\left(-x_2^* + \frac{x_2^*}{x_2^{*2}+x_3^{*2}}\right)\right.$$

$$\left. + S_i^{3I}(x)\left(\frac{1}{1-n^{(1)}}\right)\left(-x_3^* + \frac{x_3^*}{x_2^{*2}+s_3^{*2}}\right)\right.$$

$$+ S_i^{3II}(x)\left[\frac{1}{1 - n^{(3)}}\right]\left[- x_3^* + \frac{x_3^*}{x_3^{*2} + x_1^{*2}}\right]$$

$$+ S_i^{1II}(x)\left[\frac{1}{1 - n^{(3)}}\right]\left[- x_1^* + \frac{x_1^*}{x_3^{*2} + x_1^{*2}}\right]\Bigg] + O(\epsilon^2) \qquad (11.9a)$$

where

$$g^{(2)}(r_I) = \frac{1}{1 - n^{(1)}}\left[- r_I + \frac{1}{r_I}\right], \qquad (11.9b)$$

$$h^{(2)}(r_{II}) = \frac{1}{1 - n^{(3)}}\left[- r_{II} + \frac{1}{r_{II}}\right].$$

11.5 PRINCIPLE OF VIRTUAL WORK FOR SYNTHESIZED FIELD.

In a manner similar to that described for a single rebar set, the principle of virtual work for the synthesized field can be written as

$$\iiint_V \Bigg[\sum_{\alpha=1}^{3} \iiint_{V_*^{(\alpha)}} \sigma_{ij}^{(\alpha)} \delta e_{ij}^{(\alpha)}\, dV_* + \frac{1}{\epsilon}\iint_{\partial V_*^{(1)}} \tau_i^{*I}\left(\delta u_i^{(2)} - \delta u_i^{(1)}\right) dS_I^* dx_1^*$$

$$+ \frac{1}{\epsilon}\iint_{\partial V_*^{(3)}} \tau_i^{*II}\left(\delta u_i^{(2)} - \delta u_i^{(3)}\right) dS_{II}^* dx_2^*\Bigg] dV \qquad (11.10)$$

$$= \iiint_V \Bigg[\sum_{\alpha=1}^{3} \iiint_{V_*^{(\alpha)}} f_i^{(\alpha)} \delta u_i^{(\alpha)} dV_*\Bigg] dV + \iint_{\partial V_T}\Bigg[\sum_{\alpha=1}^{3} \iiint_{V_*^{(\alpha)}} \tau_i^{(\alpha)} \delta u_i^{(\alpha)} dV_*\Bigg] dS$$

where $dV = dx_1 dx_2 dx_3$, and $dV_* = dx_1^* dx_2^* dx_3^*$.

and where

$$e_{ij} = \frac{1}{2}\left[u_{i,j} + u_{j,i} + \frac{1}{\epsilon}\left(u_{i,j^*} + u_{j,i^*}\right)\right] , \tag{11.11}$$

$$\delta e_{ij} = \frac{1}{2}\left[\delta u_{i,j} + \delta u_{j,i} + \frac{1}{\epsilon}\left(\delta u_{i,j^*} + \delta u_{j,i^*}\right)\right] , \tag{11.12}$$

11.6 MIXTURE EQUATIONS OF EQUILIBRIUM.

The trial displacement functions (11.7) - (11.8) are now substituted into (11.11) and (11.12) and only those terms up to an including 0(1) are retained. The result is then substituted in (11.10), together with the displacement functions where required. Upon again retaining only 0(1) terms, one thus obtains the following form of the principle of virtual work after appropriate integrations by parts:

$$\iint_{\partial V_T}\left[\sum_{\alpha=1}^{3}\left(n^{(\alpha)}t_i^{(\alpha a)} - n^{(\alpha)}\sigma_{ij}^{(\alpha a)}\nu_j\right)\delta U_i^{(\alpha)}\right] dS$$

$$+ \iiint_{V}\Big[\left(n^{(1)}\sigma_{ji,j}^{(1a)} + n^{(1)}f_i^{(1a)} + P_i^{I}\right)\delta U_i^{(1)} + \left(n^{(3)}\sigma_{ji,j}^{(3a)} + n^{(3)}f_i^{(3a)} + P_i^{II}\right)\delta U_i^{(3)}$$

$$+ \left(n^{(2)}\sigma_{ji,j}^{(2a)} + n^{(2)}f_i^{(2a)} - P_i^{I} - P_i^{II}\right)\delta U_i^{(2)} - \left(\sigma_{12}^{(1a)} - \frac{n^{(2)}}{1 - n^{(1)}}\sigma_{12}^{(2a)}\right.$$

$$\left. + n^{(2)}Q_{12}^{I} + n^{(2)}Q_{13}^{I}\right)\delta S_1^{2I}$$

$$- \left(\sigma_{22}^{(1a)} - \frac{n^{(2)}}{1 - n^{(1)}}\sigma_{11}^{(2a)} + n^{(2)}Q_{22}^{I} + n^{(2)}Q_{23}^{I}\right)\delta S_2^{2I} - \left(2\sigma_{23}^{(1a)} + n^{(2)}R_{22}^{I}\right.$$

$$\left. + n^{(2)}Q_{33}^{I} - \frac{2n^{(2)}}{1 - n^{(1)}}\sigma_{23}^{(2a)} + n^{(2)}R_{23}^{I} + n^{(2)}Q_{32}^{I}\right)\left(\delta S_2^{3I} = \delta S_3^{2I}\right)$$

$$- \left[\sigma_{31}^{(1a)} - \frac{n^{(2)}}{1 - n^{(1)}}\sigma_{31}^{(2a)} + n^{(2)}R_{13}^{I} + n^{(2)}R_{12}^{I}\right]\delta S_1^{3I}$$

$$- \left[\sigma_{33}^{(1a)} - \frac{n^{(2)}}{1 - n^{(1)}}\sigma_{33}^{(2a)} + n^{(2)}R_{33}^{I} + n^{(2)}R_{32}^{I}\right]\delta S_3^{3I}$$

$$- \left[2\,\sigma_{31}^{(3a)} + n^{(2)}Q_{11}^{II} + n^{(2)}R_{33}^{II} - \frac{2n^{(2)}}{1 - n^{(3)}}\sigma_{31}^{(2a)} + n^{(2)}R_{31}^{II} + n^{(3)}Q_{13}^{II}\right]$$

$$\left(\delta S_1^{2II} = \delta S_3^{1II}\right) - \left[\sigma_{23}^{(3a)} - \frac{n^{(2)}}{1 - n^{(3)}}\sigma_{23}^{(2a)} + n^{(2)}Q_{23}^{II} + n^{(2)}Q_{21}^{II}\right]\delta S_2^{3II}$$

$$- \left[\sigma_{33}^{(3a)} - \frac{n^{(2)}}{1 - n^{(3)}}\sigma_{33}^{(2a)} + n^{(2)}\,Q_{33}^{II} + n^{(2)}Q_{31}^{II}\right]\delta S_3^{3II}$$

$$- \left[\sigma_{11}^{(3a)} - \frac{n^{(2)}}{1 - n^{(3)}}\sigma_{11}^{(2a)} + n^{(2)}R_{11}^{II} + n^{(2)}R_{13}^{II}\right]\delta S_1^{1II}$$

$$- \left[\sigma_{12}^{(3a)} + n^{(2)}R_{23}^{II} - \frac{n^{(2)}}{1 - n^{(3)}}\sigma_{12}^{(2a)} + n^{(2)}R_{21}^{II}\right]\delta S_2^{1II}\Bigg]dV = 0 \quad . \qquad (11.13)$$

The Euler-Lagrange equations of (11.13) lead immediately to the following mixture equilibrium equations and associated internal condensation relations which can be used to eliminate the variables $\mathbf{S}^{I}$ and $\mathbf{S}^{II}$.

Mixture Equilibrium Equations.

$$n^{(1)}\sigma_{ji,j}^{(1a)} + n^{(1)}f_i^{(1a)} + P_i^{I} = 0 \quad , \qquad (11.14a)$$

$$n^{(3)}\sigma_{ji,j}^{(3a)} + n^{(3)}f_i^{(3a)} + P_i^{II} = 0 \quad , \qquad (11.14b)$$

$$n^{(2)}\sigma_{ji,j}^{(2a)} + n^{(2)}f_i^{(2a)} - P_i^{I} - P^{II} = 0 \quad , \qquad (11.14c)$$

Internal Condensation Relations.

$$\sigma_{12}^{(1a)} - \frac{n^{(2)}}{1 - n^{(1)}} \sigma_{12}^{(2a)} + n^{(2)} \left[Q_{12}^{I} + Q_{13}^{I} \right] = 0 , \tag{11.15a}$$

$$\sigma_{22}^{(1a)} - \frac{n^{(2)}}{1 - n^{(1)}} \sigma_{11}^{(2a)} + n^{(2)} \left[Q_{22}^{I} + Q_{23}^{I} \right] = 0 . \tag{11.15b}$$

$$\sigma_{23}^{(1a)} - \frac{n^{(2)}}{1 - n^{(1)}} \sigma_{23}^{(2a)} + \frac{n^{(2)}}{2} \left[R_{22}^{I} + Q_{33}^{I} + R_{23}^{I} + Q_{32}^{I} \right] = 0 , \tag{11.15c}$$

$$\sigma_{31}^{(1a)} - \frac{n^{(2)}}{1 - n^{(1)}} \sigma_{31}^{(2a)} + n^{(2)} \left[R_{13}^{I} + R_{12}^{I} \right] = 0 , \tag{11.15d}$$

$$\sigma_{33}^{(1a)} - \frac{n^{(2)}}{1 - n^{(1)}} \sigma_{33}^{(2a)} + n^{(2)} \left[R_{33}^{I} + R_{32}^{I} \right] = 0 , \tag{11.15e}$$

$$\sigma_{31}^{(3a)} - \frac{n^{(2)}}{1 - n^{(3)}} \sigma_{31}^{(2a)} + \frac{n^{(2)}}{2} \left[Q_{11}^{II} + R_{33}^{II} + R_{31}^{II} + Q_{13}^{II} \right] = 0 , \tag{11.16a}$$

$$\sigma_{23}^{(3a)} - \frac{n^{(2)}}{1 - n^{(3)}} \sigma_{23}^{(2a)} + n^{(2)} \left[Q_{23}^{II} + Q_{21}^{II} \right] = 0 , \tag{11.16b}$$

$$\sigma_{33}^{(3a)} - \frac{n^{(2)}}{1 - n^{(3)}} \sigma_{33}^{(2a)} + n^{(2)} \left[Q_{33}^{II} + Q_{31}^{II} \right] = 0 , \tag{11.16c}$$

$$\sigma_{11}^{(3a)} - \frac{n^{(2)}}{1 - n^{(3)}} \sigma_{11}^{(2a)} + n^{(2)} \left[R_{11}^{II} + R_{13}^{II} \right] = 0 , \tag{11.16d}$$

$$\sigma_{12}^{(3a)} - \frac{n^{(2)}}{1 - n^{(3)}} \sigma_{12}^{(2a)} + n^{(2)} \left[R_{23}^{II} + R_{21}^{II} \right] = 0 , \tag{11.16e}$$

Boundary Conditions.

$$\delta U_i^{(\alpha)} = 0 \quad \text{or} \quad n^{(\alpha)} \sigma_{ji}^{(\alpha a)} = n^{(\alpha)} \Psi_i^{(\alpha a)} \tag{11.17}$$

Averages

$$\sigma_{ij}^{(\alpha a)} \equiv \frac{1}{n^{(\alpha)}\pi^{3/2}} \iiint_{V_*^{(\alpha)}} \sigma_{ij}^{(\alpha)} dV_* \tag{11.18a}$$

$$\left(R_{ij}^{I}, R_{ij}^{II}\right) = \frac{1}{n^{(2)}\pi^{3/2}} \iiint_{V_*^{(2)}} \left(h_{i,j*}^{I},\ h_{i,j*}^{II}\right) \sigma_{ij}^{(2)} dV_* \quad , \tag{11.18b}$$

$$\left(Q_{ij}^{I}, Q_{ij}^{II}\right) = \frac{1}{n^{(2)}\pi^{3/2}} \iiint_{V_*^{(2)}} \left(g_{i,j*}^{I},\ g_{i,j*}^{II}\right) \sigma_{ij}^{(2)} dV_* \quad , \tag{11.18c}$$

$$P_i^{I} = \frac{1}{\epsilon\pi^{3/2}} \iint_{\partial V_*^{(1)}} \psi_i^{I*} dS^* \tag{11.18d}$$

$$P_i^{II} = \frac{1}{\epsilon\pi^{3/2}} \iint_{\partial V_*^{(3)}} \psi_i^{*II}\ dS^* \tag{11.18e}$$

in which dS^* is an infinitesimal interface area element on $\partial V_*^{(1)}$ or $\partial V_*^{(3)}$; and

$$f_i^{(\alpha a)} = \frac{1}{n^{(\alpha)}\pi^{3/2}} \iiint_{V_*^{(\alpha)}} f_i^{(\alpha)} dV_* \quad , \tag{11.18f}$$

$$\psi_i^{(\alpha a)} = \frac{1}{n^{(\alpha)}\pi^{3/2}} \iiint_{V_*^{(\alpha)}} \psi_i^{(\alpha)} dV_* \tag{11.18g}$$

11.7 MIXTURE CONSTITUTIVE RELATIONS.

In order to generate appropriate mixture constitutive relations to accompany the equilibrium equations (11.14), one can utilize a mixed weighted residual procedure. The situation here is similar to that encountered for the case of a single rebar set.

Trial Displacement Field.

The trial displacement field (11.7) - (11.9) is again used in the mixed residual procedure. This field can be expressed in the form

$$u^{(\alpha)}(x,x^*;\epsilon) = U^{(\alpha)}(x) + \epsilon G^{(\alpha)}(x^*)S \quad , \tag{11.19a}$$

where

$$S \equiv \left[{}^{2I}_{S_1}, {}^{2I}_{S_2}, {}^{2I}_{S_3}\left(= {}^{3I}_{S_2}\right), {}^{3I}_{S_1}, {}^{3I}_{S_3}, {}^{3II}_{S_1}\left(= {}^{1I}_{S_3}\right), {}^{3II}_{S_2}, {}^{3II}_{S_3}, {}^{1II}_{S_1}, {}^{1II}_{S_2}\right]^T \quad . \tag{11.19b}$$

This trial field leads to the following strain field via (11.11) when terms of 0(1) only are retained:

$$e^{(\alpha)} = E\left(U^{(\alpha)}\right) + Q^{(\alpha)}(x^*)S(x) \tag{11.20a}$$

where

$$E\left(U^{(\alpha)}\right) \equiv \left[U_{1,1}, U_{2,2}, U_{3,3}, U_{2,3} + U_{3,2}, U_{1,3} + U_{3,1}, U_{1,2} + U_{2,1}\right]^{(\alpha)} \tag{11.20b}$$

Trial Stress Field.

The trial stress field to be used in the mixed residual procedure is selected in the form:

$$\sigma_{ij}^{(\alpha)}(x,x^*;\epsilon) = \tau_{ij}^{(\alpha)}(x) + \delta_{\alpha 2}\, T_{ijk\ell}(x^*)\, t_{k\ell}^{(2)}(x) + \epsilon \sigma_{ij(1)}^{(\alpha)} \tag{11.21a}$$

where

$$\iiint_{V_*^{(2)}} T_{ijk\ell}(x^*)\, dV_* = 0 \quad , \tag{11.21b}$$

and where $\sigma^{(\alpha)}_{ij(1)}$ are defined by

$$\begin{bmatrix} \sigma_{11(1)} \\ \sigma_{22(1)} \\ \sigma_{33(1)} \\ \sigma_{23(1)} \\ \sigma_{31(1)} \\ \sigma_{12(1)} \end{bmatrix}^{(\alpha)} = \begin{bmatrix} \frac{1}{4} P_3^{II}(x) g^{II(\alpha)}(x^*) + \frac{3}{4} P_1^{II}(x) + h^{II(\alpha)}(x^*) \\ \frac{3}{4} P_2^{I}(x) g^{I(\alpha)}(x^*) + \frac{1}{4} P_3^{I}(x^*) h^{I(\alpha)}(x^*) \\ \frac{1}{4} P_2^{I}(x) g^{I(\alpha)}(x^*) + \frac{3}{4} P_3^{I}(x) h^{I(\alpha)}(x^*) + \frac{3}{4} P_3^{II}(x) g^{II(\alpha)}(x^*) + \frac{1}{4} P_1^{II}(x) h^{II(\alpha)}(x^*) \\ \frac{1}{4} P_2^{I}(x) h^{I(\alpha)}(x^*) + \frac{1}{4} P_3^{I}(x) g^{I(\alpha)}(x^*) + \frac{1}{4} P_2^{II}(x) g^{II(\alpha)}(x^*) \\ \frac{1}{2} P_1^{I}(x) h^{I(\alpha)}(x^*) + \frac{1}{4} P_3^{II}(x) h^{II(\alpha)}(x^*) + \frac{1}{4} P_1^{II}(x) g^{II(\alpha)}(x^*) \\ \frac{1}{2} P_1^{I}(x) g^{I(\alpha)}(x^*) + \frac{1}{4} P_2^{II}(x) h^{II(\alpha)}(x^*) \end{bmatrix} \tag{11.21c}$$

or by

$$\sigma_{(1)}^{(\alpha)} = H_I^{(\alpha)}(x^*) P^I(x) + H_{II}^{(\alpha)}(x^*) P^{II}(x) \tag{11.21d}$$

where

$$P^I \equiv \left[P_1^I, P_2^I, P_3^I\right]^T , \quad P^{II} \equiv \left[P_1^{II}, P_2^{II}, P_3^{II}\right]^T . \tag{11.21e}$$

Thus, (11.21a) can be rewritten as

$$\sigma^{(\alpha)}(x, x^*) = \tau^{(\alpha)}(x) + \delta_{\alpha 2} T^{(2)}(x^*) t^{(2)}(x) + \epsilon H_I^{(\alpha)}(x^*) P^I(x) + \epsilon H_{II}^{(\alpha)}(x^*) P^{II}(x) . \tag{11.22}$$

Several remarks are in order at this point. First, the first two terms of the trial stress field (11.22), i.e.

$$\sigma_{(o)}^{(\alpha)} = \tau^{(\alpha)}(x) + T^{(2)}(x^*) t^{(2)} \delta_{\alpha 2}$$

was constructed to satisfy $\sigma^{(\alpha)}_{ji(o),j^*} = 0$ and may be obtained from the displacement $u^{(\alpha)}$ in (11.19a). Second, it is noted that

$$\iiint_{V_*^{(2)}} T^{(2)}(x^*)\,dV_* = 0\ ,\quad \iiint_{V_*^{(\alpha)}} H_I^{(\alpha)}\,dV_* = 0\ ,\quad \iiint_{V_*^{(\alpha)}} H_{II}^{(\alpha)}\,dV_* = 0$$

so that

$$\iiint_{V_*^{(2)}} \sigma_{(o)}^{(2)}\,dV_* = \pi^{3/2}\tau^{(2)}(x)$$

i.e., $\tau^{(\alpha)}$ is the average stress $\sigma^{(\alpha a)}$.

Finally, the forms $\mathbf{P}^{I}$ and $\mathbf{P}^{II}$ introduced where constructed to satisfy the integrability condition for $u^{(\alpha)}_{i(2)}$:

$$\frac{1}{\pi^{3/2}} \iiint_{\partial V_*^{(1)}} \sigma^{(1)}_{ji(1),j^*}\,dA_I = P_i^I\ ,\quad \frac{1}{\pi^{3/2}} \iiint_{\partial V_*^{(3)}} \sigma^{(3)}_{ji(i),j^*}\,dA_{II} = P_i^{II}\ .$$

Local Constitutive Relations.

The local constitutive relations for each component material are specified in the rate-form

$$\dot{\mathbf{e}}^{(\alpha)} = \mathbf{C}^{(\alpha)}\dot{\boldsymbol{\sigma}}^{(\alpha)} \tag{11.23}$$

where $\dot{\mathbf{e}}^{(\alpha)}$ is a 6x1 matrix, $\mathbf{C}^{(\alpha)}$ is a 6x6 matrix, and $\dot{\boldsymbol{\sigma}}^{(\alpha)}$ is a 6x1 matrix. The coefficients $\mathbf{C}^{(\alpha)}$ are tangent moduli. Thus, (11.23) incorporates incremental plasticity. All stresses in (11.23) are transverse stresses.

Mixed Weighted Residual Form.

The appropriate form of the mixed weighted residual for the present problem is

$$\iiint_{V} \left[\sum_{\alpha=1}^{3} \iiint_{V_*^{(\alpha)}} \left\{\delta\dot{\boldsymbol{\sigma}}^{(\alpha)T}\dot{\boldsymbol{\sigma}}^{(\alpha)T} + \delta\dot{\boldsymbol{\sigma}}^{(\alpha)T}\left[\dot{\mathbf{e}}^{(\alpha)} - \mathbf{C}^{(\alpha)}\dot{\boldsymbol{\sigma}}^{(\alpha)}\right\}dV_*\right.$$

$$+\frac{1}{\epsilon}\iint_{\partial V_*^{(1)}}\left[\delta\dot{u}^{(2)}-\delta\dot{u}^{(1)}\right]^T\dot{t}^{II}\,dS_I^*dx_1^*+\frac{1}{\epsilon}\iint_{\partial V_*^{(3)}}\left[\delta\dot{u}^{(2)}-\delta\dot{u}^{(3)}\right]\dot{t}^{*II}\,dS_{II}^*dx_2^*$$

$$=\iiint_V\left[\sum_{\alpha=1}^{2}\iiint_{V_*^{(\alpha)}}\delta\dot{u}^{(\alpha)T}f^{(\alpha)}\,dV_*\right]dV+\iint_{\partial V_T}\left\{\sum_{\alpha=1}^{2}\iiint_{V_*^{(\alpha)}}\delta\dot{u}^{(\alpha)}\dot{t}^{(\alpha)}\,dV_*\right\}dS, \tag{11.24}$$

where

$$\dot{e}^{(\alpha)}\equiv\left[\dot{e}_{11},\dot{e}_{22},\dot{e}_{33},2\dot{e}_{23},2\dot{e}_{31},2\dot{e}_{12}\right]^{(\alpha)T} \tag{11.25}$$

Homogenized Rate Constitutive Relations.

Upon substitution of the fields

$$\begin{aligned}\dot{u}^{(\alpha)}&=\dot{U}^{(\alpha)}(x)+\epsilon G^{(\alpha)}(x^*)\dot{S}(x)\quad,\\ \dot{e}^{(\alpha)}&=E\left[\dot{U}^{(\alpha)}\right]+Q^{(\alpha)}(x^*)\dot{S}\quad,\\ \dot{\sigma}^{(\alpha)}&=\dot{\tau}^{(\alpha)}+\delta_{\alpha 2}T^{(2)}(x^*)\dot{t}^{(2)}+\epsilon H_I^{(\alpha)}(x^*)\dot{p}^{I}(x)+\epsilon H_{II}^{(\alpha)}(x^*)\dot{p}^{II}(x)\end{aligned} \tag{11.26}$$

into (11.24), one obtains, as the Euler-Lagrange equations, the rate form of (11.14) - (11.16) together with the rate constitutive relations

$$E\left[\dot{U}^{(\alpha)}\right]+\left[\frac{1}{V_*}\iiint_{V_*^{(\alpha)}}Q^{(\alpha)}(x^*)\,dV_*\right]\dot{S}-\left[\frac{1}{V_*}\iiint_{V_*^{(\alpha)}}C^{(\alpha)}\,dV_*\right]\dot{\tau}^{(\alpha)}$$

$$-\delta_{\alpha 2}\left[\frac{1}{V_*}\iiint_{V_*^{(\alpha)}}C^{(\alpha)}T^{(2)}\,dV_*\right]\dot{t}^{(2)}+\epsilon\left[\frac{1}{V_*}\iiint_{V_*}C^{(\alpha)}H_I^{(\alpha)}\,dV_*\right]\dot{p}^{I}$$

$$+ \epsilon \left[\frac{1}{V_*} \iiint_{V_*^{(\alpha)}} C^{(\alpha)} H_{II}^{(\alpha)} dV_* \right] \dot{\beta}^{II} = 0 \quad , \; \alpha = 1\text{-}3 \; ; \tag{11.27}$$

$$\left[\iiint_{V_*^{(2)}} T^{(2)^T} Q^{(2)} dV_* \right] \dot{S} - \left[\iiint_{V_*^{(2)}} T^{(2)^T} C^{(2)} dV_* \right] \dot{\tau}^{(2)} - \left[\iiint_{V_*^{(2)}} T^{(2)^T} C^{(2)} T^{(2)} V_* \right] \dot{t}^{(2)}$$

$$+ \epsilon \left[\iiint_{V_*^{(2)}} T^{(2)^T} C^{(2)} H_I^{(2)} dV_* \right] \dot{\beta}^{I} + \epsilon \left[\iiint_{V_*^{(2)}} T^{(2)^T} C^{(2)} H_{II}^{(2)} dV_* \right] \dot{\beta}^{II} = 0 \quad , \tag{11.28}$$

$$\left[\dot{U}^{(2)} - \dot{U}^{(1)} \right] + \epsilon \left[\sum_{\alpha} \frac{1}{V_*} \iiint_{V_*^{(\alpha)}} H_I^{(\alpha)^T} Q^{(\alpha)} dV_* \right] \dot{S} - \epsilon \left[\sum_{\alpha} \frac{1}{V_*} \iiint_{V_*^{(\alpha)}} H_I^{(\alpha)^T} C^{(\alpha)} dV_* \right] \dot{\tau}^{(\alpha)}$$

$$- \epsilon \left[\frac{1}{V_*} \iiint_{V_*^{(2)}} H_I^{(2)^T} C^{(2)} T^{(2)} dV_* \right] \dot{t}^{(2)} - \epsilon^2 \left[\sum_{\alpha} \frac{1}{V_*} \iiint_{V_*^{(\alpha)}} H_I^{(\alpha)^T} C^{(\alpha)} H_I^{(\alpha)} dV_* \right] \dot{\beta}^{I}$$

$$- \epsilon^2 \left[\sum_{\alpha} \frac{1}{V_*} \iiint_{V_*^{(\alpha)}} H_I^{(\alpha)^T} C^{(\alpha)} H_{II}^{(\alpha)} dV_* \right] \dot{\beta}^{II} = 0 \; , \tag{11.29}$$

$$\left[\dot{U}^{(2)} - \dot{U}^{(3)} \right] + \epsilon \left[\sum_{\alpha} \frac{1}{V_*} \iiint_{V_*^{(\alpha)}} H_{II}^{(\alpha)^T} Q^{(\alpha)} dV_* \right] \dot{S} - \epsilon \left[\sum_{\alpha} \frac{1}{V_*} \iiint_{V_*^{(\alpha)}} H_{II}^{(\alpha)^T} C^{(\alpha)} dV_* \right] \dot{\tau}^{(\alpha)}$$

$$- \epsilon \left[\frac{1}{V_*} \iiint_{V_*^{(2)}} H_{II}^{(2)^T} C^{(2)} T^{(2)} dV_* \right] \dot{t}^{(2)} - \epsilon^2 \left[\sum_{\alpha} \frac{1}{V_*} \iiint_{V_*^{(\alpha)}} H_{II}^{(\alpha)^T} C^{(\alpha)} H_I^{(\alpha)} dV_* \right] \dot{\beta}^{I}$$

$$- \epsilon^2 \left[\sum_{\alpha} \frac{1}{V_*} \iiint_{V_*^{(\alpha)}} H_{II}^{(\alpha)^T} C^{(\alpha)} H_{II}^{(\alpha)} dV_* \right] \dot{\beta}^{II} = 0 \quad . \tag{11.30}$$

Section 12
LIST OF REFERENCES

Bazant, Z. P., and P. Gambarova (1980), "Rough Cracks in Reinforced Concrete," *J. of the Struct. Div.*, ASCE 106 (ST4), 819.

Bazant, Z. P., and T. Tsubaki (1980), "Slip Dilatancy Model for Cracked Reinforced Concrete," *J. of the Struct. Div.*, ASCE 101 (ST9), 1947.

Drucker, D. C., and W. Prager (1952), "Soil Mechanics and Plastic Analysis or Limit Design," *Quart. Appl. Math.*, 10, 157.

Hegemier, G. A., and G. A. Gurtman (1974), "Finite-Amplitude Elastic-Plastic Wave Propagation in Fiber-Reinforced Composites," *J. Appl. Phys.*, 45.

Hegemier, G. A., H. Murakami and A. Maewal (1979), "On Construction of Mixture Theories for Composite Materials by the Method of Multivariable Asymptotic Expansion," Proceedings, Third International Symposium on Continuum Models of Discrete Systems, Freudenstad, Germany.

Murakami, H., A. Maewal and G. A. Hegemier (1981), "A Mixture Theory with a Director for Linear Elastodynamics of Periodically Laminated Media," *Intl. J. Solids and Structs.*, 17, 155.

Murakami, H., and G. A. Hegemier (1986), "On Simulating Steel-Concrete Interaction in Reinforced Concrete, Part I: Theoretical Development," *Mechanics of Materials*, 5.

Reissner, E. (1984), "On a Certain Mixed Variational Theory and a Proposed Application," *Intl. J. Numer. Meths. in Engrg.*, 20, 1366.

Reissner, E (1986), "On A Mixed Variational Theorem and On Shear Deformable Plate Theory," *Intl. J. Numer. Meths. in Engng.*, 23, 193.

Seguchi, Y., A. Sindo, Y. Tomita and M. Sunohars (1974), "Sliding Rule of Friction in Plastic Forming of Metal," in J. T. Oden *et al.*, Proc. Intl. Confr. Comp. Methods. in Nonlinear Mechs., University of Texas at Austin, TX, 23-24 September, 603.

APPENDIX B
SSS-R-89-9848

ENDOCHRONIC PLASTIC-FRACTURING THEORY WITH APPLICATION TO PLAIN CONCRETE

H. E. Read

Topical Report

Prepared for

Air Force Office of Scientific Research
Bolling AFB, DC 20332

under

AFOSR Contract No. F49620-84-C-0029

December, 1988

PREFACE

This Topical Report describes a portion of the research conducted by S-CUBED for the Air Force Office of Scientific Research (AFOSR) under Contract F49260-84-C-0029. The research was performed during the period from September 1, 1987 to August 31, 1988. The Principal Investigator for this portion of the research effort was Dr. H. E. Read, while Dr. Spencer T. Wu was the AFOSR Contract Technical Monitor.

The author is indebted to Dr. K.C. Valanis of ENDOCHRONICS, INC., who shared with him early unpublished versions of the formulation of the endochronic plastic-fracturing theory and graciously and patiently participated in numerous discussions of the theory during the course of the research. Also, a special note of appreciation is due to Professor Hidenori Murakami, University of California, San Diego, for a number of helpful discussions. In addition, the author thanks Mr. R. G. Herrmann, S-CUBED, for his expert computational support.

ABSTRACT

A new internal variable theory of plastic-fracturing solids is described. The key concept upon which the theory rests is a mapping that transforms the current, damaged and generally anisotropic state of a material into an isotropic undamaged state. The effect of cracking on the constitutive behavior is accounted for through a second-order integrity tensor ϕ, which is governed by an evolution equation. The integrity tensor also allows anisotropy to be described in a convenient way without introducing a fourth-order tensor, as is the usual approach. The model describes both stiffness degradation and yield limit degradation due to developing damage, as well as dilatancy, and contains, as special cases, several models that are noteworthy, including the classical elastic-fracturing model and the endochronic plasticity model. Finally, the model is applied to recent data on the response of plain concrete to simple tension in the presence of developing damage.

TABLE OF CONTENTS

Section			Page
	PREFACE		2
	ABSTRACT		3
1	INTRODUCTION		6
2	FORMULATION OF MODEL		8
	2.1	Mapping from Current State to Transformed State	8
	2.2	Constitutive Equation for the Transformed State	12
	2.3	Constitutive Equation for the Current State	14
3	UNIAXIAL LOADING		19
	3.1	Governing Equations	19
	3.2	Comments on the Model	22
	3.3	An Incremental Scheme for Integrating the Governing Equations	25
	3.4	Application to Plain Concrete	29
		3.4.1 Determination of Material-Dependent Parameters and Functions	30
		3.4.2 Predicted and Measured Responses	36
4	CONCLUSIONS		39
5	LIST OF REFERENCES		41

LIST OF ILLUSTRATIONS

Figure		Page
1	Various states of the plastic-fracturing body B	10
2	Special cases of the general endochronic plastic-fracturing model for simple tension	24
3	Plot of ϕ versus ϵ^p for two different functions $\phi(\epsilon^p)$, showing their relationship to the critical curve $\phi^*(\epsilon^p)$	26
4	Stress versus strain in the transformed space, showing the corresponding responses for the two different functions $\phi(\epsilon^p)$ depicted in Figure 3	26
5	Response of plain concrete to uniaxial tension, as measured in four different types of tests (from Gopalaratnam and Shah, 1985)	32
6	Schematic of stress-strain curve, showing the manner in which ϵ^e, ϵ^p and ϕ are defined at an arbitrary unloading point P	32
7	Dependence of ϕ on plastic strain for monotonic extension under simple tension	34
8	Stress versus plastic strain in the transformed state for monotonic extension under simple tension, showing yield degradation	34
9	Response of plain concrete to simple tension	37
10	Dependence of ϕ on ϵ and ϵ^p, as predicted by the present constitutive model for plain concrete	38

Section 1

INTRODUCTION

Many of the important questions faced by the Air Force today regarding the hardness of concrete defense structures require a knowledge and understanding of the likelihood that a given structure will fail under a prescribed loading environment. To address this issue in the most cost-effective manner, analytic methods must be available to allow system designers to systematically vary design parameters in an expedient and efficient manner so that an optimum structural design can be achieved. Finite element methods are now available for this purpose, but the results obtained with these methods can only be as accurate as the constitutive relations used in conjunction with them. To examine the hardness of concrete structure requires a constitutive model of plain concrete which not only is capable of describing the inelastic behavior of intact, unfractured material but is capable of describing developing damage and cracking and their effect on the overall constitutive behavior. For a constitutive model to be useful in addressing these important issues, it must be able to treat both elastic, plastic and cracking behavior.

Recently, Valanis and Read (1986) developed an advanced nonlinear constitutive model for plain concrete, on the basis of the endochronic theory of plasticity. The model was applied to an extensive set of laboratory data for a medium strength plain concrete reported by Scavuzzo, *et al.* (1983). The test program consisted of a variety of complex loading paths designed to explore different facets of concrete behavior. The stress paths were selected, however, so that no significant (macroscopic) cracking of the concrete occurred during the tests. As shown by Valanis and Read (1986), the endochronic model for concrete was remarkably successful in describing the behavior of the concrete over the wide variety of complex stress paths explored in the laboratory.

The constitutive model for concrete mentioned above has several limitations, however, which restrict its application to stress states below failure. First, the model is incapable of accounting for the effect of macrocracking on material behavior. Secondly, since the model is isotropic, it is unable to account for the anisotropy that develops when significant macrocracking occurs in preferred directions. Finally, in the case of shearing at fixed hydrostatic pressure, the model exhibits only compaction; the dilatant behavior observed when cracked concrete is sheared cannot be described by this model.

Recently, Valanis (1987, 1988a) developed an approach for extending the endochronic theory to include the effects of damage and fracture. The result is a new endochronic plastic-damaging model which possesses all of the attractive features of the earlier concrete model (Valanis and Read, 1986) but which also can treat cracking, anisotropy and dilatancy. The resulting model appears to have the desired features for describing the complete spectrum of concrete response, including plastic flow, cracking and dilatancy. Anisotropy is accounted for in a clever way through the use of the second-order integrity tensor ϕ rather than by a fourth-order tensor, as is the usual approach. The use of a second-order tensor for this purpose greatly reduces the analytic complexity of the model and simplifies the experimental determination of the material parameters. The model describes both stiffness degradation and yield limit degradation due to developing damage and contains, as special cases, several models that are noteworthy, such as the classical elastic-fracturing model.

Parenthetically, it should be noted that since the endochronic theory contains classical plasticity as a special case (as shown by Valanis, 1980), the approach described herein can also be used to determine the form taken by classical plasticity theory when there is cracking, although this has not been done in the work reported herein.

The present study represents the first attempt to explore the application of the new endochronic plastic-fracturing theory to plain concrete and to develop a numerical approach for dealing with the system of governing equations computationally. After the basic formulation of the new theory is given, attention is focussed on the special case of uniaxial loading to elucidate some of the basic features of the theory. The model is applied to the problem of the response of plain concrete to uniaxial tension in the presence of developing damage, using the recent laboratory data reported by Gopalaratnam and Shah (1985). It is shown that the resulting model describes the observed behavior very well, including the post-peak response and the unloading-reloading behavior. The observed hysteresis during the unload-reload cycles is, however, somewhat greater than the model predicts.

Section 2

FORMULATION OF MODEL

In this section, the basic formulation of the endochronic plastic fracturing model is given, following the work of Valanis (1988a). The key concept, upon which the formulation rests, is a mapping that transforms the current, damaged and generally anisotropic state of a material into an isotropic undamaged state, which is called the "transformed state". Since the standard endochronic plasticity theory applies to isotropic, undamaged material, it is taken here as the constitutive model for the material in the transformed state.*** Then, by using the mapping from the transformed state to the current state, the constitutive relations for an endochronic plastic-fracturing model are found. The effect of cracking is reflected through a second-order integrity tensor $\underset{\sim}{\phi}$, which is governed by an evolution equation.

2.1 MAPPING FROM CURRENT STATE TO TRANSFORMED STATE.

To begin, we note that damage and fracture produce a reduction in material integrity. With this in mind, an integrity tensor, $\underset{\sim}{\phi}$, is introduced which has the following properties: It is a second-order symmetric tensor which is equal to the unit tensor $\underset{\sim}{\delta}$ in the undamaged virgin material and to the null tensor in fully fractured materials, i.e., material which cannot support tensile stress in any direction. The integrity tensor $\underset{\sim}{\phi}$ is positive semi-definite but can be regarded as positive definite in the sense that its norm may be made as close to zero as one wishes, without it actually being zero; this proves to be a useful concept for the purposes of the ensuing analysis. Inasmuch as $\underset{\sim}{\phi}$ is symmetric and may be regarded as positive definite, it can be represented in the polar form

$$\underset{\sim}{\phi} = \underset{\sim}{B}^{T}\,\underset{\sim}{B} \tag{2-1}$$

where $\underset{\sim}{B}^{-1}$ exists and is unique, i.e.,

$$B^{-1}_{ir}\,B_{rj} = \delta_{ij} \tag{2-2}$$

In indicial notation, Eq. (2-1) reads

$$\phi_{ij} = B_{ki}B_{kj} \tag{2-3}$$

*** Other constitutive models, such as those from classical plasticity, for example, could also be used to describe the material in the transformed state.

On the basis of the above considerations, the free energy density ψ for a plastic-fracturing solid may be expressed in the following form:

$$\psi = \frac{1}{2} \sum_{r} C^{r}_{ijk\ell}(\underset{\sim}{\phi}) \left(\epsilon_{k\ell} - q^{r}_{k\ell}\right)\left(\epsilon_{ij} - q^{r}_{ij}\right) \tag{2-4}$$

where

$$C^{r}_{ijk\ell}(\underset{\sim}{\phi}) = A^{r}_{1}\, \phi_{ij}\, \phi_{k\ell} + A^{r}_{2}\, \phi_{ij}\phi_{j\ell} \tag{2-5}$$

Here, in the formalism of internal variable theory, the integrity tensor $\underset{\sim}{\phi}$ is an internal variable which characterizes damage, while the internal variables $\underset{\sim}{q}^{r}$ characterize plastic deformation.

The stress $\underset{\sim}{\sigma}$ is obtained from ψ in the usual manner, i.e.,

$$\underset{\sim}{\sigma} = \frac{\partial \psi}{\partial \underset{\sim}{\epsilon}} \tag{2-6}$$

which, on the basis of Eq. (2-4), leads to the result:

$$\sigma_{ij} = \sum \left\{A^{r}_{1}\phi_{ij}\phi_{k\ell} + A^{r}_{2}\, \phi_{ik}\phi_{j\ell}\right\}\left\{\epsilon_{k\ell} - q^{r}_{k\ell}\right\} \tag{2-7}$$

We now consider a mapping $\hat{\underset{\sim}{x}} = \hat{\underset{\sim}{x}}(\underset{\sim}{x})$ from the current damaged state to the "transformed" state, as shown in Figure 1. If $\underset{\sim}{B}$ is taken as the transpose of the deformation gradient $\underset{\sim}{F}$ between the current and transformed states, i.e.,

$$\underset{\sim}{B} = \underset{\sim}{F}^{T} \tag{2-8}$$

then the strain tensor $\underset{\sim}{\epsilon}$ and internal variables $\underset{\sim}{q}^{r}$ in the transformed state can be defined in terms of the strain tensor $\underset{\sim}{\epsilon}$ and internal variables $\underset{\sim}{q}^{r}$ in the current state as follows:

$$\hat{\epsilon}_{k\ell} = B_{ki}B_{\ell j}\epsilon_{ij} \tag{2-9}$$

or

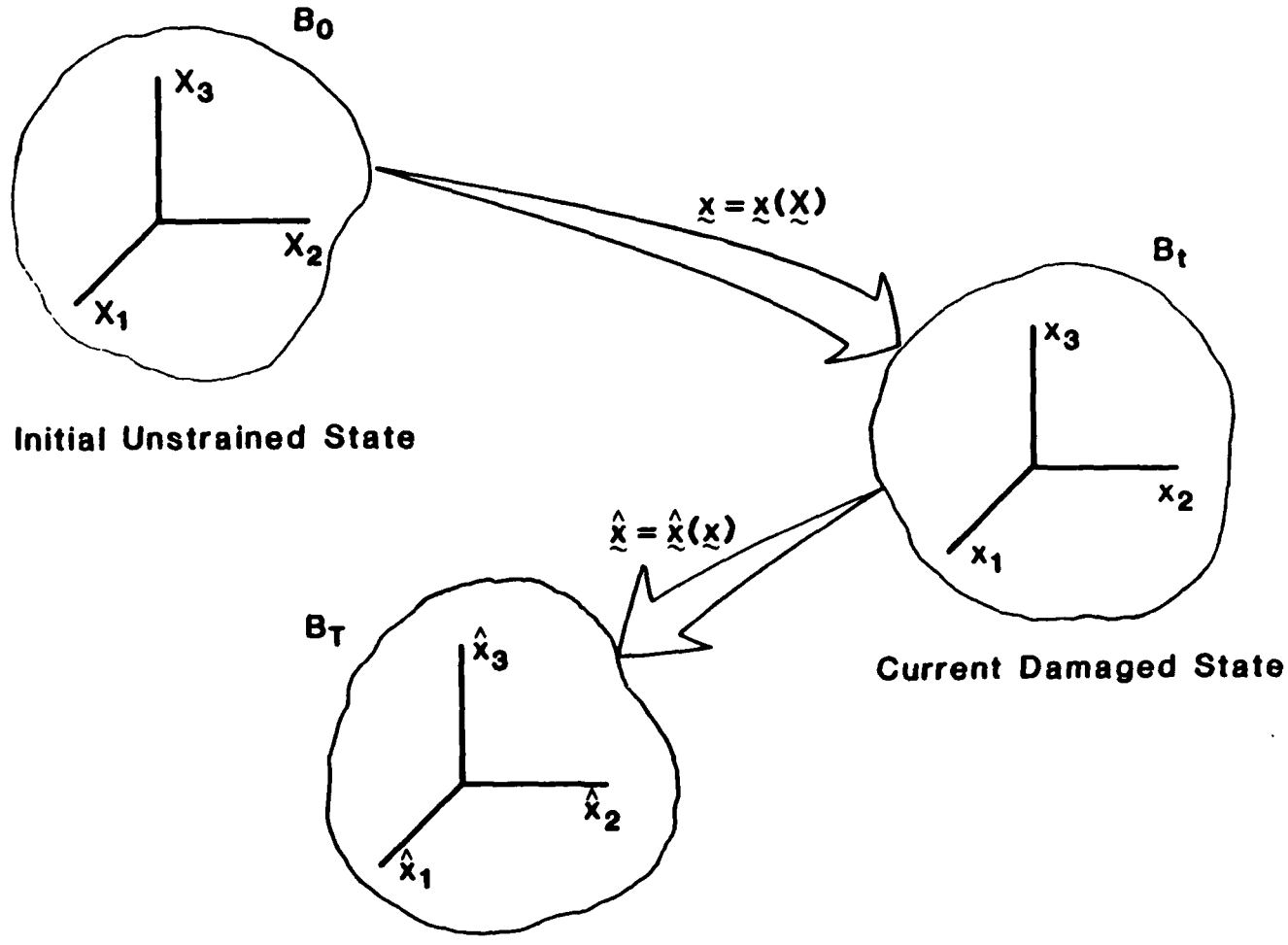

Figure 1. Various states of the plastic-fracturing body B.

$$\epsilon_{k\ell} = B^{-1}_{ki} B^{-1}_{\ell j} \hat{\epsilon}_{ij} \tag{2-10}$$

and

$$\hat{q}^r_{k\ell} = B_{ki} B_{\ell j} q^r_{ij} \tag{2-11}$$

or

$$q^r_{k\ell} = B^{-1}_{ki} B^{-1}_{\ell j} \hat{q}^r_{ij} \tag{2-12}$$

The use of Eqs. (2-2), (2-3) and (2-9) to (2-12) in Eq. (2-4) "normalizes" this last equation and leads to the following simple expression:

$$\psi = \frac{1}{2} \sum_r \left(A^r_1 \delta_{ij} \delta_{k\ell} + A^r_2 \delta_{ik} \delta_{j\ell} \right) \left(\hat{\epsilon}_{ij} - \hat{q}^r_{ij} \right) \left(\hat{\epsilon}_{k\ell} - \hat{q}^r_{k\ell} \right) \tag{2-13}$$

which implies that the material in the transformed state is <u>isotropic</u> and <u>undamaged</u>.

The stress $\underline{\sigma}$ in the transformed state may be obtained by differentiating Eq. (2-13) with respect to $\underline{\epsilon}$, leading to the expression:

$$\hat{\sigma}_{ij} = \sum_r \left\{ A^r_1 \delta_{ij} \left(\hat{\epsilon}_{kk} - \hat{q}^r_{kk} \right) + A^r_2 \left(\hat{\epsilon}_{ij} - \hat{q}^r_{ij} \right) \right\} \tag{2-14}$$

Upon comparing Eqs. (2-7) and (2-14), we find that

$$\hat{\sigma}_{k\ell} = B^{-1}_{ik} B^{-1}_{j\ell} \sigma_{ij} \tag{2-15}$$

or

$$\sigma_{k\ell} = B_{ik} B_{j\ell} \hat{\sigma}_{ij} \tag{2-16}$$

In view of the above developments, it is concluded that the thermodynamic analysis may be done in the transformed state, where the deformed material is both isotropic and undamaged, and then mapped back to the current deformed state, in which the material is both damaged and anisotropic, by means of the transformations (2-9), (2-10), (2-15) and (2-16).

2.2 CONSTITUTIVE EQUATION FOR THE TRANSFORMED STATE.

Consider now the evolution equation for the plastic internal variables $\underset{\sim}{g}^r$ in the transformed state, which we take in the usual form:

$$\frac{\partial \psi}{\partial \hat{\underset{\sim}{g}}^r} + \hat{\underset{\sim}{b}}^r \frac{d\hat{\underset{\sim}{g}}^r}{dz} = 0 \quad , \tag{2-17}$$

Here, $\underset{\sim}{b}^r$ is an isotropic tensor of the fourth order (the "resistance" tensor), in which case it has the following representation:

$$\hat{b}^r_{ijk\ell} = b_1^r \delta_{ij}\delta_{k\ell} + b_2^r \delta_{ik}\delta_{j\ell} \tag{2-18}$$

Note that the tensor $\underset{\sim}{b}^r$ in the current state is related to $\hat{\underset{\sim}{b}}^r$ in the transformed state by the tensor transformation:

$$b^r_{ijk\ell} = B_{ir}B_{js}B_{kt}B_{\ell q}\,\hat{b}^r_{rstq} \tag{2-19}$$

Therefore, in view of Eqs. (2-18) and (2-19), it follows that:

$$b^r_{ijk\ell} = b_1^r \phi_{ij}\phi_{k\ell} + b_2^r \phi_{ik}\phi_{j\ell} \, , \tag{2-20}$$

which shows that the integrity tensor $\underset{\sim}{\phi}$ affects the resistance tensor $\underset{\sim}{b}^r$.

The solution of Eq. (2-17) for a generic r is given elsewhere (see Valanis and Read, 1989), and will not be repeated here. Briefly, $\underset{\sim}{g}^r$ is found from Eq. (2-17), using Eqs. (2-13) and (2-18). The result is substituted into Eq. (2-14), leading to the following result:

$$\hat{\sigma}_{ij} = 2\int_0^{z_D} \mu(z_D - z')\frac{d\hat{e}_{ij}}{dz'}\,dz' + \delta_{ij}\int_0^{z_H} K(z_H - z')\frac{d\hat{\epsilon}_{kk}}{dz'}\,dz' \qquad (2\text{-}21)$$

where

$$dz_D = \frac{d\zeta}{F_D} \quad , \quad dz_H = \frac{d\zeta}{kF_H} \qquad (2\text{-}22)$$

and

$$d\zeta^2 = \left|\left|d\hat{\underset{\sim}{e}}^p\right|\right|^2 + k^2\left(d\hat{\epsilon}^p_{kk}\right)^2 \qquad (2\text{-}23)$$

Here, F_D and F_H are hardening functions for deviatoric and hydrostatic response which satisfy the conditions:

$$F_D > 0 \quad , \quad F_H > 0 \qquad (2\text{-}24)$$

Furthermore, the double bars around a symbol denote its Euclidean norm, and

$$\mu(z_D) = \sum_r \mu_r e^{-\alpha_r z_D}$$
$$K(z_H) = \sum_r K_r e^{-\beta_r z_H} \quad , \qquad (2\text{-}25)$$

where μ_r, K_r, α_r and β_r are all positive constants. Specifically:

$$\mu_r = A_2^r \qquad K_r = A_1^r + \tfrac{1}{3} A_2^r$$
$$\alpha_r = \frac{R_r}{b_2^r} \qquad \beta_r = \phi_r \Big/ \left(b_1^r + \tfrac{1}{3} b_2^r\right) \qquad (2\text{-}26)$$

The above constitutive equation can alternately be expressed in terms of plastic strain integrals with singular kernels. The details for accomplishing this are also given by Valanis and Read (1989). Thus, Eq. (2-20) may be written in the form:

$$\hat{\sigma}_{ij} = \int_0^{z_D} \rho(z_D - z') \frac{d\hat{e}^p_{ij}}{dz'} dz' + \delta_{ij} \int_0^{z_H} \phi(z_H - z') \frac{d\hat{\epsilon}^p_{kk}}{dz'} dz' \qquad (2\text{-}27)$$

where $\rho(z)$ and $\phi(z)$ are weakly singular kernel functions that satisfy the conditions $\rho(0) = \phi(0) = \infty$ such that the integrals

$$\int_0^{z_D} \rho(y)\,dy \quad , \quad \int_0^{z_H} \phi(y)\,dy$$

exist for all $z_D \geq 0$ and $z_H \geq 0$.

To complete the specification of the constitutive model for the transformed state, we must add Hooke's law:

$$\hat{\sigma}_{ij} = \lambda\left(\hat{\epsilon}_{kk} - \hat{\epsilon}^p_{kk}\right)\delta_{ij} + 2\mu\left(\hat{\epsilon}_{ij} - \hat{\epsilon}^p_{ij}\right) \qquad (2\text{-}28)$$

where λ and μ are the Lamé constants.

2.3 CONSTITUTIVE EQUATION FOR THE CURRENT STATE.

The relation between $\underline{\sigma}$ and $\underline{\xi}$ in the current deformed, damaged configuration is found by using Eqs. (2-8) and (2-16) in Eq. (2-26), with the result:

$$\sigma_{rs} = B_{ri}B_{sj} \int_0^{z_D} \rho(z_D - z') \frac{d}{dz'} \left(B_{ik}B_{j\ell}e^p_{k\ell}\right) dz' + \phi_{rs} \int_0^{z_H} \phi(z_H - z') \frac{d}{dz'} \left(\phi_{k\ell}\epsilon^p_{k\ell}\right) dz' \qquad (2\text{-}29)$$

To eliminate the tensor $\underset{\sim}{B}$ from the above expression in favor of the tensor $\underset{\sim}{\phi}$ we proceed according to Valanis (1988b) in the following manner. Since $\underset{\sim}{\phi}$ is a symmetric, second-order tensor, it can be expressed in the form:

$$\underset{\sim}{\phi} = \underset{\sim}{N}\, \underset{\sim}{\phi}^{*}\, \underset{\sim}{N}^{T} \tag{2-30}$$

where $\underset{\sim}{N}$ denotes the matrix of the eigenvectors of $\underset{\sim}{\phi}$, and $\underset{\sim}{\phi}^{*}$ is the (diagonal) matrix of the eigenvalues of $\underset{\sim}{\phi}$. Then, in view of Eqs (2-1) and (2-30), $\underset{\sim}{B}$ can be expressed in terms of $\underset{\sim}{\phi}$ as follows:

$$\underset{\sim}{B} = (\underset{\sim}{\phi}^{*1/2})\, \underset{\sim}{N}^{T} \tag{2-31}$$

which, in indicial notation, reads

$$B_{ij} = (\phi^{*}_{ik})^{1/2}\, N_{jk} \tag{2-32}$$

Thus, on the basis of Eq (2-32), Eq (2-29) can be expressed solely in terms of $\underset{\sim}{\phi}$.

It should also be noted that there are conditions under which Eq (2-29) reduces to a more simplified form. Consider, for instance, the following conditions:

(i) $\underset{\sim}{B}$ is a slowly varying function of z

(ii) ρ and ϕ are rapidly decaying functions such that $F(z')$ may be evaluated at $z' = z$ in the integrals on the righthand side of Eq. (2-29).

In view of (i), we can write:

$$\frac{d}{dz'}\left(B_{ik}B_{j\ell}e^{p}_{k\ell}\right) \sim \underset{\sim}{B}_{ik}\underset{\sim}{B}_{j\ell}\frac{de^{p}_{k\ell}}{dz'}$$

$$\frac{d}{dz'}\left(\phi_{k\ell}\epsilon^{p}_{k\ell}\right) \approx \phi_{k\ell}\frac{d\epsilon^{p}_{k\ell}}{dz'} \tag{2-33}$$

Therefore, on the basis of Eqs. (2-33), Eq. (2-29) can be written as

$$\sigma_{rs} = \phi_{rk}\phi_{s\ell}\int_0^{z_D} \rho(z_D - z')\frac{de^p_{k\ell}}{dz'}\,dz' + \phi_{rs}\phi_{k\ell}\int_0^{z_H} \phi(z_H - z')\frac{d\epsilon^p_{k\ell}}{dz'}\,dz' \tag{2-34}$$

Consider now the expression (2-23) for the intrinsic time scale $d\varsigma$. Upon using Eqs. (2-8) and (2-9), Eq. (2-23) transforms to the following expression for $d\varsigma$ in the current state:

$$d\varsigma^2 = \phi_{mp}\,\phi_{qn}\,de^p_{pq}\,de^p_{mn} + k^2\left(\phi_{mn}d\epsilon^p_{mn}\right)^2 \tag{2-35}$$

Note that the tensor $d\underset{\sim}{e}^p$ in the current configuration is not deviatoric, i.e., $\mathrm{tr}(d\underset{\sim}{e}^p) \neq 0$; this follows from the fact that the current state is, in general, anisotropic. To see this, recall the expression for the deviatoric plastic strain $\underset{\sim}{e}^p$ in the transformed state:

$$\hat{\underset{\sim}{e}}^p = \hat{\underset{\sim}{\epsilon}}^p - \frac{1}{3}\,\mathrm{tr}\left(\hat{\underset{\sim}{\epsilon}}^p\right)\underset{\sim}{\delta} \tag{2-36}$$

Then from Eqs. (2-9) and (2-10), we can write, using matrix notation:

$$\underset{\sim}{e}^p = \underset{\sim}{B}^{-1}\,\hat{\underset{\sim}{e}}^p\left(\underset{\sim}{B}^{-1}\right)^T \quad , \quad \underset{\sim}{\epsilon}^p = \underset{\sim}{B}^{-1}\,\hat{\underset{\sim}{\epsilon}}^p\left(\underset{\sim}{B}^{-1}\right)^T \tag{2-37}$$

Substituting Eqs. (2-37) into (2-36) leads to the result:

$$\underset{\sim}{e}^p = \underset{\sim}{\epsilon}^p - \frac{1}{3}\,\underset{\sim}{B}^{-1}\left(\underset{\sim}{B}^{-1}\right)^T\,\mathrm{tr}\left(\hat{\underset{\sim}{\epsilon}}^p\right) \tag{2-38}$$

It can be shown that

$$\mathrm{tr}\left[\hat{\underset{\sim}{\varepsilon}}^{p}\right] = \mathrm{tr}\left[\underset{\sim}{\ell}\ \underset{\sim}{\varepsilon}^{p}\right] \tag{2-39}$$

Thus, Eq. (2-38) can be written as

$$\underset{\sim}{e}^{p} = \underset{\sim}{\varepsilon}^{p} - \frac{1}{3}\,\underset{\sim}{\ell}^{-1}\ \mathrm{tr}\left[\underset{\sim}{\ell}\ \underset{\sim}{\varepsilon}^{p}\right] \tag{2-40}$$

since, from Eq. (2-1), we have $\underset{\sim}{\ell}^{-1} = \underset{\sim}{B}^{-1}(\underset{\sim}{B}^{-1})^{T}$. As a result, it follows that

$$\mathrm{tr}\left[\underset{\sim}{e}^{p}\right] = \mathrm{tr}\left[\underset{\sim}{\varepsilon}^{p}\right] - \frac{1}{3}\,\mathrm{tr}\left[\underset{\sim}{\ell}\ \underset{\sim}{\varepsilon}^{p}\right]\mathrm{tr}\left[\underset{\sim}{\ell}^{-1}\right] \tag{2-41}$$

An inspection of Eq. (2-41) shows that $\mathrm{tr}(\underset{\sim}{e}^{p}) = 0$ only when $\underset{\sim}{\ell} = \underset{\sim}{\delta}$, i.e., in the initial undamaged (isotropic) state.

To express the righthand side of Eq. (2-35) solely in terms of the tensor $d\underset{\sim}{\varepsilon}^{p}$, we proceed as follows. First, it can be shown from Eq. (2-40) that

$$\underset{\sim}{\ell} \cdot \underset{\sim}{e}^{p} = \underset{\sim}{\ell} \cdot d\underset{\sim}{\varepsilon}^{p} - \frac{1}{3}\,\mathrm{tr}\left[\underset{\sim}{\ell} \cdot d\underset{\sim}{\varepsilon}^{p}\right]\underset{\sim}{\delta} \tag{2-42}$$

Equation (2-35) can be written in the following matrix form:

$$d\varsigma^{2} = \mathrm{tr}\left\{\left[\underset{\sim}{\ell} \cdot d\underset{\sim}{e}^{p}\right]\left[d\underset{\sim}{e}^{p} \cdot \underset{\sim}{\ell}\right]^{T}\right\} + k^{2}\left\{\mathrm{tr}\left[\underset{\sim}{\ell} \cdot d\underset{\sim}{\varepsilon}^{p}\right]\right\}^{2} \tag{2-43}$$

Upon substituting Eq. (2-42) into (2-43), we find:****

$$d\varsigma^{2} = \mathrm{tr}\left\{\left[\underset{\sim}{\ell} \cdot d\underset{\sim}{\varepsilon}^{p}\right]\left[d\underset{\sim}{\varepsilon}^{p} \cdot \underset{\sim}{\ell}\right]^{T}\right\} + \left[k^{2} - \frac{1}{3}\right]\left\{\mathrm{tr}\left[\underset{\sim}{\ell} \cdot d\underset{\sim}{\varepsilon}^{p}\right]\right\}^{2} \tag{2-44}$$

In the isotropic, undamaged transformed configuration, Hooke's law has the following form, which was given earlier in Eq. (2-28):

$$\hat{\underset{\sim}{\sigma}} = \lambda\ \mathrm{tr}\left[\hat{\underset{\sim}{\varepsilon}} - \hat{\underset{\sim}{\varepsilon}}^{p}\right]\underset{\sim}{\delta} + 2\mu\left[\hat{\underset{\sim}{\varepsilon}} - \hat{\underset{\sim}{\varepsilon}}^{p}\right] \tag{2-45}$$

**** This expression was first developed by H. Murakami.

To express Eq. (2-45) in the current damaged state, we introduce the transformations given by Eqs. (2-9) and (2-16). Proceeding in this manner, it follows that

$$\underset{\sim}{q} = \lambda\, \underset{\sim}{\phi}\, \mathrm{tr}\left[\underset{\sim}{\phi}\left(\underset{\sim}{\varepsilon} - \underset{\sim}{\varepsilon}^{p}\right)\right] + 2\mu\, \underset{\sim}{\phi}\left(\underset{\sim}{\varepsilon} - \underset{\sim}{\varepsilon}^{p}\right)\underset{\sim}{\phi} \tag{2-46}$$

which, in indicial notation, reads

$$\sigma_{ij} = \lambda\, \phi_{ij}\phi_{k\ell}\left(\varepsilon_{k\ell} - \varepsilon^{p}_{k\ell}\right) + 2\mu\, \phi_{ik}\phi_{j\ell}\left(\varepsilon_{k\ell} - \varepsilon^{p}_{k\ell}\right) \tag{2-47}$$

For many geomaterials, including concrete, the hardening functions are typically of the general form:

$$F_H = F_H\left(\varepsilon^{p}\right)$$

$$F_D = F_D\left(\sigma\right) \tag{2-48}$$

where ε^{p} and σ denote, respectively, the plastic volume strain and the hydrostatic pressure in the current configuration.

To summarize the main results from this section, the system of equations which govern the behavior of the endochronic plastic-fracturing model in the current damaged state consist of Eqs. (2-22), (2-29), (2-44), (2-46) and an evolution equation for $\underset{\sim}{\phi}$.

The key to the success of the damage model described above lies in having the appropriate evolution equation for $\underset{\sim}{\phi}$ for the material of interest. Ideally, it would be desirable to have the evolution equation reflect the underlying micromechanical fracture mechanisms. A research effort to develop such an evolution equation for $\underset{\sim}{\phi}$ is currently being conducted by Valanis in a separate AFOSR-funded program, but the results from this study are not expected to be available for sometime.

In the following section, the response of the model to the special case of uniaxial loading is considered in detail to explore some of the general features of the theory. The model is then applied to the recent data by Gopalaratnam and Shah (1985) on the response of plain concrete to simple tension in the presence of developing damage and unloading-reloading cycles. For this purpose, an evolution equation suggested by the data is adopted and successfully used.

Section 3

UNIAXIAL LOADING

In this section, the case of uniaxial loading is considered in detail to illustrate some basic features of the endochronic plastic-fracturing model described in the preceding section. First, the governing equations for uniaxial loading are deduced from the general equations given in Section 2. Then, several interesting features of the model are discussed, including the several important special cases that the model reduces to under certain conditions. Following this, an incremental scheme is developed for integrating the system of governing equations. Finally, the model is applied to the recent laboratory data of Gopalaratnam and Shah (1985) for the response of plain concrete to uniaxial tension, and it is shown that the model provides an excellent description of the observed behavior.

3.1 GOVERNING EQUATIONS.

Consider the case of uniaxial tension in which the applied stress is directed along the x_i-axis. In this case, we have $B_{ij} = 0$ for $i \neq j$ and $\sigma_{22} = \sigma_{33}$. From Eqs. (2-9) and (2-16) we therefore find that

$$\sigma_{11} = \phi_{11}\, \hat{\sigma}_{11}$$

$$\hat{\epsilon}_{11} = \phi_{11}\, \epsilon_{11} \tag{3-1}$$

$$\hat{\epsilon}^p_{11} = \phi_{11}\, \epsilon^p_{11}$$

The constitutive behavior of the endochronic plastic-fracturing model in the transformed state is described by the system of equations given in Section 2.2 which, for the case of uniaxial loading and plastic incompressibility, reduce to the following form:

$$\hat{\sigma}_{11} = \int_0^z E(z - z') \frac{d\hat{\epsilon}^p_{11}}{dz'}\, dz' \tag{3-2}$$

$$\hat{\sigma}_{11} = E_o\left(\hat{\epsilon}_{11} - \hat{\epsilon}^p_{11}\right) \tag{3-3}$$

$$d\varsigma = \sqrt{\frac{3}{2}}\left|d\hat{\epsilon}^p_{11}\right| \tag{3-4}$$

$$dz = \frac{d\varsigma}{F} \tag{3-5}$$

Here, $E(z)$ is a weakly singular kernel function.***** E_o denotes Young's modulus, z is the intrinsic time and ς is the intrinsic time scale. In addition, F represents the shear softening function, and the vertical bars surrounding a symbol denote its absolute value. Note that Eqs. (3-2) to (3-5) are the governing equations for the standard (undamaged) endochronic theory.

The kernel function $E(z)$ is given, in the usual manner, by the Dirichlet series:

$$E(z) = \sum_{r=1}^{\infty} A_r e^{-\alpha_r z} \tag{3-6}$$

where, in order to satisfy the conditions imposed by the weakly singular nature of $E(z)$, i.e., $E(0) = \infty$ and $\int_o^\infty E(y)dy < 0$, the positive constants A_r and α_r must satisfy the following conditions:

$$\sum_{r=1}^{\infty} A_r = \infty$$

$$\sum_{r=1}^{\infty} \frac{A_r}{\alpha_r} < 0 \tag{3-7}$$

***** As shown by Valanis and Read (1989), $E(z)$ is related to $\rho(z)$ according to the expression $E(z) = 3/2\ \rho(z)$.

From experience, we have found that, for most materials, only two or three terms of the series (3-6) are necessary to provide an adequate modeling capability. In view of this, we write

$$E(z) = \sum_{r=1}^{n} A_r e^{-\alpha_r z} \tag{3-8}$$

where n is finite and care is taken to insure that the infinitely large value of E(0) is suitably approximated by a large finite value.

The above system of equations, which apply to the transformed state, are now mapped to the current (damaged) state through the use of Eqs. (3-1). The following set of equations are then obtained for the current state:

$$\sigma = \phi \int_0^z E(z - z') \frac{d(\phi \epsilon^p)}{dz'} dz' \tag{3-9}$$

$$\sigma = \phi^2 E_o (\epsilon - \epsilon^p) \tag{3-10}$$

$$d\varsigma = \sqrt{\frac{3}{2}} \left| d(\phi \epsilon^p) \right| \tag{3-11}$$

$$dz = \frac{d\varsigma}{F} \tag{3-12}$$

where the subscripts have been suppressed for convenience. To the above equations, we must add an expression which defines the manner in which ϕ depends upon the deformation.

In uniaxial loading, it is reasonable to assume that ϕ will depend upon a variable related to the axial extension, and the three likely candidates are the total axial strain ϵ, the elastic axial strain ϵ^e and the plastic axial strain ϵ^p. During the course of applying the model to the uniaxial concrete data of Gopalaratnam and Shah (1985) (see Section 3.4), we investigated the dependence of ϕ on each of the three strain variables noted above and found that a dependence on the axial plastic strain ϵ^p was preferred. The reasons for this are as follows. For the case in which ϕ is taken to depend on the total strain ϵ, it was found that the model was overly sensitive to the form adopted for $\phi(\epsilon)$. Very slight deviations from a form which gave good

agreement with the Gopalaratnam-Shah data lead to difficulties in numerically integrating the system of governing equations; this was not the case when ϕ was taken to depend on the axial plastic strain, ϵ^p. Furthermore, on the basis of the results described in Section 3.4, it was found that ϕ could not be described uniquely as a function of the axial elastic strain, ϵ^e, i.e., for a range of values of ϵ^e, ϕ was double-valued. Again, this was not the case when ϕ depended on the axial plastic strain, ϵ^p. For the reasons cited above, ϕ is taken to depend on ϵ^p. We therefore adopt the general form:

$$\phi = \phi\left[\epsilon_m^p\right] \tag{3-13}$$

where ϵ^p denotes the plastic component of the total tensile strain ϵ, i.e., $\epsilon^p = \epsilon - \epsilon^e$, and the subscript m indicates the maximum value attained.

The corresponding evolution equation for ϕ is then

$$d\phi = \begin{cases} H\left[\epsilon_m^p\right] d\epsilon^p & , \text{ if } d\epsilon^p > 0 \text{ on } \epsilon^p \geq \epsilon_m^p \\ 0 & , \text{ otherwise} \end{cases} \tag{3-14}$$

where $H \equiv d\phi/d\epsilon^p$. Thus, in the event of unloading from a tensile strain state, we have $d\epsilon_m^p = 0$ and therefore $d\phi = 0$, as should be.

3.2 COMMENTS ON THE MODEL.

The model described above contains, as special cases, several models which are particularly noteworthy, whose responses are depicted in Figure 2. We note, first of all, that there are ideally two kinds of damage (or degradation) that are observed in materials (see Bazant and Lin, 1988):

1. Degradation of material stiffness, which is caused by microcracking, nucleation and void growth, and elasto-plastic coupling (Maier and Hueckel, 1979).

2. Degradation of yield limit, resulting from a reduction in the areas of cohesive or plastic-fractional connections. Such degradation does not produce a reduction in the material stiffness.

The observed behavior of many real materials, including concrete and rock, suggests that their responses involve some combination of the above two types of degradation. The endochronic plastic-fracturing model described above contains both types of degradation. The softening function F describes yield limit degradation, while the function ϕ reflects degradation in stiffness.

With the above discussion in mind, let us consider the special cases of the model shown in Figure 2. First, if the plasticity of the model is suppressed and ϕ is taken to depend, say, on the axial tensile strain ϵ, then the model reduces to the classic elastic-fracturing model (see Dougill, 1976, for example), which exhibits only stiffness degradation. In this case, the slope ofthe unloading/reloading path decreases with increasing strain, but all unloading paths pass through the origin. The response of this special case is shown in Figure 2(a). Secondly, the general model reduces to the standard (non-softening) endochronic plasticity model when there is no damage, i.e., $\phi = F = 1$. In this case, the response of the model is depicted in Figure 2(b). Thirdly, if one sets $\phi = 1$, the general model reduces to an endochronic plastic-fracturing model with yield limit degradation, whose response is shown in Figure 2(c). Note in this case that the model unloads and reloads with the same slope as the initial elastic slope. Finally, when both yield limit degradation and stiffness degradation are present ($\phi \neq 1$, $F \neq 1$), the model has the response features illustrated in Figure 2(d). Here, the slope of the unloading-reloading path decreases with increasing strain, and the unloading paths no longer pass through the origin due to the development of plastic strains. These features are representative of many materials, including concrete, as we will demonstrate in the sequel.

There is also another interesting feature of the model which should be noted. If the model is subjected to monotonic increasing tensile strain, the corresponding behavior in the transformed space (σ - ϵ) may or may not involve unloading, depending upon the relationship of the function ϕ to a critical curve, which we will call ϕ^*. This critical curve is the curve in ϕ - ϵ^p space which satisfies the condition $d(\phi\epsilon^p) = 0$. Given a functional relation for ϕ, say $\phi = \phi(\epsilon^p)$, the critical curve is defined by the expression.

$$\phi^*(\epsilon^p) = 1 - \int_0^{\epsilon^p} \frac{\phi(x)}{x}\, dx \qquad (3\text{-}15)$$

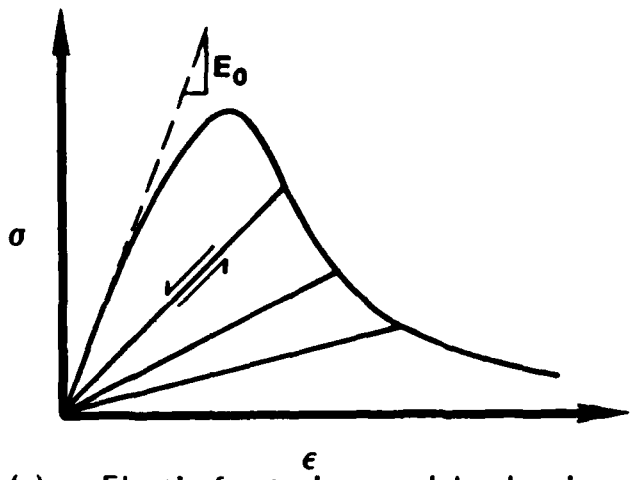

(a) Elastic-fracturing model, showing stiffness degradation ($\phi \neq 1$, $F = 1$).

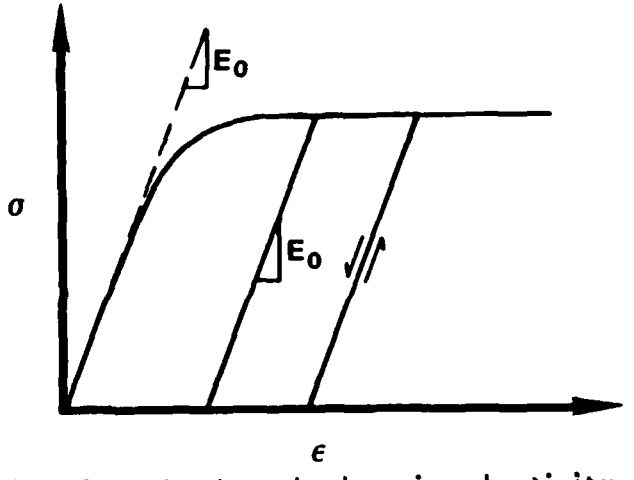

(b) Standard endochronic plasticity model ($\phi = F = 1$)

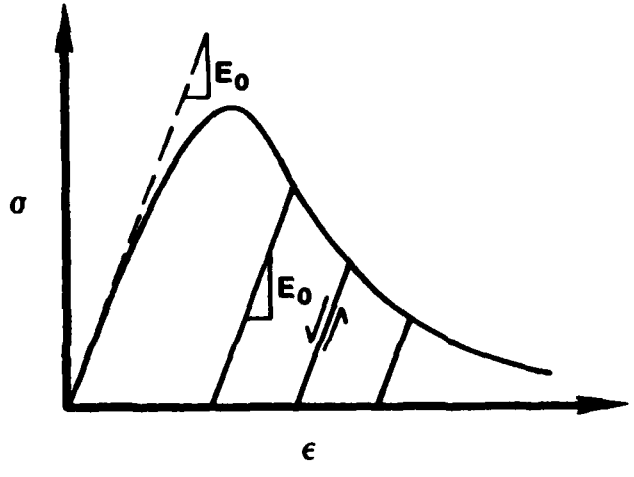

(c) Endochronic plastic-fracturing modelwith yield limit degradation($\phi = 1$, $F = 1$)

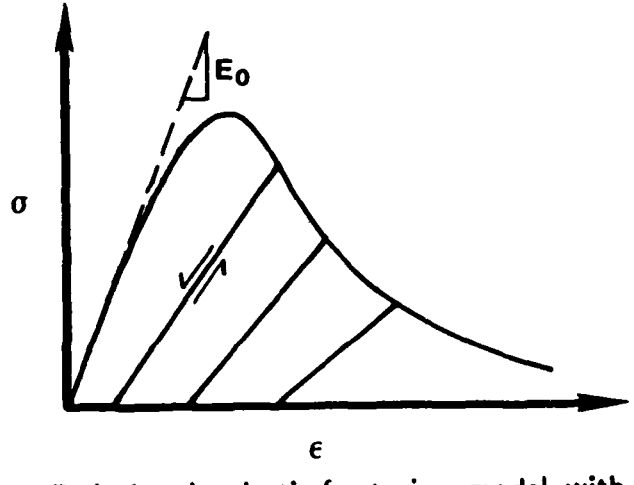

(d) Endochronic plastic-fracturing model with both yield limit degradation and stiffness degradation ($\phi \neq 1$, $F \neq 1$).

Figure 2. Special cases of the general endochronic plastic-fracturing model for simple tension.

If the curve $\phi(\epsilon^p)$ lies above the critical curve in the region where $d(\phi\epsilon^p) > 0$, such as curve A in Figure 3, the response in the transformed state will involve only loading, as shown in Figure 4. This follows immediately from the relation (3-1c), i.e.,

$$d\hat{\epsilon}^p = d(\phi\epsilon^p) \tag{3-16}$$

On the other hand, if the curve $\phi(\epsilon^p)$ falls below the critical curve at some point P in the region where $d(\phi\epsilon^p) < 0$, such as curve B in Figure 3, unloading will take place in the transformed state, since, as shown in Figure 4, in view of Eq. (3-16), $d\epsilon^p$ will be negative. The occurence of unloading in the transformed state does not, however, affect the continuity or the smoothness of the response in the current state, as our numerical studies have shown. Thus, the model allows unloading ($d\epsilon < 0$) to take place in the transformed space concurrently with loading ($d\epsilon > 0$) in the current state.

In the following section, an incremental numerical scheme is presented for integrating the system of equations (3-9) to (3-12) in conjunction with the evolution equation (3-14).

3.3 AN INCREMENTAL SCHEME FOR INTEGRATING THE GOVERNING EQUATIONS.

Let us now consider the governing equations for the current states which are given by Eqs. (3-9) to (3-12) and (3-14), with $E(z)$ defined by Eq. (3-8). If we substitute Eq. (3-8) into Eq. (3-9), we find that

$$\sigma = \phi \sum_{r=1}^{n} Q_r \tag{3-17}$$

where

$$Q_r = A_r e^{-\alpha_r z} \int_0^z e^{\alpha_r z'} \frac{d}{dz'} \left(\phi\epsilon^p\right) dz' \tag{3-18}$$

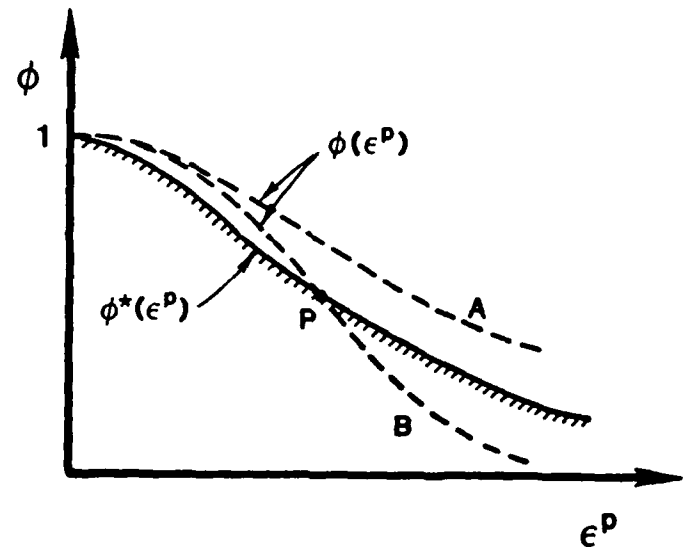

Figure 3. **Plot of ϕ versus ϵ^p for two different functions $\phi(\epsilon^p)$, showing their relationship to the critical curve $\sigma^*(\epsilon^p)$.**

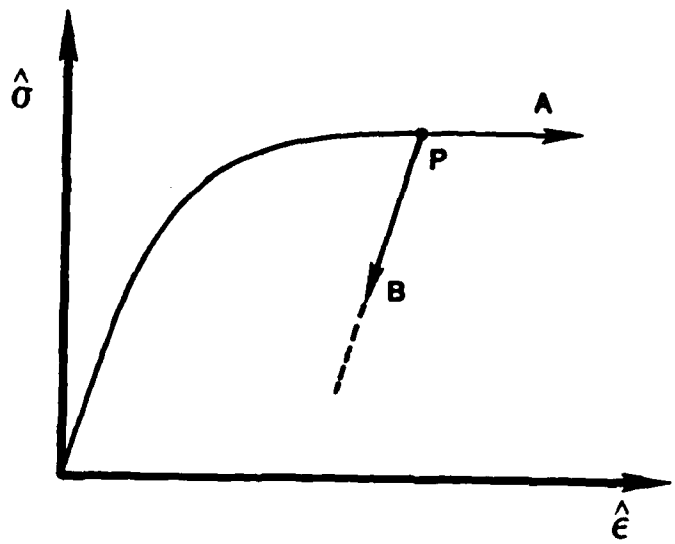

Figure 4. **Stress versus strain in the transformed space, showing the corresponding responses for the two diffeent function $\phi(\epsilon^p)$ depicted in Figure 3.**

Differentiation of Eq. (3-18) with respect to z leads to the expression

$$dQ_r + \alpha_r Q_r dz = A_r d\left(\phi\epsilon^p\right) \tag{3-19}$$

If we now set:

$$A \equiv \sum_{r=1}^{n} A_r \tag{3-20}$$

$$Q \equiv \sum_{r=1}^{n} \alpha_r Q_r \quad , \tag{3-21}$$

then, in view of Eqs. (3-17) and (3-19), we can write:

$$d\sigma = \left[A\, d\left(\phi\epsilon^p\right) - Q\, dz\right] + \frac{\sigma}{\phi}\, d\phi \tag{3-22}$$

Also, Eq. (3-10) may be differentiated to give:

$$d\sigma = \phi^2 E_o \left(d\epsilon - d\epsilon^p\right) + 2\phi E_o \left(\epsilon - \epsilon^p\right) d\phi \tag{3-23}$$

Returning now to the evolution equation (3-14), we rewrite this in the form:

$$d\phi = H\, d\epsilon^p \tag{3-24}$$

where

$$H = \begin{cases} H\left(\epsilon_m^p\right) , & \text{if } d\epsilon^p > 0 \text{ and } \epsilon^p \geq \epsilon_m^p \\ 0 , & \text{otherwise} \end{cases} \tag{3-25}$$

Equation (3-24) may now be combined with Eqs. (3-22) and (3-23) to give the following expressions:

$$d\sigma = \left(A\phi^2 + A\phi\epsilon^p H + \frac{\sigma H}{\phi}\right) d\epsilon^p - \phi Q dz \tag{3-26}$$

$$d\sigma = \left[\phi^2 E_o\right] d\epsilon - \left[\phi^2 E_o - 2\phi E_o H(\epsilon - \epsilon^p)\right] d\epsilon^p \tag{3-27}$$

Upon eliminating $d\sigma$ from the above equations and solving for $d\epsilon^p$, we obtain the expression:

$$d\epsilon^p = \alpha_o d\epsilon + \alpha_1 dz \tag{3-28}$$

where

$$\alpha_o = \frac{\phi^2 E_o}{\phi^2 (A + E)\phi + H\left[A\phi\epsilon^p - \frac{\sigma}{\phi}\right]}$$

$$\alpha_1 = \frac{\phi Q}{(A + E)\phi^2 + H\left[A\phi\epsilon^p - \frac{\sigma}{\phi}\right]} \tag{3-29}$$

From Eqs. (3-11), (3-12) and (3-14), we can write

$$dz = \sqrt{\frac{3}{2}} \frac{1}{F} \left| \left(\phi + H\,\epsilon^p\right) d\epsilon^p \right| \tag{3-30}$$

For the case of loading, we have $d\epsilon^p > 0$, so that Eq. (3-30) may be written as

$$dz = \sqrt{\frac{3}{2}} \frac{1}{F} \left| \phi + H\epsilon^p \right| \left(\alpha_o d\epsilon + \alpha_1 dz\right) \tag{3-31}$$

where Eq. (3-28) has been used. Solving Eq. (3-31) for dz, we obtain

$$dz = \left\{ \frac{\sqrt{\frac{3}{2}} \frac{\alpha_o}{F} \left| \phi + H\epsilon^p \right|}{1 - \sqrt{\frac{3}{2}} \frac{\alpha_1}{F} \left| \phi + H\epsilon^p \right|} \right\} d\epsilon \qquad (d\epsilon > 0) \tag{3-32}$$

Similarly, for the case of unloading ($d\epsilon^p > 0$), we find

$$dz = \left\{ \frac{-\sqrt{\frac{3}{2}} \frac{\alpha_o}{F} \left| \phi - H\epsilon^p \right|}{1 + \sqrt{\frac{3}{2}} \frac{\alpha_1}{F} \left| \phi + H\epsilon^p \right|} \right\} d\epsilon \qquad (d\epsilon < 0) \tag{3-33}$$

On the basis of the above developments, the following algorithm provides a numerical method for incrementally integrating the system of equations (3-9) to (3-12) and (3-14) when $\Delta\epsilon$, σ, ϕ, ϵ, ϵ^p, F and H are known at time t:

1. Depending upon the sign of $\Delta\epsilon$, use either Eqs. (3-32) or (3-33) to obtain Δz.

2. Determine $\Delta\epsilon^p$ from Eq. (3-28).

3. Compute $\Delta\phi$ from Eq. (3-14).

4. Using Eq. (3-19), calculate ΔQ_r for $r = 1,2, \ldots n$.

5. Evaluate ΔQ from Eq. (3-21).

6. Determine $\Delta\sigma$, using Eq. (3-27)

The numerical scheme described above is first-order accurate. It can be made second-order accurate by using Richardson extrapolation in conjunction with the above first-order scheme. For further details, see Murakami and Read (1988).

3.4 APPLICATION TO PLAIN CONCRETE.

There are little data presently available on the complete load-deformation response of plain concrete to uniaxial tension, and the data that do exist are often conflicting and confusing (compare the results of Evans and Marathe (1968) with those of Petersson (1981), for example). The testing of brittle, tension-weak materials, such as plain concrete, presents two major experimental problems, namely, (1) the tendency of a specimen to fail near the grips where the state of stress is not uniaxial and (2) the inability of the testing device to maintain stable post-peak response.

Recently, Gopalaratnam and Shah (1985) developed experimental techniques which overcome the difficulties noted above, and measured the complete load-deformation response of plain concrete to simple tension, including the post-peak behavior. Seven different mix proportions were used to provide data on the influence of aggregate size, water-cement ratio, and volume content of aggregates. To insure stable post-peak response, a small notch was introduced into each specimen at its center and on both sides, and the displacement across the notch was used to control the loading.

Studies showed that the average responses of notched and unnotched specimens were identical and that both notched and unnotched specimens failed at a single critical section.

Typical results from the study by Gopalaratnam and Shah (1985) are depicted in Figure 5, where the stress-strain response of a medium strength concrete (f_c' = 6,364 psi) to simple tension is shown. Note that the data shown in this figure were obtained from four different types of tests. Three tests were done under monotonic axial straining while a fourth test was conducted under cyclic straining conditions. One test was peformed with an unnotched specimen, while the rest were notched. The axial displacement for one specimen was determined from optical measurements of the crack width, while local strain measurements were made on another specimen. Despite these differences in testing procedure, the curves show a remarkable consistency, when one considers the usual difficulties of testing concrete in tension.

In the following section, the endochronic plastic-fracturing model described in Section 3.1 is applied to the data of Gopalaratnam and Shah (1985) shown in Figure 5. The procedures used to determine the various material-dependent parameters and functions in the model are described. The response of the resulting model to monotonic and cyclic tensile straining under uniaxial loading is then compared with the corresponding data.

3.4.1 Determination of Material-Dependent Parameters and Functions.

The endochronic plastic-fracturing model for simple tension defined by Eqs. (3-9) to (3-12), with an evolution equation for ϕ having the form of Eq. (3-14) will now be applied to Gopalaratnam-Shah (1985) data for plain concrete. As an inspection of this system of equations reveals, the material-dependent functions and parameters that must be evaluated from data are E_o, the Young's modulus of the undamaged material; E(z), the weakly singular kernel function that depends on the intrinsic time, z; the hardening/softening function F; and the evolution equation (3-14) for ϕ. The data shown in Figure 5 permit a direct determination of E_o and ϕ, but are not sufficient to allow us to determine E(z) and F directly. Because of this, an interative approach was used to determine these functions in the present study.

From the initial slope of the loading curve shown in Figure 5, we find that E_o = 500 psi. Figure 6 describes the way in which the elastic strain ϵ^e, the plastic strain ϵ^p and finally ϕ may be obtained directly from the unloading-reloading paths shown in Figure 5. Note from Eq. (3-10) that the instantaneous Young's modulus E at any damage level is given by $E = \phi^2 E_o$. In this manner, the following table was constructed from the data given in Figure 5 for the five unloading-reloading paths.

Table I
Information on Current State Inferred Directly from Figure 5.

$\epsilon(10^{-4})$	σ(psi)	E(psi)	ϕ	$\epsilon^e(10^{-4})$	$\epsilon^p(10^{-4})$
0	0	500	1	0	0
1.4	295	357	0.85	0.80	0.60
2.1	170	192	0.62	0.90	1.20
2.9	130	125	0.50	1.00	1.90
3.7	95	81	0.40	1.10	2.60
4.4	68	59	0.34	1.20	3.20

Using the results given in the above table, together with Eqs. (3-1), the information given below in Table II was derived for the transformed state.

Table II

Information on Transformed State Derived from Table I Using Eq. (3-1).

$\epsilon(10^{-4})$	$\epsilon(10^{-4})$	σ(psi)	$\epsilon^e(10^{-4})$	$\epsilon^p(10^{-4})$
0	0	0	0	0
1.4	1.18	349	0.68	0.51
2.1	1.30	27	0.56	0.77
2.9	1.45	260	0.50	1.00
3.7	1.48	237	0.44	1.04
4.4	1.51	198	0.41	1.13

The function ϕ describes the degradation of material stiffness, caused by microcracking, void growth and elastic-plastic coupling (Maier and Hueckel, 1979). As noted earlier, we found that ϕ is most naturally described in terms of the plastic strain ϵ^p. Guided by the data given in Table I, ϕ was taken in the form:

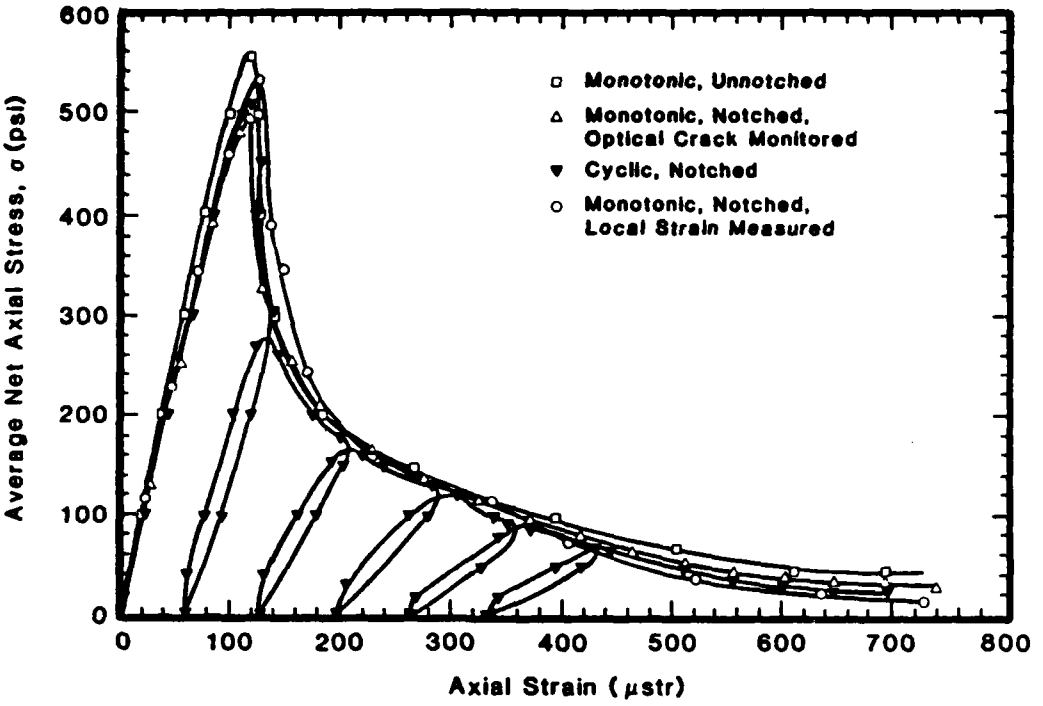

Figure 5. Response of plain concrete to uniaxial tension, as measured in four different types of tests (from Gopolaratnam and Shah, 1985).

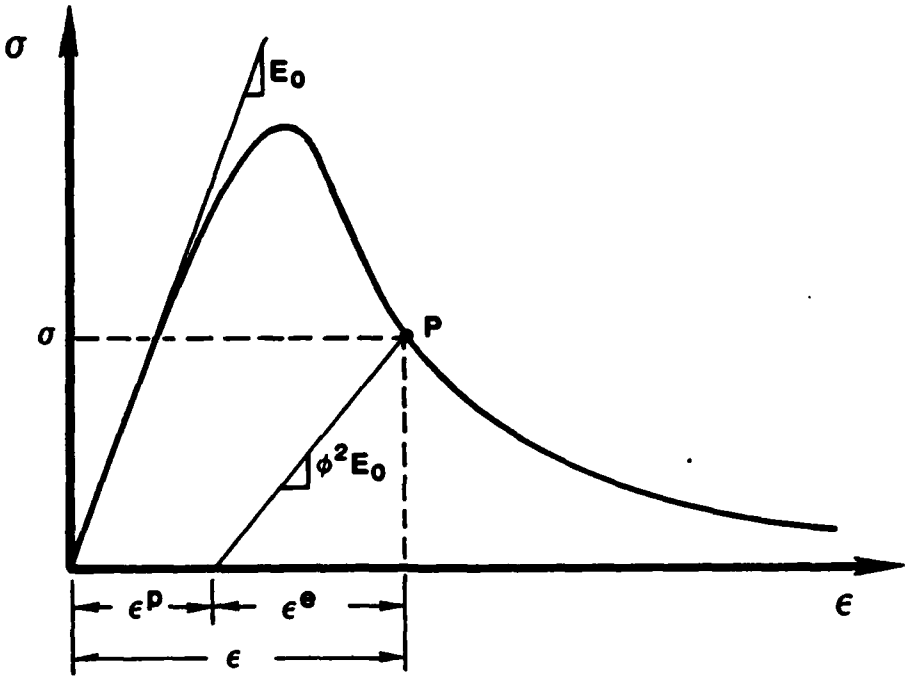

Figure 6. Schematic of stress-strain curve, showing the manner in which ϵ^e, ϵ^p and ϕ are defined at an arbitrary unloading point P.

$$\phi = 1 - (1 - \phi_\infty) \exp\left[- \left(\frac{k}{\epsilon^p}\right)^m \right] \tag{3-34}$$

where

$$k = 9.33 \times 10^{-5}$$

$$m = 1.21 \tag{3-35}$$

$$\phi_\infty = 0.20$$

Figure 7 depicts this relationship and demonstrates its ability to describe the data.

With ϕ defined, the evolution equation for ϕ is then simply obtained by differentiating Eq. (3-34), which leads to the result

$$d\phi = H(\epsilon^p) d\epsilon^p \tag{3-36}$$

where

$$H(\epsilon^p) = - C_o (\epsilon^p)^{-(1+m)} \exp\left[- \left(\frac{k}{\epsilon^p}\right)^m \right] \tag{3-37}$$

and

$$C_o \equiv k^m (1 - \phi_\infty) \tag{3-38}$$

Equation (3-36), with $H(\epsilon^p)$ defined by Eq. (3-37) together with the values of the parameters given in Eq. (3-35), is the evolution equation for ϕ used in the present study.

Turning now to the kernel function $E(z)$ and the softening function F, we note that they are both associated with the plasticity of the model and, as such, are most naturally defined with respect to the response in the transformed state, particularly, the response in the $\sigma - \epsilon^p$ plane. We note that the response of the model in the $\sigma - \epsilon^p$ plane is governed by Eqs. (3-2), (3-4) and (3-5). Assuming that F depends upon ϵ^p, these equations may be combined to give the expression:

$$\hat{\sigma} = \sqrt{\frac{2}{3}} \int_o^z E(z - z') \, F[\hat{\epsilon}^p(z')] \, dz' \tag{3-39}$$

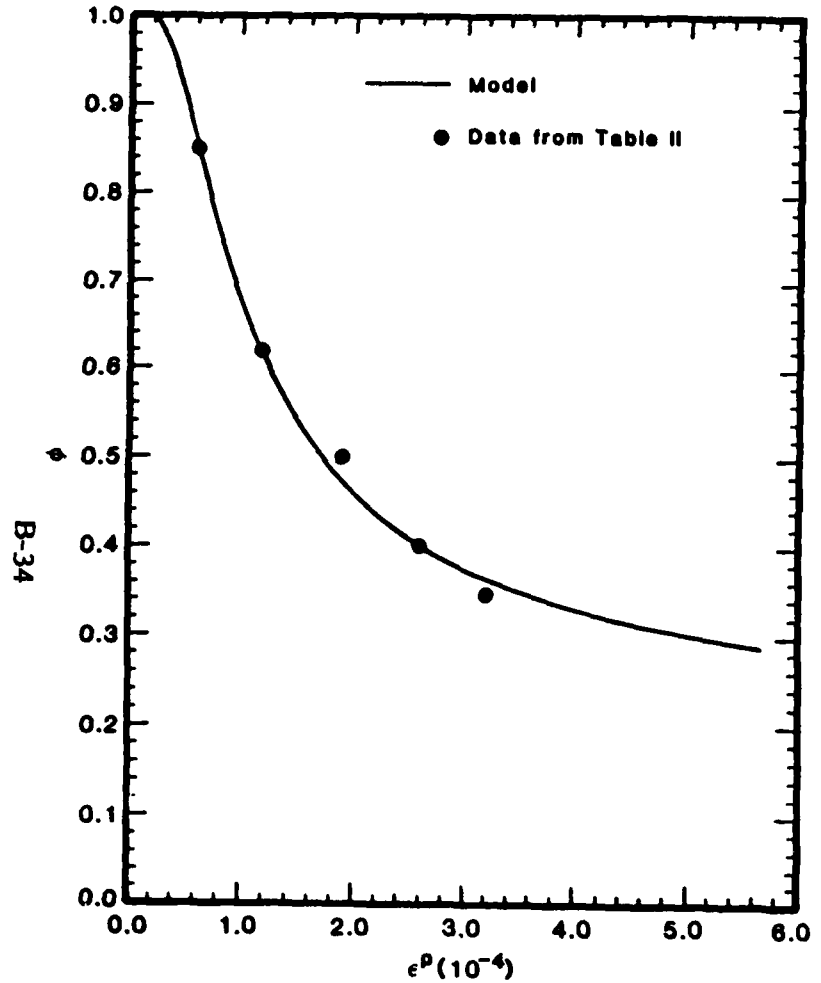

Figure 7. **Dependence of ϕ on plastic strain for monotonic extension under simple tension.**

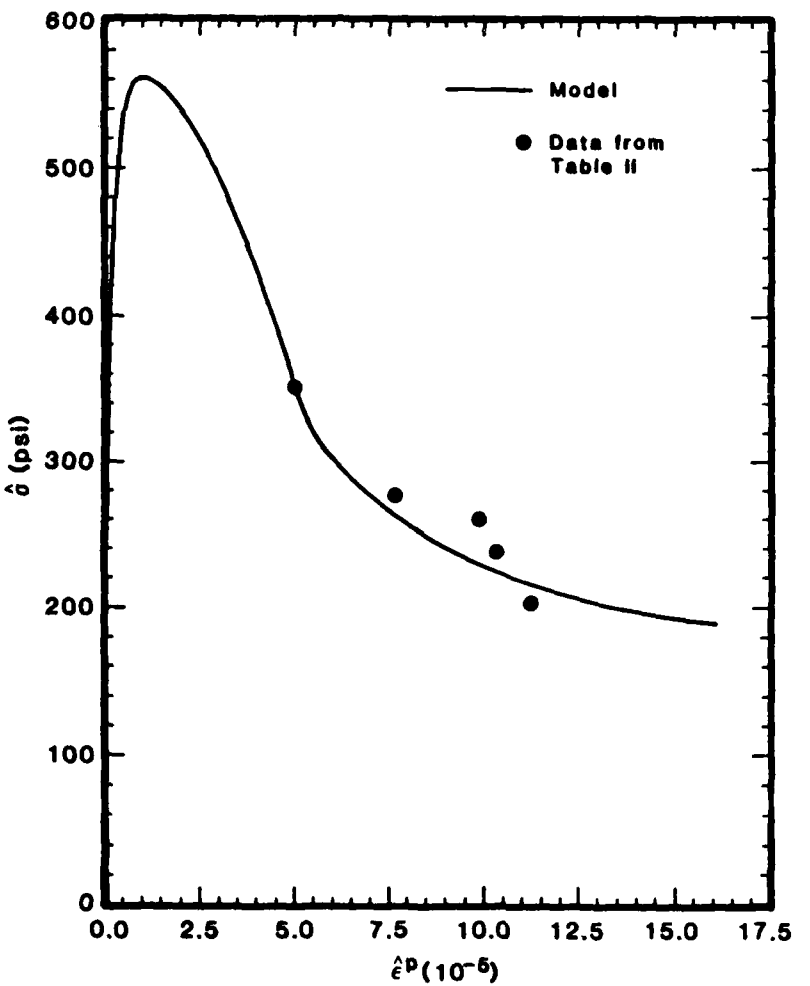

Figure 8. ***Stress versus plastic strain in the*** **transformed state for monotonic extension under simple tension, showing yield limit degradation.**

where

$$dz = \sqrt{\frac{3}{2}} \frac{|d\hat{\epsilon}^p|}{F(\hat{\epsilon}^p)} \tag{3-40}$$

and the unknown functions $E(z)$ and $F(\epsilon^p)$ are to be determined. As Eq. (3-39) reveals, these functions appear in product form, which adds complexity to their determination.

As reference to Table II will show, the data defining the behavior in the σ - ϵ^p plane are very sparse (5 points) and there are no data points for small values of ϵ^p, where information is required if $E(z)$ is to be evaluated directly. As a result, it was necessary to determine $E(z)$ and $F(\epsilon^p)$ indirectly, using an iterative approach. Proceeding in this manner, the following expressions for $E(z)$ and $F(\epsilon^p)$ were found to describe the behavior of the concrete quite well:

$$E(z) = \sum_{r=1}^{2} A_r e^{-\alpha_r z} \tag{3-41}$$

where

$$\begin{aligned} A_1 &= 1.62 \times 10^7 \text{ psi} & \alpha_1 &= 8.82 \times 10^4 \\ A_2 &= 2.69 \times 10^8 \text{ psi} & \alpha_2 &= 3.99 \times 10^5 \end{aligned} \tag{3-42}$$

and

$$F(\hat{\epsilon}^p) = F_\infty + (1 - F_\infty) \exp[-\alpha(\hat{\epsilon}^p)^n] \tag{3-43}$$

where

$$\begin{aligned} \alpha &= 6.71 \times 10^3 \\ n &= 0.866 \\ F_\infty &= 0.20 \end{aligned} \tag{3-44}$$

Based on the forms for $E(z)$ and $F(\epsilon^p)$ given above, the response of the model in the transformed (σ - ϵ^p) space to monotonic uniaxial loading is given in Figure 8. The corresponding data points from Table II are also shown in this figure for comparison. As the figure shows, the model describes the data quite well in this space.

The specification of the parameters and functions in the model is now complete.

3.4.2 Predicted and Measured Responses.

Using the parameters and functions given above, response of the endochronic plastic-fracturing model defined by Eqs. (3-9) to (3-12) was examined for both monotonic and cyclic tensile strain paths over the range of tensile strains studied by Gopalaratnam and Shah (1985). The governing equations of the model were integrated using the numerical scheme described in Section 3.3. The results obtained in this manner are depicted in Figure 9, where both the model predictions and the corresponding data are shown for comparative purposes. As the figure reveals, the model describes the data quite well. The only noticeable difference between the predicted and observed responses is that the data show significant hysteresis during the unloading-reloading processes while the model does not. Overall, however, the agreement is considered very encouraging.

Finally, we note that during the course of calculating the response to monotonic straining shown in Figure 9, the dependence of ϕ on both the total strain ϵ and the elastic strain ϵ^e was monitored. The resulting curves are shown in Figure 10, where it is seen that ϕ decreases in a monotonic manner with ϵ, but is a double-valued function of ϵ^e. This clearly shows why attempts to define ϕ as a simple monotonic decreasing function of ϵ^e proved futile.

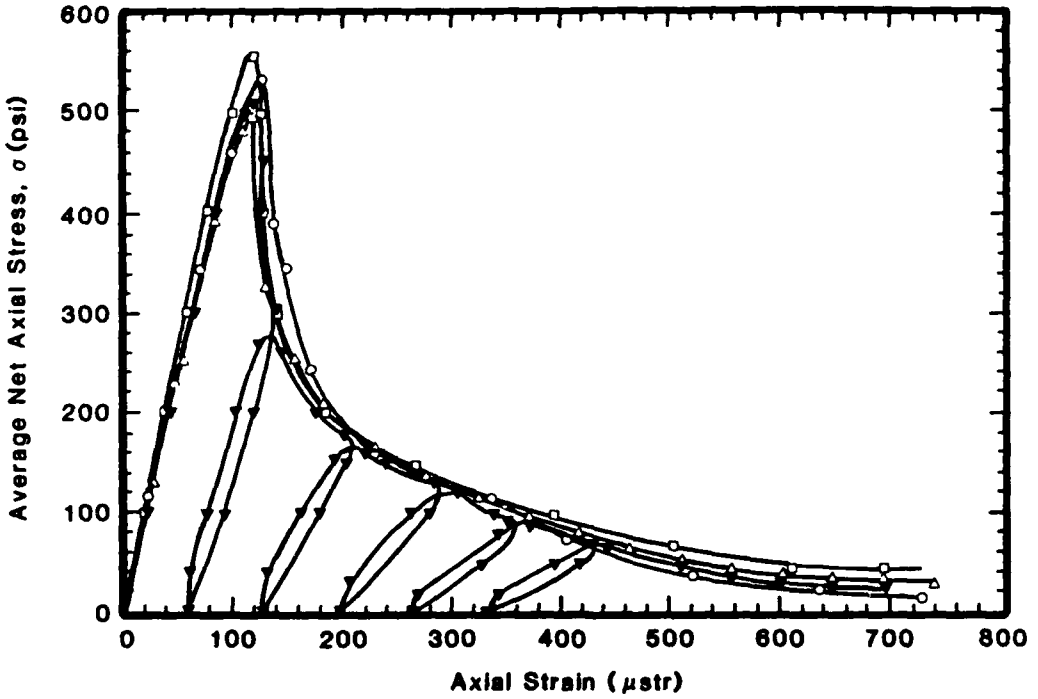

(a) Response measured by Gopalaratnam and Shah (1985).

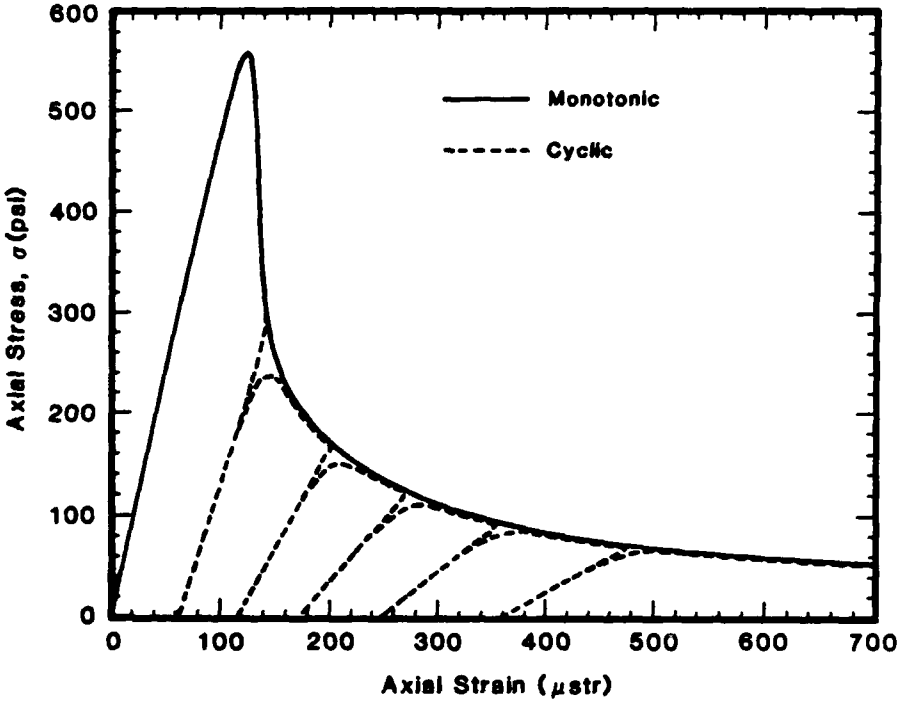

(b) Response predicted by present model.

Figure 9. Response of plain concrete to simple tension.

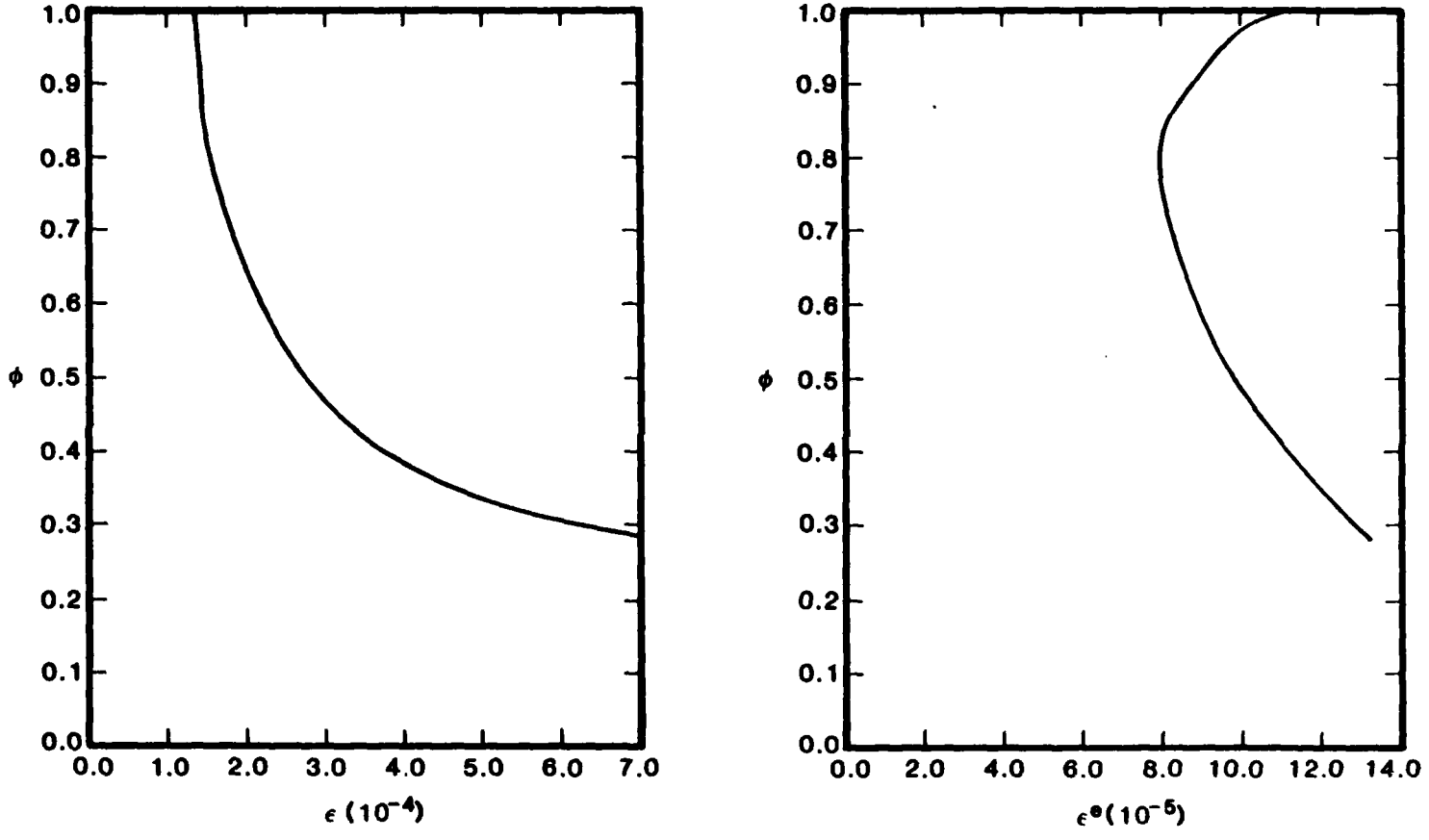

(a) ϕ versus total strain.

(b) ϕ versus elastic strain.

Figure 10. **Dependence of ϕ on ϵ and ϵ^e, as predicted by the present constitutive model for plain concrete.**

Section 4

CONCLUSIONS

This study represents the first attempt to explore the application of the new endochronic plastic-fracturing theory to plain concrete. For this purpose, attention was focussed on the behavior of the model under uniaxial loading conditions. On the basis of the results presented herein, the following conclusions are drawn.

1. To the extent that the model has been explored in the present study, i.e., under conditions of simple tension, the model appears to provide an excellent description of the observed behavior of plain concrete during progressive failure under tensile straining conditions.

2. In addition to elasto-plastic effects, the model can describe both stiffness degradation, through ϕ, and yield limit degradation through F.

3. The endochronic plastic-fracturing model contains, as special cases, several models that are noteworthy. This includes the classic elastic-fracturing model, the standard plasticity model and a plastic-fracturing model with yield degradation. The general model includes both stiffness degradation and yield limit degradation.

4. The key to the success of the model lies in having the appropriate evolution equation for ϕ for the material of interest. Ideally, it would be desirable to have the evolution equation reflect the underlying micromechanical fracture mechanisms, but the technology has not advanced to that point. A research effort to develop such an evolution equation for ϕ is currently underway (Valanis, 1988), but the results from this study are not expected to be available for sometimes.

5. In the present study, an evolution equation for ϕ suggested by the data was used. We found that this equation was most naturally expressed in terms of the plastic strain ϵ^p. The dependence of ϕ on the elastic strain was found to be double-valued.

6. A simple and efficient numerical scheme was developed for integrating the governing equations of the model for simple tension, and this suggest an approach for numerically dealing with the more general three-dimensional version of the model.

7. Procedures were developed for determining the materials-dependent parameters and functions in the model from standard data. However, because of the sparseness of the available data, several of the functions had to be determined indirectly.

8. On the basis of the very encouraging results presented herein, further studies should be undertaken to explore and validate the model under more general loading conditions, such as uniaxial compression and triaxial compression. These cases involve cracking patterns that are considerably more complex than occurs under simple tension and thus should provide a stringent test of the theory.

Section 5
LIST OF REFERENCES

Bazant, Z. P., and F-B Lin (1988), "Non-Local Yield Limit Degradation," *Intl. J. of Num. Meths. in Engrg.*, 26, 1805.

Dougill, J. W., (1976), "On Stable Progressively Fracturing Solids," *Zeits. für Angewandte Math. und Phys.*, 27 (4), 423.

Gopalaratnam, V. S., and S. P. Shah (1985), "Softening Response of Plain Concrete in Direct Tension," *ACI Journal*, May-June, 310.

Maier, G., and T. Hueckel (1979), "Nonassociated and Coupled Flow Rules of Elastoplasticity for Rock-Like Materials," *Intl. J. Rock Mech. Min. Sci. and Geomech. Abstr.*, 16, 77.

Murakami, H., and H. E. Read (1988), "A Second-Order Numerical Scheme for Integrating the Endochronic Plasticity Equations," *Computers and Structures*, 18.

Scavuzzo, R., T. Stankowski, K. H. Gerstle and H. Y. Ko (1983), "Stress-Strain Curves for Concrete Under Multiaxial Load Histories," CEAE Department, University of Colorado, Boulder, CO.

Valanis, K. C. (1980), "Fundamental Consequences of a New Intrinsic Time Measure, Plasticity as a Limit of the Endochronic Theory," *Archives of Mechanics*, 32, 171.

Valanis, K. C., and H. E. Read (1986), "An Endochronic Plasticity Theory for Concrete," *Mechanics of Materials*, 5, 277.

Valanis, K. C. (1987), "A Comprehensive Study of Internal Damage in Brittle and Cementitious Materials," A proposal submitted to the AFOSR by ENDOCHRONICS, INC., Vancouver, WA.

Valanis, K. C. (1988a), "An Internal Variable Theory of Plasticity and Fracture," (informal report) ENDOCHRONICS, INC., Vancouver, WA.

Valanis, K.C. (1988b), ENDOCHRONICS, INC., Vancouver, WA., Private Communication, November 10.

Valanis, K. C., and H. E. Read (1989), Endochronic Plasticity, A. A. Balkema, The Netherlands (to appear).